UNIVERSITÀ
DEGLI STUDI
DI TRIESTE

UNIVERSITÀ DEGLI STUDI DI TRIESTE

XXXVIII CICLO DEL DOTTORATO DI RICERCA IN

Scienze della terra, fluidodinamica e matematica.

Interazioni e metodiche

Impact of high resolution convection permitting climate projections on the description of the hydrological cycle over Italian rivers and the added value of improved land surface and hydrology in the two-way regional model coupled system.

Settore scientifico-disciplinare: **GEO/12 Oceonografia e fisica dell'Atmosfera**

DOTTORANDA
Luiza Vargas de Oliveira Heinz

COORDINATORE
PROF. Stefano Maset

SUPERVISORE DI TESI
Dr. Erika Coppola

CO-SUPERVISORE
Dr. Filippo Giorgi

ANNO ACCADEMICO 2024/2025

UNIVERSITÀ DEGLI STUDI DI TRIESTE

ABDUS SALAM INTERNATIONAL CENTRE FOR THEORETICAL PHYSICS

Scienze della terra, fluidodinamica e matematica.
Interazioni e metodiche - 38°Ciclo del Dottorato di Ricerca

Impact of high resolution convection permitting climate projections on the description of the hydrological cycle over Italian rivers and the added value of improved land surface and hydrology in the two-way regional model coupled system.

GEO/12 Oceonografia e fisica dell'Atmosfera

December 19, 2025

Candidate
Luiza Vargas de Oliveira Heinz

Supervisor
Prof. Erika Coppola

Co-Supervisor
Filippo Giorgi

Coordinator
Stefano Maset

A.Y. 2024/2025

Author's note

This thesis has been compressed for uploading. The original version, containing full-resolution images and hyperlinks, can be requested to luiza.v.heinz@gmail.com.

Hoje, todos nós sabemos que somos finitos como raça.
E, além de não saber como lidar com a
imprevisibilidade dos fenômenos climáticos,
temos pouco tempo para aprender como fazê-lo.

Marina Silva

Abstract

This thesis aims at improving our understanding of the evolution of the hydrological cycle under climate change by mean of hydrological and climate modelling and high resolution simulations. Through model development and increased spatio-temporal resolution, we have aimed to improve the quality of our modelling efforts, such as to reliably reproduce the evolution of the river discharge both in time and space in the regions of interest. Understanding hydrological behaviour in relation to past and future periods is of key importance as global warming may have drastic effects on the river flow. Having a solid comprehension of current hydroclimate interactions and of how they may evolve in the coming decades is essential to establish which adaptation measures may be needed for preserving water resources.

The climate modelling community has come together to help research efforts advance towards a better understanding of the climate system by several coordinated efforts. The Coupled Model Intercomparison Project (CMIP, [1]) has created over the years different ensembles of Global Climate Models (GCMs) in order to better understand past, present, and future climate through model intercomparison and to address key scientific questions. The CORDEX (Coordinated Regional Climate Downscaling Experiment) community has done the same for Regional Climate Models (RCMs). The CORDEX ([2]) project focuses on generating high-resolution regional simulations covering the main inhabited regions of the world and, as CMIP, has produced several ensemble of downscaled climate projections for all the domains involved. The ICTP Regional Climate Model (RegCM) has been used in the CORDEX community for decades and, in its current version (RegCM5.0, [3]), the kilometre scale resolution can be achieved.

The land-surface schemes inside GCMs and RCMs do not always have good representations of hydrological processes, nor reliable river routing modules. Therefore, in order to simulate a river discharge based on climate projections, it may be needed to use a hydrological model. In this work, the CETEMPS Hydrological Model (CHyM, [4]) was adopted to complete several simulations forced by the output variables of either GCMs or RCMs.

The CORDEX community has recently made available an ensemble of models

of the Great Alpine Domain ([5], [6]) that are at the convection permitting (CP) resolution, i.e. their nominal resolution is $\sim 3km$. This finer grid is expected to, for example, better reproduce the precipitation distribution as the local scale process and interaction are better reproduced. Moreover, since the CP simulations do not use the convection parametrization, which is one of the main sources of uncertainty in climate projections ([7]), we could also expect a reduction of the model spread in the projections of this ensemble([8]).

The most recently developed land-surface model CLM (Community Land Model) version 5.0 ([9]) contains in itself a hydrological component, MOSART, which constitutes an improvement from its predecessor. RegCM5.0, however, uses CLM4.5 as its standard land-surface scheme. In CLM4.5, the river routing process is done with a simple linear reservoir model, whereas MOSART performs physically based river routing. This, combined with the several other improvements relevant for the hydrological cycle in the land scheme of the CLM5.0, could improve the description of hydrological variables inside the RegCM5.0 model, once coupled with CLM5.0. In this configuration, the atmosphere, land-surface and hydrological process are fully coupled. Therefore, the runoff will be in balance with the precipitation and the evapotranspiration through the water balance equation, and the expectation is that final river discharge would be more realistic.

Given the above, two different approaches were used in this work. First, we completed an ensemble of offline coupled hydrological simulations to assess the added value of using the kilometre scale regional climate model projections as input. After, we proceeded with model development to implement improved land-surface schemes in the RegCM model to assess the added value of the fully coupled system versus the off-line one. For the former approach, we have forced the CHyM model over Italy with the CORDEX CP ensemble. We have used two different settings of CHyM according to which input variables were used. In one configuration the model is forced with temperature and precipitation, and, in the second configuration, it is forced with the runoff output of the CP RCM models. These new simulations were compared to previously completed lower resolution CHyM runs, forced with Euro-CORDEX RCMs and CMIP5 GCMs. All these ensembles were firstly compared against observations in order to evaluate our methodology. Once validated, we have assessed how climate change is expected to affect river flow in the coming decades by comparing the historical period (1996-2005) to a mid-century (2040-2049) and an end-of-century (2090-2099) period.

For the second approach, a new coupling mechanism was implemented in RegCM5.0 to enable the transition from CLM4.5 to CLM5.0 as its land-surface scheme. This was achieved through the CLM5.0 fork eCLM, which uses the OASIS3-MCT coupler to exchange data with other models ([10], [11]). Several structural adjustments were made to ensure compatibility between RegCM and

eCLM, while maintaining their physical process representations unchanged. In this approach, a new control RegCM5.0-CP simulation was completed and used to force off-line the eCLM model with MOSART scheme active. Afterwards, a preliminary run was executed with on-line coupling enabled between RegCM5.0 and eCLM, again with the MOSART scheme active. The resulting eCLM runs were evaluated against observations and compared with hydrological simulations of the Great Alpine experiment.

The results of the CP forced runs of the CHyM model show some clear added value connected with the use of the forcing at the kilometre scale resolution. The validation of CHyM runs driven by different ensembles showed that, when forced with CP models, the model spread was similar to the observations spread. However, Euro-CORDEX and CMIP5 driven hydrological runs had a noticeably higher spread. Moreover, the two settings of CHyM (temperature and precipitation driven or runoff driven) have equivalent performances when describing the discharge of the Italian river network. The hydrological simulation driven by the RegCM runs of the CP ensemble was also compared with hydrological simulation of the eCLM/MOSART driven by the new RegCM5.0 simulation. The comparison showed no noticeable difference in the evaluation of the analysed time period, except for more intense extremes discharge values and low flow values being found with CHyM than with eCLM/MOSART. A long time series of the coupled eCLM and RegCM run is not yet available, and these are preliminary results, thus the investigation is expected to continue with extended runs.

The hydrological ensemble climate projections completed with the CHyM model forced by the high resolution CP ensemble showed an intensification of extreme events, with the flood proxy Q_{100} indicating an increase in extreme discharge (up to 60%) and the drought proxy $Q_{7,10}$ indicating a decrease in low discharge (up to 50%). The behaviour of these two variables were found to be driven respectively by the extreme and the average precipitation change, which respectively increased and decreased for the majority of the territory. The average change in discharge over Italy was mainly driven by average precipitation but modulated by extreme precipitation, specially during summer and spring months. Furthermore, a very clear altitude dependence was seen when analysing the hydrological year. By the end of the century, regions in the Po Valley over 2000m in altitude are expected to reach 25% of their cumulated yearly discharge up to 6 weeks earlier, whereas the 50% mark should be reached only 2 weeks earlier. This phenomenon, which was poorly or even not at all captured by the lower resolution hydrological simulations, is linked to the change in the snow regime with warming temperatures. As less solid precipitation falls in winter and snow melt occurs earlier in the spring, we expect wetter winters and drier springs. In terms of model spread in the hydrological projections, the high resolution ensemble shows a decrease up to 5 times when

looking at average discharge changes and comparing them to lower-resolution results. These findings reinforced the importance of high-resolution when studying hydrological processes in region with complex topography.

The interest in improving hydroclimate modelling extends beyond theoretical research, as its results can be used for real-time and impact-based applications. To illustrate this, we conducted a case study using hydrological modelling simulations in an attribution study of a major flood event that occurred in Southern Brazil between the late April and early May 2024. The extreme precipitation during this period caused record-breaking levels of river floods, resulting in over 16 billion dollars in damages ([12]) and nearly 200 deaths ([13]).

Given the importance of the fluvial network for the region, we assembled a long time series of local station observations for precipitation and river discharge, which are rarely available in regions affected by similar events. As such, we first conducted a statistical attribution study based on this data, where we compared a factual (F, i.e. with climate change) scenario to a counterfactual (CF, i.e. without climate change) scenario according to the World Weather Attribution protocol ([14]). A GEV (generalized extreme value) distribution was fitted to both precipitation and discharge under the F and CF periods, with the distribution from the CF period derived assuming a 1.2°C cooler global mean temperature. We computed the return period of the observed flood event in both the F and CF periods. The probability of occurrence of events, of similar or higher magnitude than the observed one, has increased by a factor of eight for precipitation and of 1.7 for discharge, highlighting a clear rise in frequency with climate change.

The ClimaMeter attribution scheme ([15]) was also used to study the same event. The mean sea level pressure pattern averaged over the nine days between 26/04/2024 and 04/05/2024 was used to identify analogue events in different time periods, based on the similarity of their synoptic pattern. Three associated variables (precipitation, discharge and temperature) were analysed to assess any changes in time of the composite of these events. Using both the ERA5 reanalysis dataset ([16]) divided into past and present periods and the observations from local stations in the flood region, we found an increase in precipitation in the areas most affected by the floods, and a widespread increase in discharge throughout the Rio Grande do Sul region. Notably, precipitation from station data and reanalysis showed consistent results. We also examined the natural variability contribution to the event and, according to the ClimaMeter protocol, natural variability cannot alone explain the observed increases in precipitation and discharge between the past and present periods.

Following the ClimaMeter protocol, we also included global and regional climate models and repeated the analogue analysis for each model. We assessed whether any significant differences emerged when comparing different Global Warm-

ing Levels (GWLs, [17]) to a reference period in different ensembles. These were also used as input of the hydrological model CHyM, providing us with supplementary information on river discharge, not typically available in similar studies. Our analysis indicates that, starting from 1.5°C of warming, both precipitation and discharge associated with analogue events increases. Moreover, several models analysed show more intense and consistent increases at higher degrees of warming.

This work has explored avenues for improving the quality of hydroclimate modelling and highlighted the potential of high-resolution and enhanced land-surface schemes in better representing river discharge. We have also presented one application of the results of this work in an attribution study. Further work could build upon the results presented in this thesis, notably by continuing the validation simulations within the newly established eCLM-RegCM coupled framework. Additionally, research similar to the analysis done with CP-RCMs driven CHyM runs could be extended to other models/ensembles, not limited to the Italian domain. Finally, as demonstrated by our attribution study, the results generated by this study could be used for a wide range of applications and could be relevant for more policy oriented climate change research.

Contents

Author's note **I**

Abstract **III**

1 Introduction **1**
1.1 Overview and objectives 1
1.1.1 Scientific significance and research questions 1
1.1.2 Structure of the thesis 3
1.2 Climate change impact on hydrological phenomena 3
1.3 Hydrological extremes 5
1.4 High resolution modelling 8

2 Methodology: Using High-Resolution Convection-Permitting Climate Simulations for Hydrological Projections **14**
2.1 Data used 15
2.1.1 Observations 15
2.1.2 Climate simulations 15
2.2 CETEMPS Hydrological Model (CHyM) 15
2.2.1 Hydrological simulations performed 20
2.3 Evaluation methodology 21
2.4 Methodology for analysing discharge projections 24
2.4.1 Lower-resolution results 25
2.4.2 Model uncertainty 25

3 Impacts of High-Resolution Convection-Permitting Simulations on Hydrological Projections Under Climate Change **29**
3.1 Validation Period 30
3.2 Climate Change Projection Results 37
3.2.1 Hydrological Year 47
3.2.2 Model uncertainty 53
3.3 Discussion 53

4 Integrating eCLM into RegCM5: online hydrological coupling at high resolutions. 58
4.1 Modelling and coupling framework . . . 59
4.1.1 The OASIS3-MCT coupler . . . 60
4.1.2 RegCM5 . . . 61
4.1.3 eCLM . . . 62
4.1.4 RegCM5.0 and eCLM coupled system . . . 64
4.2 Preliminary Simulations . . . 65
4.2.1 Offline simulations . . . 65
4.2.2 Coupled simulations . . . 66
4.2.3 Evaluation methodology . . . 67
4.3 Results . . . 68
4.4 Discussion . . . 74

5 Application of regional hydrological projections in real world events: attribution of a flood event in Southern Brazil in 2024. 76
5.1 Event Description . . . 77
5.2 Methodology . . . 78
5.2.1 Observations . . . 78
5.2.2 Statistical Attribution of the Event . . . 79
5.2.3 Discharge Modelling . . . 80
5.2.4 Attribution of the event with the analogue method . . . 83
5.3 Results . . . 85
5.3.1 Event definition . . . 85
5.3.2 Statistical Attribution . . . 86
5.3.3 Model validation . . . 88
5.3.4 Analogue Method . . . 92
5.4 Discussion and applications of hydrological modelling . . . 102

Conclusion 108

A Pre-processing Protocol for MOSART 112
A.1 External Files . . . 112
A.2 Generation of variables . . . 113

Bibliography 116

Chapter 1

Introduction

1.1 Overview and objectives

This research thesis aims to investigate the evolution of the hydrological cycle under a climate change scenario. A combined approach of hydrological and climate models was adopted to assess their ability to reproduce present day river discharge and its projected evolution under climate change. The main region of interest of this work is the Italian peninsula, for which state-of-the-art kilometre scale climate projections are available. Simulations were validated against discharge observations to ensure the robustness of the results.

Furthermore, this work explores the added value of an improved land-surface scheme and hydrological representation within a two-way regional modelling coupled system. To enable this evaluation, significant model development was carried out. Notably, a new coupling scheme was implemented between the Regional Climate Model RegCM version 5.0 (RegCM5.0, [3]) and the Fork of the Community Land Model version 5.0 (eCLM; [9], [10]). Preliminary results for the Italian domain obtained with the updated system were evaluated against the same observational dataset.

Finally, a case-study combining hydrological and climate modelling is presented in the last chapter. It investigates a flood event that occurred in southern Brazil using different climate change attribution protocols, with the novel inclusion of hydrological simulations. This component highlights how hydrological modelling can shed light on the influence of warming temperatures on specific extreme events.

1.1.1 Scientific significance and research questions

Climate change is one of the major challenges of the 21st century. With each passing year, its effects on the biosphere and on human society become increasingly clear, and the actions needed to address them increasingly urgent. Effective

adaptation and mitigation strategies are required in most, if not all, sectors of human activity. For these strategies to be successful, they must be grounded in a thorough understanding of the risks posed by global warming.

There is scientific consensus on the role of anthropogenic emissions in increasing Earth's average temperature ([18], [19], [20]). However, projecting the evolution of other variables remains more complex. Among the possible consequences of a warming climate are changes in precipitation patterns and river flow. River discharge is influenced by several atmospheric and land processes, and can display location-dependent responses (e.g. [21]). Rising temperatures can increase evapotranspiration rates ([22], [23]), and alter the snow cycle, shifting precipitation from solid to liquid forms as the climate warms ([24]). Moreover, precipitation is often controlled by phenomena that occur at very local scales, with convective and orographic processes remaining challenging to simulate accurately ([25],[26],[27]). Capturing extreme discharge events also requires very high temporal resolution and detailed topographic representation, as floods are affected by local characteristics such as the subsurface flow and soil moisture. While an overall increase in extreme events is expected, simulating discharge extremes remains a significant challenge ([28], [29], [30]).

Advancing our ability to understand and model these processes is not only of scientific interest, but also has direct societal implications. Water resources are fundamental to human societies, and their future availability will strongly influence sustainable development. High-resolution climate projections offer a way of improving our understanding of local processes in regions of complex topography or areas prone to localized intense precipitation events. These simulations must also incorporate state-of-the-art land-surface and hydrological schemes to ensure reliability. With such high-quality information available, attribution studies, such as presented at the end of this thesis, can be conducted, allowing for a more direct use of scientific knowledge by the community at large.

Accordingly, this thesis addresses the following research questions:

- What are the effects of using kilometre scale climate projections on the description of the hydrological cycle and river discharge?
- What is the added value of enhancing the land-surface and hydrology representation in a two-way coupled regional modelling system?
- Can hydrological modelling of river discharge be included in attribution studies of flood events?

1.1.2 Structure of the thesis

This thesis is organized into 6 chapters. The present chapter introduces the research context, scientific questions posed, and the main objectives. Chapter 2 details the methodology and datasets used to perform a high-resolution study on hydrological behaviour of Italian rivers. Chapter 3 presents the results of these analyses and the projections of river discharge of Italy under a warming climate. Chapter 4 focuses on the technical developments carried out to implement a new two-way coupled system between RegCM and eCLM, and evaluates its preliminary results. Chapter 5 presents a case-study on the attribution of an extreme flood event in Southern Brazil, in which hydrological modelling has been incorporated. Finally, the Chapter 6 summarizes the main findings, highlights the scientific contributions and indicates perspectives for future research work.

1.2 Climate change impact on hydrological phenomena

The latest Intergovernmental Panel on Climate Change (IPCC) Assessment Report (AR6, [20]) states with *high confidence* that anthropogenic greenhouse gas (GHGs) emissions are a major driver of substantial changes in the global water cycle. Global mean precipitation is expected to increase globally at a rate "*very likely of between 2-3%*" per degree of warming. However, extreme precipitation is expected to have an even more intense increase, following the Clausis-Clapeyron or super Clausis-Clapeyron scaling ([31], [32], [33], [34]). In addition, continued climate change is projected to alter large scale atmospheric circulation patterns ([20]), leading to spatial variations of precipitation regimes.

Global warming is also expected to amplify the contrast of wet and dry seasons. The differential warming over land compared to the ocean, together with higher evapotranspiration rates, is expected to lead to more intense drought events ([20]). This drying tendency, combined with the increase in extreme precipitation, will exacerbate both types of hydrological extremes. Since the IPCC Fifth Assessment Report (AR5, [35]), there is *high confidence* that the difference between wet and dry seasons will become more pronounced under global warming. Nonetheless, identifying the most affected regions remains a challenge, as circulation changes may have a determining role in it.

Beyond precipitation, many other forcings influence runoff and river discharge. The hydrological cycle involves several interconnected water fluxes, such as evaporation, infiltration, surface runoff and groundwater recharge (Figure 1.1). These natural processes interact with and influence each other, but are also affected by human activities (e.g. [36]). Land-use change, for example, can substantially mod-

ify local water balances ([37], [38]). Urban expansion and deforestation can reduce infiltration and enhance surface runoff, while irrigation and groundwater extraction directly alter river discharge ([39], [40], [41], [42]). Although these processes are not a direct consequence of global warming, the anthropogenization of the landscape can mask the natural hydrological signals and hinder our ability to detect climate driven trends. For instance, dams can effectively manage water availability during dry seasons, but are also known to camouflage low-flow conditions and drought indicators ([43]).

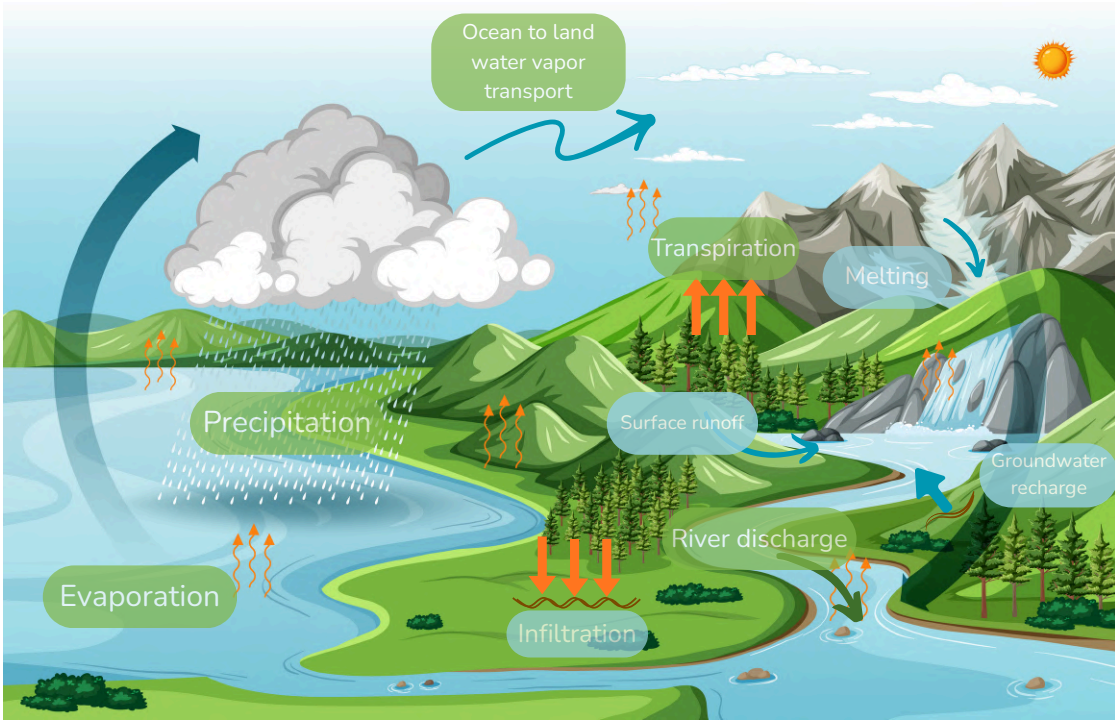

Figure 1.1: Depiction of natural fluxes on the water cycle.

There is *high confidence* that snow covering and glacier mass will continue to decrease ([20]) with warming temperatures, which is bound to affect the river recharge in affected areas. Decreased snowfall in winter and earlier spring snowmelt are expected to alter the seasonality of river discharge, affecting downstream water resources. With glaciers, their melting processes will increase runoff until a tipping point is reached, after which runoff will decrease until the glacier has vanished completely ([44]).

Observing the direct influence of climate change on hydrological phenomena remains challenging, as climate related signals often interact with and are masked by other human-driven forcings. As such, the magnitude and even the direction of hydrological trends can vary strongly by region. The Mediterranean region,

one of the focal points of this thesis, has already experienced increasing drought severity due to anthropogenic emissions, with future projections indicating further intensification ([45]). In Figure 1.2 (reproduced from [20]), an ensemble mean of climate models shows the expected seasonal runoff change under different emission scenarios. There, the drying of the Italian region strengthens with higher degrees of warming, worsening present conditions. In contrast, Figure 1.3 (reproduced from [20]) displays the high-discharge magnitude changes projected across Europe, indicating an increase in extreme flows for the same region.

According to the AR6 Report, projections indicate that *global mean annual runoff increases with global surface temperature increase*, but this change remains highly dependent on season and location. The seasonality of rivers is not projected to change drastically, though the contrast between wet and dry months is expected to become more pronounced. In Europe, the summer months (JJA) are projected to be drier, particularly in the Mediterranean region. Even under low emissions scenarios, this signal is consistent among models across Italy. However, during the winter season (DJF), a dipole pattern is observed, with a wettening of northern Europe and a drying of the Mediterranean. This change displays less model agreement. Figure 1.3 from the IPCC AR6 WGI report shows the projected discharge by mid century of the 1-in-100 year event. It is evident a projected decrease for the Iberian Peninsula and a large parts of the northern Europe. In contrast, Italy, along with much of western and central Europe, displays an increase in extreme discharges.

The Northern-most regions of America and and Asia are projected to experience drier summers and wetter winters (Figure 1.2). The projected increase in runoff during the winter months is already present for low-emission scenarios, and with high model agreement. In southern Brazil, a region also examined in this thesis, a severe wettening is projected for all seasons, which intensifies under higher emission scenarios. This wettening extends across the La Plata basin, with Amazon region and continental Central American displaying a drying in both seasons depicted. A large portion of Africa, as well as the Indian subcontinent, also experience severe wettening. Nevertheless, uncertainties remain large in many regions. Different strategies for reducing them can be explored, such as higher model resolution and improved process representation, in order to produce more reliable regional climate projections.

1.3 Hydrological extremes

The hydrological cycle encompasses various interconnected processes which lead to extreme events such as droughts and floods. In this thesis, hydrological extremes are primarily studied in terms of changes of river discharge, which corresponds to

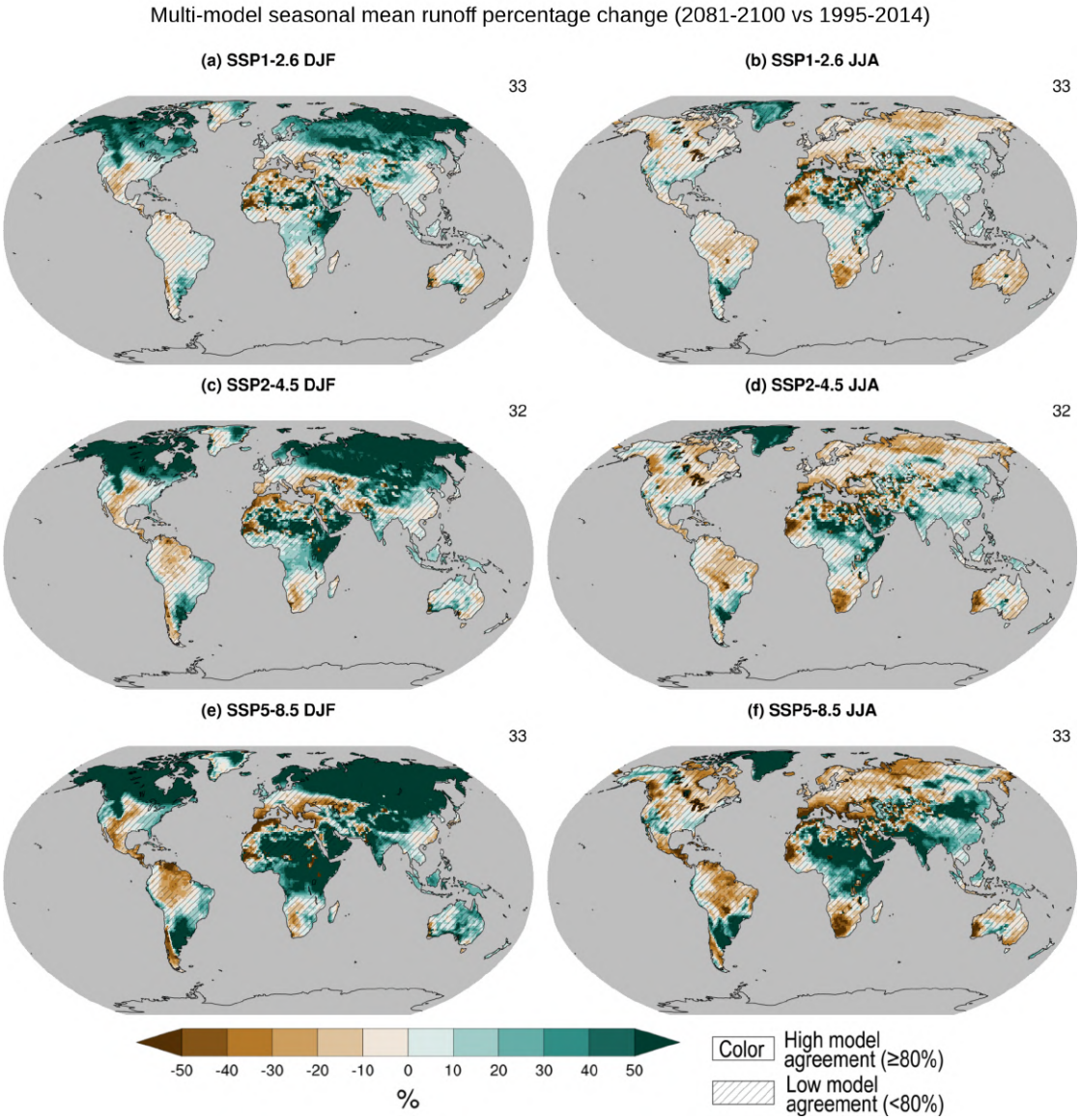

Figure 1.2: Figure 8.18 in [20]. Changes in the average seasonal runoff between the 1995 to 2014 and 2081 to 2100 periods [%]. Left column refers to DJF (December, January and February) averages and right to JJA (June, July and August). Multi-model ensemble obtained from CMIP6 models (number of models in each panel on the top right corner). Scenarios depicted correspond to SSP1.2-6 for panels a and b; SSP2-4.5 for panels c and d; and SSP5-8.5 for panels e and f. Diagonal hatching indicates low model agreement on the signal of the change (<80%)

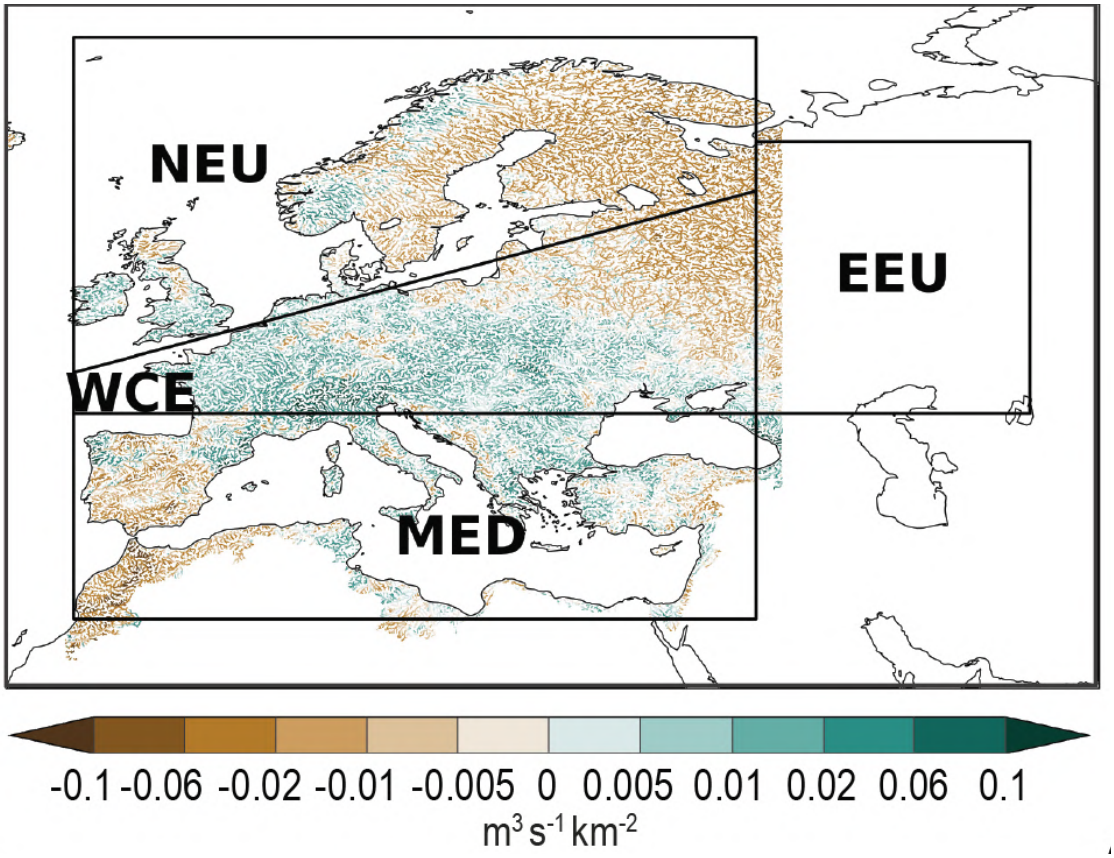

Figure 1.3: Figure 12.9 in [20]. Projected discharge changes for 1-in-100-year events per unit catchment area $[m^3/s.km^2]$ between 1995-2014 to 2041-2060, from the EURO-CORDEX models under the RCP8.5 scenario.

a response of several atmospheric and land-surface processes. While this thesis focuses on streamflow extremes, it is important to acknowledge that droughts and floods can be characterized through other indicators.

Droughts can be classified into the meteorological, agricultural and hydrological categories ([46], [47]). Meteorological droughts are defined by prolonged precipitation deficits, whereas agricultural drought arises from dry soils and increased evapotranspiration demand experienced by crops due to unfavourable meteorological conditions. Ecological droughts are often considered together with agricultural droughts, as it is defined by water stress conditions experienced in natural ecosystems. Hydrological droughts occur when there is a decrease in the water supply available, including groundwater, streamflow or even reservoir levels. In this thesis, when discussing drought occurrence, the focus will be only on the streamflow aspect of hydrological droughts. Although these classifications are distinct, they

are all interlinked, as they are caused by dry meteorological conditions and how they propagate in different components of the biosphere.

Floods can also be grouped into different types, namely are coastal floods, river floods and flash floods ([48]). River floods, which are the focus of this work, occur when sustained high discharge leads to an overflow the riverbanks into neighbouring terrain. These events are often related to prolonged periods of intense rainfall, but can be amplified by factors such as snowmelt and bad soil draining conditions. Flash floods, in contrast, result from extreme precipitation falling within a short time span, and might be worsened by the failing of a local drainage system in urban areas. Coastal floods, or storm surges, occur when low pressure systems with very intense winds cause tides to move offshore water inland.

Understanding the mechanisms that lead to these hydrological extremes is essential for projecting their occurrence under climate change. As demonstrated in later chapters, integrating high-resolution climate and hydrological modelling allows us to improve the simulation of both droughts and floods, especially in regions with complex topography and localized precipitation processes.

Moreover, scientific efforts have been made in recent years to establish a direct link between specific extreme events and climate change through attribution studies. Using different methodologies, the role of anthropogenic emissions in a given extreme is examined to determine whether its frequency and/or intensity may be altered under a warming climate. Advances in climate modelling and in the understanding of climate processes can improve attribution studies, which are not yet widespread for hydrological variables such as river discharge. Robust attribution research can support societal actors in structural planning by improving their understanding of future risks and needs. For example, an increased likelihood of severe floods may require stricter building standards for bridges and dams, as return periods decrease. Similarly, an expected increase in drought severity may indicate a greater need for alternative water sources and reservoir capacity.

1.4 High resolution modelling

Understanding past, present, and future climate dynamics relies on the use of climate models that represent different components of the Earth system. Climate models have evolved significantly since the early works of [49]. Currently, climate models can go from covering the global scale (spatial resolution of 50-250 km), passing through the regional scale (10-25 km), and arriving to the local convection-permitting scale (1-3 km). Each spatial scale presents distinct challenges and capabilities: whereas the global models are suited to project changes in the large scale circulation patterns, the kilometre scale can resolve local processes influenced by small scale interactions.

Global climate models (GCMs) are numerical models that simulate the main components of the climate system and their interactions at a global scale, including the atmosphere, the land surface, the oceans and the sea ice, among others ([20]). These models respond to distinct large-scale forcings, including the increase in GHGs from human activity. Since 1995, the climate modelling community has worked together to advance the field through the Coupled Model Intercomparison Project (CMIP) ([1]). The project provides a standardized framework for GCM development. It aims to create a consistent foundation for answering important research questions of the field through model inter-comparison. GCM developers are currently working on Phase 7 (CMIP7, [50]) and outputs from the last two phases (CMIP5 and CMIP6,[51] and [1]) are used in this work.

To obtain finer scale information, downscaling methods can be applied to GCM outputs. Statistical downscaling is based on statistical relationships found between GCM outputs and existing observations, assuming these relationships hold for periods not covered by observations. Dynamical downscaling, in contrast, relies on Regional Climate Models (RCMs) that explicitly simulate physical processes over limited domain ([20], [52] [**giorgi2019**]). They need to be forced at their boundary with either reanalysis data or information from their lower-resolution counterpart, the GCMs. RCMs simulate at the continental or sub-continental scale, with resolutions typically between 10-50km.

Analogously to CMIP, the RCM community has developed the Coordinated Regional Climate Downscaling Experiment (CORDEX) initiative ([2]). The principal goals of the initiative are to further the understanding of local and regional processes through downscaling, and to coordinate and exchange information on these downscaling efforts. The CORDEX simulations aim to dynamically downscale the GCM climate projections on each CORDEX domain from either CMIP GCMs or from a reanalysis product like ERA-Interim ([53]), ERA5 ([16]), MERRA-2 ([54]), the NCEP-NCAR Reanalysis 1 ([55]) and JRA-55 ([56]). Within the CORDEX project the CORDEX-CORE (Coordinated Output for Regional Evaluations, [57], [58]) simulations have been completed by downscaling three CMIP5 GCMs on all continental regions by means of two RCMs (RegCM, [59]; and REMO, [60], [61]) A second phase of the CORDEX-CORE project is underway and has as its main objective downscaling both ERA5 reanalysis and CMIP6 GCMs.

In the last decade another project has been developed within the CORDEX initiative to reach the kilometre scale by means of the so-called convection permitting (CP) RCMs. This is referred to as the CORDEX Flagship Pilot Study (CORDEX-FPS, [62], [5], [6]) for Convection Permitting Scale. Within this FPS, an ensemble of CP-RCMs was used to simulate an area covering the Greater Alpine Region at a nominal resolution of 3km with hourly outputs. Such fine scale can better represent, for example, complex topography and, more in general, local

land-surface interactions, which are known to be essential in simulating local scale weather and climate extremes ([**giorgi2019**], [63]).

By explicitly resolving convection, CP-RCMs reduce the number of parametrizations needed in the models, which are often the reason of the greatest climate uncertainty ([20]), potentially improving the signal of simulated precipitation and related hydrological processes. Climate models have three main sources of uncertainty ([8], [7], [64]): scenario uncertainty, which relates to the different assumptions about future GHG emissions and forcings used to define a projection scenario; natural variability, caused by the inherent nature of the climate system and its internal oscillations on decadal and multi-decadal scales; and model uncertainty, tied to the assumptions made and the parametrizations chosen when developing climate models. The latter is particularly relevant at the regional scale ([7]). At the kilometre scale resolution, deep convection is explicitly simulated rather than parametrized. Given that this parametrization can be a large source of uncertainty in climate models, it is expected that CP resolutions will have decreased model uncertainty than those with coarser grids.

A recent study by [8] supports this hypothesis. Their analysis of RCMs and CP-RCMs shows that CP-RCMs have a lower relative contribution of model uncertainty to total uncertainty for precipitation intensity in the Great Alpine Domain for the summer (JJA) season. This can be explained by the seasonality of convective systems, which are much more prevalent during summer. Therefore, the explicit representation of convection by CP-RCMs versus the parametrized RCMs helps to lower the model uncertainty. CP-RCMs have been also been shown to outperform coarser-resolution models when simulating intense short-duration precipitation events and convective systems happening at hourly scales ([5], [65], [8]). All these findings are expected to be reflected in the representation of the hydrological cycle at the high resolution basin scale.

Hydrological processes are represented inside climate models through their land-surface models (LSMs). Nonetheless, these schemes are often simplified and may no fully capture key aspects of the water cycle. This can be improved by coupling the climate model with a hydrological model. Additionally, many LSMs do not have physically based river routing modules, often leading to unrealistic representation of local hydrology ([66], [67], [68]). Increasing the complexity of LSMs, or coupling of the existing climate models with dedicated hydrological models, can help to improve the knowledge on this topic ([30]). By improving our capacity to predict how climate change will affect the hydrological cycle, adaptation and mitigation strategies can be taken for long term trends and for changes in extreme events. Chapter 5 presents a case study illustrating how hydroclimate modelling can help elucidate the climatic influence of an observed extreme flood event.

Temporal resolution also plays a crucial role in hydrological modelling. Ex-

treme events are more accurately captured when studied at the sub-daily scale, even though this fine temporal resolution can also limit the ability to generate long time series due to computational demands. Notably, flood simulations have been shown to improve in small basins at sub-daily resolution ([69]). The hydrological cycle is particularly sensitive to small-scale processes, such as orographic and convective precipitation, which are difficult to simulate in coarser grids with longer time steps ([25], [26], [27]). Figure 1.4 (sourced from [20]) indicates how the response of precipitation to warming, expressed in percentage of increase per degree of warming, depends on the temporal scale analysed. Sub-daily extremes show a much more intense and broader response to warming than daily extremes. Coarse grid GCMs are not able to capture these signals, as they do not have the resolving capabilities to do so. Therefore, to study extreme precipitation events and their hydrological consequences, such as floods, RCMs, and specially CP-RCMs, can enhance our ability to capture the full range of relevant processes.

Another aspect of the hydrological cycle that can be challenging to model is the role of groundwater in soil moisture dynamics and discharge generation. Often, LSMs rely on simplified descriptions of soil moisture processes that do not account for two-way vertical and lateral interactions with the groundwater. For example, the use of free drainage approaches does not allow deep groundwater to supply moisture to the soil layers, whereas more complex descriptions can include such interactions, including even lateral flows, which become increasingly relevant at very high spatial resolutions. Previous research has shown that the inclusion of two-way exchanges between the land-surface and deep groundwater can help reduce temperature biases and has a particularly strong influence during dry periods ([70]). Moreover, [71] demonstrated the impact that soil moisture can have on precipitation through a convective mechanism, highlighting both the importance of accurately resolving the soil moisture and of representing convective processes. At CP resolution, there is therefore potential to improve the hydrological description of both components. Improving the modelling of these processes could help address current gaps in understanding the response of groundwater to anthropogenic climate change and provide further insights into land surface atmosphere feedbacks ([72]).

Despite their clear advantages, high resolution modelling present substantial challenges due to its high computational cost, both in terms of processing time and storage. Therefore, many research works combining CP resolution climate simulations with hydrological models have been constrained to a limited number of ensemble members or to small domains ([73], [74]). However, to fully capture the hydrological processes that drive runoff and river discharge at finer spatial resolutions, it is essential to have high resolution ensemble projections. Higher model resolution also demands an improved parametrization of hydrological pro-

cesses, which becomes increasingly important in order to produce reliable climate projections. Therefore, both reliable climate data and physically sound descriptions of hydrological mechanisms are necessary for generating robust hydrological projections.

In an ideal framework, the surface hydrological cycle representation should interact directly with the atmosphere to allow feedbacks relevant for the climate evolution. Therefore, they should be effectively represented. This thesis advances towards that goal by exploring how the recently developed kilometre-scale CP-RCMs contribute to the representation of river discharge over Italy, and by evaluating the potential of improving the LSM of RegCM to achieve more realistic hydroclimate projections. Both these efforts aim to contribute to a more physically consistent understanding of the hydrological cycle in a changing climate and to lay the groundwork for future high-resolution, fully coupled hydroclimate modelling studies.

The following chapters describe the datasets, models, and methodologies used to conduct these high-resolution analyses, outlining the experimental framework through which the research questions introduced above are addressed.

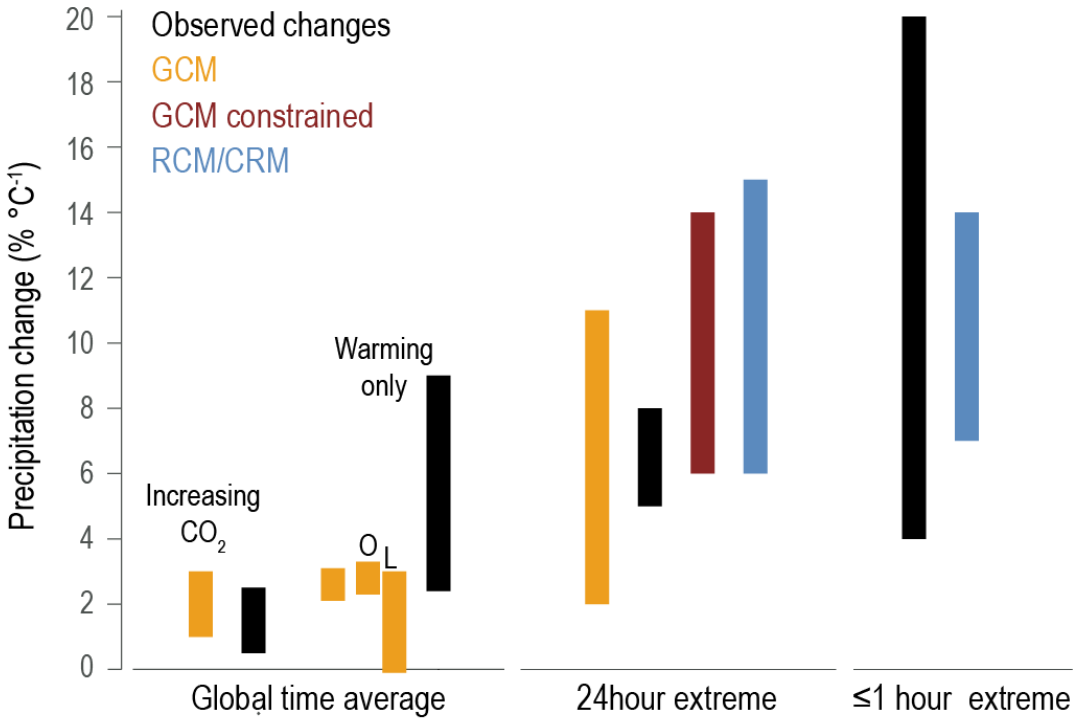

Figure 1.4: Figure 8.4 in [20]. Precipitation increase with global mean surface warming [%/°C] for different ensemble of experiences (estimations in the 5-95% range). The global time average refers to either the apparent hydrological sensitivity (responses to increased CO_2 emissions) or the hydrological sensitivity (response to warming only) for observations and GCMs, the latter of which was divided into a land (L) and ocean (O) response. The 24 hour extreme is obtained with the 99.9^{th} percentile of GCMs, a observationally constrained set of GCM experiments, RCMs and observations. For $\leq$ 1 hour extremes, only observations and RCMs (including CP-RCMs) are shown.

Chapter 2

Methodology: Using High-Resolution Convection-Permitting Climate Simulations for Hydrological Projections

This chapter describes the use of high-resolution convection permitting (CP) climate simulations as input for a hydrological model. The datasets, model configurations, and validation methodology used to investigate the hydrological impact of climate change on the Italian river system are presented, and the metrics employed for both model evaluation and future projection analyses are defined.

The analyses presented here provide the basis for the results discussed later in Chapter 3, which examines the influence of kilometre scale resolution on the simulated discharge behaviour of the Italian river network. Hydrological simulations at lower resolution, previously published in [75], are also described in the chapter for comparative purposes.

Section 2.1 introduces the data used in this work, including both observational datasets and climate model inputs. Section 2.2 describes in detail the hydrological model setup. Finally, Sections 2.3 and 2.4 describe the methodologies employed to evaluate, respectively, the validation experiments and the projection simulations.

2.1 Data used

2.1.1 Observations

Two river discharge datasets provided by the University of l'Aquila were used as observational references, covering the Po river catchment in northern Italy. The first, referred to as the Po river dataset, contains hourly data from the year 1995 to 2005, while the second, the Upper Po river dataset, spans 2000 to 2010. Both datasets have been previously employed in literature to evaluate hydrological simulations (e.g. [76]). In this study, they will be used to validate the river discharge simulated by CHyM over the region and assess the model's performance.

2.1.2 Climate simulations

A CP ensemble of regional climate models has recently been made available through the CORDEX-FPS convection project. These CP simulations cover the Greater Alpine region, from which a subdomain corresponding to the Italian river network was selected for the hydrological analyses conducted in this study. No further validation of the CORDEX-FPS convection ensemble is presented here, as these simulations have already been extensively evaluated against observations ([5] [6]).

There are two different ensemble that will be examined: the first corresponds to a validation sub-ensemble (val) covering the years 2000-2009, in which the CP models are nested inside RCMs driven by Era-Interim reanalysis data ([53]). The second sub-ensemble consists of the projection sub-ensemble, including three time slices: a historical period (his, 1996-2005), a mid-century period (mid, 2040-2049) and an end-of-century period (end, 2090-2099). For the projections, the CP models are nested inside RCMs that are themselves nested inside various GCMs driven by the Representative Concentration Pathway (RCP) 8.5 scenario ([77]).

2.2 CETEMPS Hydrological Model (CHyM)

The CETEMPS Hydrological Model (CHyM, [4]) is a grid-based model developed at the University of l'Aquila to simulate river discharge based on input from climate data. It reconstructs an eight-direction flow river network from on a Digital Elevation Model (DEM). The DEM is smoothed with a Cellular-Automata based algorithm to ensure a coherent drainage structure, even in regions of complex topography ([78]). CHyM has been successfully applied in various climatological and hydrological studies across different regions in the world ([76], [75], [79], [80]).

To simulate the routing of surface runoff through the generated river network, CHyM employs a kinematic wave approximation of the shallow water equations

Table 2.1: Ensemble of models used for the validation period (2000-2009) for CP TP driven by Era-Interim data. Table shows CP-RCMs and their driving intermediate RCMs.

Institute	CPRCM	RCM
Aristotle University of Thessaloniki	WRF381BF	WRF
BCCR The Bjerknes Centre for Climate Research	WRF3.8	WRF3.8.1CA
Center for International Climate and Environmental	WRF381BJ	WRF
BTU Brandenburg University of Technology	CCLM5	CCLM4
ETHZ Federal Institute of Technology	CCLM	CCLM
Justus-Liebig-University Giessen	CCLM	-
KIT Karlsruhe Institute of Technology	CCLM5	CCLM4
Centro Euro-Mediterraneo sui Cambiamenti Climatici	CCLM	CCLM
Centre National de Recherches Meteorologique	CNRM-AROME41t1	CNRM-ALADIN63
Research Centre Jülich	WRF381BB	WRF
Climate Service Center Germany	REMO	REMO
HARMONIE-Climate community	HCLIM38-AROME	HCLIMcom
ICTP Abdus Salam Internatinal Centre for Theoretical Physics	RegCM4	RegCM4
KNMI The Royal Netherlands Meteorological Institute	HCLIM38-AROME	RACMO
Institut Pierre-Simon-Laplace	WRF381BE	WRF
University of Hohenheim	WRF381BD	WRF
Wegener Center for Climate and Global Change, University of Graz	WRF381BL	WRF

([81]). The average cross-sectional velocity (V) is computed using Equation 2.2.1, where S represents the slope of the channel, R is the hydraulic radius and n is a function of the manning coefficient M.

$$V = \frac{\sqrt{S} R^{\frac{2}{3}}}{n} \tag{2.2.1}$$

The hydraulic radius (R) is defined as a function of the drainage area (D), with coefficients α, β, and γ determined during the model's calibration process(see Table 2.6). When D is smaller than a minimum threshold D_{min}, D_{min} is used to compute R.

$$R = \alpha + \beta \max\left(D, D_{min}\right)^{\gamma} \tag{2.2.2}$$

The value of n can be estimated using either by Equation 2.2.3 or 2.2.4, depending on the drainage area. When $D > D_{min}$, Equation 2.2.3 is applied. Otherwise,

Table 2.2: Ensemble of models used for the validation period (2000-2009) for CP Roff driven by Era-Interim data. Table shows CP-RCMs and their driving intermediate RCMs.

Institute	**CPRCM**	**RCM**
BCCR The Bjerknes Centre for Climate Research	WRF3.8	WRF3.8.1CA
Center for International Climate and Environmental	WRF381BJ	WRF
BTU Brandenburg University of Technology	CCLM5	CCLM4
ETHZ Federal Institute of Technology	CCLM	CCLM
Justus-Liebig-University Giessen	CCLM	-
KIT Karlsruhe Institute of Technology	CCLM5	CCLM4
HARMONIE-Climate community	HCLIM38-AROME	HCLIMcom
ICTP Abdus Salam Internatinal Centre for Theoretical Physics	RegCM4	RegCM4
Instituto Dom Luiz	WRF381BH	WRF
KNMI The Royal Netherlands Meteorological Institute	HCLIM38-AROME	RACMO
Institut Pierre-Simon-Laplace	WRF381BE	WRF
University of Hohenheim	WRF381BD	WRF
Wegener Center for Climate and Global Change, University of Graz	WRF381BL	WRF

Table 2.3: Ensemble of models CP Roff for the mid and end of century periods (2040-2049 and 2090-2099). Table shows CP-RCMs, their driving intermediate RCMs and their driving GCMs.

Institude	**CPRCM**	**RCM**	**GCM**
BTU Brandenburg University of Technology	CCLM5	CCLM4	CNRM-CM5
Justus-Liebig-University Giessen	CCLM	-	MPI
KIT Karlsruhe Institute of Technology	CCLM5	CCLM4	MPI-ESM-LR
HARMONIE Climate Modelling Community	HCLIM38-AROME	HCLIMcom	EC-Earth
ICTP Abdus Salam Internatinal Centre for Theoretical Physicss	RegCM4	RegCM4	HadGEM
ETHZ Federal Institute of Technology	CCLM	CCLM	MPI

Table 2.4: Ensemble of models CP TP for the mid-century period (2040-2049). Table shows CP-RCMs, their driving intermediate RCMs and their driving GCMs.

Institude	**CPRCM**	**RCM**	**GCM**
BTU Brandenburg University of Technology	CCLM5	CCLM4	CNRM-CM5
KNMI The Royal Netherlands Meteorological Institute	HCLIM38-AROME	RACMO	EC-Earth
Climate Service Center Germany	REMO	REMO	MPI
Justus-Liebig-University Giessen	CCLM	-	MPI
Institut Pierre-Simon-Laplace	WRF381BE	WRF	IPSL-CM5
KIT Karlsruhe Institute of Technology	CCLM5	CCLM4	MPI-ESM-LR
HARMONIE Climate Modelling Community	HCLIM38-AROME	HCLIMcom	EC-Earth
ICTP Abdus Salam Internatinal Centre for Theoretical Physicss	RegCM4	RegCM4	HadGEM
Centro Euro-Mediterraneo sui Cambiamenti Climatici	CCLM	CCLM	EC-Earth
ETHZ Federal Institute of Technology	CCLM	CCLM	MPI

Table 2.5: Ensemble of models CP TP for the end of century period. Table shows CP-RCMs, their driving intermediate RCMs and their driving GCMs.

Institude	**CPRCM**	**RCM**	**GCM**
BTU Brandenburg University of Technology	CCLM5	CCLM4	CNRM-CM5
Justus-Liebig-University Giessen	CCLM	-	MPI
Institut Pierre-Simon-Laplace	WRF381BE	WRF	IPSL-CM5
KIT Karlsruhe Institute of Technology	CCLM5	CCLM4	MPI-ESM-LR
HARMONIE Climate Modelling Community	HCLIM38-AROME	HCLIMcom	EC-Earth
Centre National de Recherches Meteorologique	CNRM-AROME41t1	CNRM-ALADIN63	CNRM-CM5
ICTP Abdus Salam Internatinal Centre for Theoretical Physicss	RegCM4	RegCM4	HadGEM
Centro Euro-Mediterraneo sui Cambiamenti Climatici	CCLM	CCLM	EC-Earth
Wegener Center for Climate and Global Change, University of Graz	WRF381BL	WRF	IPSL-CM5
ETHZ Federal Institute of Technology	CCLM	CCLM	MPI

Table 2.6: Parameters used

Parameter	Value	Units
δ	4.5	-
α	0.0015	-
β	0.05	-
γ	$\frac{1}{3}$	-
D_{min}	100	km^2

n is computed with Equation 2.2.4. In both cases, δ is a calibration constant and M is the Manning coefficient determined by the land-use type specified in CHyM.

$$n(M) = \frac{M}{\delta} \tag{2.2.3}$$

$$n(M) = \frac{M}{1 + (\delta - 1)\frac{1+(D-D_{min})}{D_{min}}} \tag{2.2.4}$$

The flow of water through the river network is then described by the following equations:

$$\frac{\partial A}{\partial t} + \frac{\partial Q}{\partial x} = q_c \tag{2.2.5}$$

$$Q = VA(x,t) \tag{2.2.6}$$

where A is the cross-section area of the river, Q is the river discharge, and q_c is a source term representing the input runoff per unit of length.

Potential evapotranspiration (ET_p) is also accounted for in the model and calculated as a fraction of the evapotranspiration under saturated soil conditions (ET_0, Equation 2.2.7). This fraction is defined by the crop factor (k_c), which varies according to land use type (lu) and directly influences the value of ET_0.

$$ET_p = k_c \cdot ET_0 \tag{2.2.7}$$

In addition, an infiltration term (I) is computed with Equation 2.2.8, where I_{lu} represents the maximum water storage capacity for a given land use type before

saturation, and k is an empirical coefficient controlling the fraction of rainfall ($r(t)$) that infiltrates the soil.

$$I(t) = I_{lu} - kr(t) \tag{2.2.8}$$

Furthermore, a freezing/melting component is included in CHyM to represent hydrological processes under and around freezing temperatures. When air temperatures fall below 0°C, all precipitation is assumed to be solid and will accumulate as snow in the surface. In contrast, when temperatures exceed 1°C, the water stored as snow begins to melt. The amount of snowmelt is determined as a function of the air temperature and the solar irradiation incident on the surface area of the snow cover. The resulting meltwater is then routed through the river network as liquid flow.

Recently, a new irrigation module has been incorporated into the model ([82]). This module estimates the percentage of river discharge extracted for irrigation based on empirical relationships, which depend on both crop type and season. However, this module has not been activated for the simulations presented in the following chapters.

Two configurations of CHyM are currently available, both of which were used in the work presented in the following chapters. The first configuration uses temperature and precipitation as input data (CHyM-TP), which can be obtained from climate models or observational datasets. This configuration simulates the complete sequence of hydrological processes described above, going from a precipitation input to river discharge generation.

The second configuration, the CHyM-Roff, instead uses runoff data as input, being thus primarily applied in combination with climate models. In this setting, it is assumed hydrological processes have been represented by the land-surface scheme of the driving climate model which generated the runoff information. As a consequence, CHyM-Roff does not compute evaporation, infiltration and freezing/melting processes present in its CHyM-TP option. Only the river routing component of the model is present in this configuration (Equations 2.2.1 to 2.2.6).

2.2.1 Hydrological simulations performed

Hydrological simulations were performed with the CHyM model at a kilometre-scale resolution over the Italian territory, which was divided into seven different sub-regions, according to the country's major river basins. This river network has been calibrated and validated in previous studies, and has been shown to provide reliable hydrological representation across these basins ([83], [78], [76]). Two additional sub-regions of the Italian territory, corresponding to Sicily and

Calabria, were used in previous studies but not included here, as they are not fully covered by the CP input domain of the Greater Alpine Region. The river network was constructed using the HydroSheds Hydrologically-conditioned DEM at 90 m resolution, and all CHyM simulations were conducted at an hourly resolution.

To execute the CHyM simulations, input data from the CP models was remapped using a nearest neighbour interpolation algorithm to match the domains of the seven sub-regions. Both CHyM TP (version 6.09) and CHyM Roff configurations were run using the same river network. Each CHyM simulation is forced with the output of a single CP model, and the results were subsequently aggregated to produce ensemble statistics (Tables 2.1 to 2.5). Due to the different availability of CP models simulations, the different sub-ensembles have an unequal number of members. Nonetheless, preliminary tests indicated that the analyses conducted throughout this and the next chapter remained consistent and comparable across ensembles. Therefore, the maximum available number of models was used for each decade and input variable, in order to maximize the robustness of results.

2.3 Evaluation methodology

To validate the study, CHyM simulations driven by CP models forced by the Era-Interim dataset were used, as summarized in Tables 2.1 and 2.2. The specific models included in the validation ensemble were chosen according to their availability. The following analyses were performed to evaluate the modelling framework.

The observational datasets described in Section 2.1.1 were employed, consisting of river discharge measurements in the Po Valley in Northern Italy due to availability constrains in other regions. Stations were selected only if they contained less than 20% missing data during the validation time period, ensuring that the overlapping period between simulations and observations had sufficient data. Each selected observation point was spatially matched to a corresponding location in CHyM's river network, and these cells will be henceforth referred to as validation points. In these points, direct comparisons were made between simulated and observed discharges. The validation points were clustered into five different categories to analyse the model's behaviour, according to their position in the drainage basin, drainage area and local topography. The categories are defined as follows: Po delta, central Po, upper Po, French alps and Swiss alps (Figure 2.1). Among these, the Po delta and the Swiss Alps were investigated in greater detail, as they represent very distinct hydrological regimes.

The first validation metric computed was the Kling-Gupta Efficiency (KGE) hydrological index (Equations 2.3.1 to 2.3.4) which was calculated for each validation point to evaluate the performance of the simulations against local observation ([84], [85]). The KGE values range from $-\infty$ to 1, with 1 corresponding to a

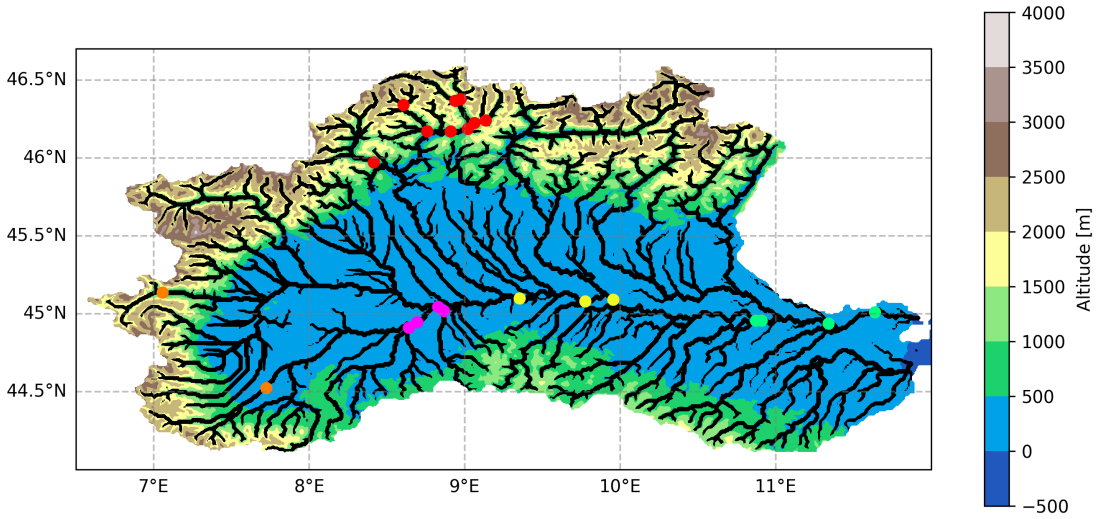

Figure 2.1: Altitude of the Po valley region with its river network in black. Dots represent the location of discharge stations used in the validation of the study. Clusters of stations were established according to their hydrological characteristics and are divided by colour: Po delta (green), central Po (yellow), upper Po (magenta), French alps (orange) and Swiss alps (red).

perfect representation of the observed discharge. Positive values are seen as good performance from the model, whereas negative values indicate poor performance. However, anything above -0.41 represents an improvement on the mean flow benchmark ([86]).

The KGE index combines three statistical components: the Pearson's coefficient (r) measures the correlation between simulated discharge (Q_{sim}) and observed discharge (Q_{obs}); β calculates the ratio between simulated and observed mean discharge ($\bar{Q}$) to assess the mean bias; and α computes the ratio between simulated and observed standard deviation (σ) to assess the variability. If β is lower (higher) than 1, there is an underestimation (overestimation) of the average simulated values, whereas a value of α lower (larger) than 1 implies an underestimation (overestimation) of the variability of the river discharge.

$$KGE = 1 - \sqrt{(r-1)^2 + (\beta-1)^2 + (\alpha-1)^2} \tag{2.3.1}$$

$$r = \frac{\sum_{i=1}^{n}(Q_{sim}(i) - \bar{Q}_{sim})(Q_{obs}(i) - \bar{Q}_{obs})}{\sqrt{\sum_{i=1}^{n}(Q_{sim}(i) - \bar{Q}_{sim})^2 \sum_{i=1}^{n}(Q_{obs}(i) - \bar{Q}_{obs})^2}} \tag{2.3.2}$$

$$\beta = \frac{\bar{Q}_{sim}}{\bar{Q}_{obs}} \tag{2.3.3}$$

$$\alpha = \frac{\sigma_{sim}}{\sigma_{obs}} \tag{2.3.4}$$

Flow-duration curves were constructed for each cluster of validation points using both simulated and observed river discharge. In these curves, a given discharge magnitude is plotted against the percentage of time at which this magnitude of discharge is equalled or exceeded, providing a comprehensive view of discharge variability and persistence across different flow regimes.

Peak flow curves were also constructed for both observed and simulated data to evaluate the model's ability to represent high discharge values and, by extension, flood events. For each validation point, the yearly peak values were extracted and fitted to a Gumbel distribution. Analytical estimates for the peak flow (Q_{RP}) were derived for a range of return periods (RP) between 2 and 100 years ([76], [75], [87]). The Gumbel distribution is a specific case of the Generalized Extreme Value (GEV) family, and has been shown to effectively represent extreme discharge events (e.g. [88]). Using a specific case of the GEV distribution avoids inconsistencies related to the limited sample sizes available, which can lead to different GEV types being fitted at different locations without a physical basis.

Additionally, low flow curves were constructed for both simulated and observed river discharge. The yearly minimum seven-day flow was used to estimate flows of different RPs ($Q_{7,RP}$), ranging from 2 to 30 years. Employing a seven-day moving average provides a more realistic representation of drought conditions, as sustained periods of low discharge are more hydrological relevant and impactful than single day minima.

In regions characterized by cold winter climates, special attention must be given to excluding frozen season data when computing the seven-day minimum of each year. The Po Valley includes, for example, the Italian Alps, where significant snow accumulation can occur during winter, producing distinct hydrological behaviour compared to warmer months. With temperature below freezing conditions, precipitation and surface water may be stored as snow or as ice, temporarily reducing streamflow. In these cases, low discharge values results from storing water in solid form and not from precipitation deficits. Analysing these low flow values together with those of warmer seasons would violate the assumption of independent and identically distributed (i.i.d.) events required by extreme value theory ([43]). Consequently, low-flow events that occurred under freezing conditions are excluded when constructing the low discharge curve. Therefore, all months with an average contributing basin temperature below 0°C during a given decade are defined as the frost season for that particular point. The corresponding discharge values were thus excluded from the minimum seven-day analysis ([43] [89]).

The yearly minimum seven-day average discharge was then computed and fitted to a Gumbel distribution to obtain low-flow estimates. While the GEV distribution may be directly used for this purpose ([43] [89]), the limited sample size available may lead to unphysical results. Preliminary tests confirmed this issue, and showed that the Gumbel distribution had satisfactory performance in representing the low discharge data.

Lastly, the hydrological year was analysed, defined for the region as starting on October 1st and ending in September 30th. Cumulated discharge values were calculated throughout the year in relation to this starting date. The amount of days that the cumulated discharge took to reach respectively 25, 50 and 75 % of total yearly flow were identified (d_{25}, d_{50} and d_{75}) and compared across ensembles. These indices provide insight into the timing and progression of annual river discharge and help evaluate the model's ability to capture its seasonality.

2.4 Methodology for analysing discharge projections

The CHyM model was forced with climate data from the CP projection sub-ensemble for the three distinct decades available (his, mid and end) and run using both possible configurations, TP and Roff (Tables 2.3, 2.4 and 2.5). The effects of a warming climate in the river discharge were investigated by comparing results from the two future periods against the historical one.

The projection results were used to compute ensemble statistics for both mean and extreme discharge values, including yearly and seasonal means. Analogously to the validation methodology, the minimum seven-day discharge with a 10-year return period ($Q_{7,10}$), henceforth also referred to as *drought index*, and the peak flow for a 100 return period (Q_{100}), henceforth synonymous with *flood index*, were calculated. To obtain the flood and drought indices, Gumbel distributions were fitted to the corresponding simulated extreme, from which values for the corresponding RTs were derived, as described in Section 2.3. Frozen season months were identified in each time slice analysed, ensuring only non-frozen conditions were considered in the drought index computation. The dates of the hydrological year when the cumulated discharge reached its main percentiles (d_{25}, d_{50} and d_{75}) were also computed to assess the seasonality of streamflow.

To assess the statistical significance of the projected changes relative to the historical period, the Student t test (see Equation 2.4.1, [90]) was used. Here, $\overline{\Delta Q}$ represents the average discharge change, $\sigma_{\Delta Q_i}$ is the standard deviation of the discharge changes (ΔQ_i) across models (i), N is the number of ensemble members, and t is the corresponding critical t-value (i.e. obtained from the Student's t-

distribution) with N-1 degrees of freedom and significance level (α) of 0.05. A change is considered significant in this and the following chapters whenever the inequality below is satisfied.

$$\frac{\overline{\Delta Q}}{\sigma_{\Delta Q_i}} > \frac{t}{\sqrt{N}} \tag{2.4.1}$$

2.4.1 Lower-resolution results

The CHyM model has been previously used to investigate the effects of climate change on the European river network ([75]). Those simulations have used the CHyM-Roff configuration at lower spatial and temporal resolutions (6km, daily) in comparison to the CP models, and were performed under the RCP8.5 scenario. The input runoff data for these experiments was obtained from the CMIP5 GCM and CORDEX RCM ensembles (Tables 2.7 and 2.8). With a coarser spatial resolution, the river network represented in these simulations does not be exactly match that obtained when CP-RCMs are used as forcing. Therefore, validation points are not identical between lower and higher resolution simulations. Despite this caveat, the validation for each cluster of points remains comparable, as they correspond to the same set of observational stations, and results are expected to be consistent across the different networks.

To assess the effects on the hydrological cycle of increased kilometre scale model resolution, the simulations from these lower-resolution ensembles were incorporated in the present analysis. Therefore, the same calculations described in Section 2.4 were done for the CORDEX and CMIP5 forced CHyM simulations. Although these two ensembles offer longer time series than the CP simulations, only the decades overlapping with the CP ensemble (Section 2.1.2) were selected and used for the analysis for consistency across comparisons

It should be noted that there is no direct equivalent to the CP validation ensembles in the lower-resolution simulations, as the CORDEX inputs used by CHyM are driven by GCMs and not Era-Interim reanalysis data. Nonetheless, the 2000 to 2009 period from the CORDEX and CMIP5 simulations was selected for comparison with CP TP and CP Roff validation ensembles. Excluding the KGE index, which requires reanalysis driven simulations, all other validation metrics (see Section 2.3) were computed for the lower resolution ensembles.

2.4.2 Model uncertainty

Model uncertainty was quantified using Equation 2.4.2, where ΔQ_i represents the change in discharge for each model relative to the historical period, and $\sigma_{\Delta Q_i}$

the standard deviation of these changes across ensemble members. This standard deviation is normalized by the average discharge of the historical period ($\overline{Q_{his}}$) to obtain the uncertainty u. Higher (lower) values of u indicate higher (lower) variability in the projected change amongst different ensemble members.

$$u = \frac{\sigma_{\Delta Q_i}}{\overline{Q_{his}}} \tag{2.4.2}$$

This metric reflects the degree of model uncertainty ([7]). To evaluate the uncertainty across different ensembles, u was calculated for both the mean discharge (Q_{mean}) and the flood index (Q_{100}), the latter representing an extreme discharge condition. As all the projections are under the same emission scenario, RCP8.5, the level of scenario uncertainty is considered comparable across ensembles.

This chapter has described the data, models and analyses used to assess the impacts of climate change on high-resolution hydrological simulations over Italy. The methodology combines high-resolution climate models with hydrological modelling to evaluate the effects of spatial and temporal resolution on hydrological projections. The results obtained from the methodology described in this chapter are presented in Chapter 3, which discusses the outputs of the different ensembles and analyses the behaviour of the various variables and indices obtained.

Table 2.7: Ensemble of models used for the CORDEX Roff ensemble (RCMs and driving GCMs)

RCM	Driving Model	Ensembles
CLMcom-CCLM4-8-17	CCCma-CanESM2	r1
CLMcom-CCLM4-8-17	CNRM-CERFACS-CNRM-CM5	r1
CLMcom-CCLM4-8-17	ICHEC-EC-EARTH	r12
CLMcom-CCLM4-8-17	MIROC-MIROC5	r1
CLMcom-CCLM4-8-17	MOHC-HadGEM2-ES	r1
CLMcom-CCLM4-8-17	MPI-M-MPI-ESM-LR	r1
CLMcom-ETH-COSMO-crCLIM-v1-1	MPI-M-MPI-ESM-LR	r1
CNRM-ALADIN63	CNRM-CERFACS-CNRM-CM5	r1
CNRM-ALADIN63	MOHC-HadGEM2-ES	r1
DMI-HIRHAM5	CNRM-CERFACS-CNRM-CM5	r1
DMI-HIRHAM5	ICHEC-EC-EARTH	r12
DMI-HIRHAM5	ICHEC-EC-EARTH	r1
DMI-HIRHAM5	ICHEC-EC-EARTH	r3
DMI-HIRHAM5	MOHC-HadGEM2-ES	r1
DMI-HIRHAM5	NCC-NorESM1-M	r1
GERICS-REMO2015	CCCma-CanESM2	r1
GERICS-REMO2015	CNRM-CERFACS-CNRM-CM5	r1
GERICS-REMO2015	ICHEC-EC-EARTH	r12
GERICS-REMO2015	MIROC-MIROC5	r1
GERICS-REMO2015	MOHC-HadGEM2-ES	r1
GERICS-REMO2015	MPI-M-MPI-ESM-LR	r3
GERICS-REMO2015	NCC-NorESM1-M	r1
ICTP-RegCM4-6	MOHC-HadGEM2-ES	r1
ICTP-RegCM4-6	MPI-M-MPI-ESM-LR	r1
IPSL-WRF381P	CNRM-CERFACS-CNRM-CM5	r1
IPSL-WRF381P	NCC-NorESM1-M	r1
KNMI-RACMO22E	CNRM-CERFACS-CNRM-CM5	r1
KNMI-RACMO22E	ICHEC-EC-EARTH	r12
KNMI-RACMO22E	ICHEC-EC-EARTH	r1
KNMI-RACMO22E	ICHEC-EC-EARTH	r3
KNMI-RACMO22E	MOHC-HadGEM2-ES	r1
KNMI-RACMO22E	MPI-M-MPI-ESM-LR	r1
KNMI-RACMO22E	NCC-NorESM1-M	r1
MPI-CSC-REMO2009	MPI-M-MPI-ESM-LR	r1
MPI-CSC-REMO2009	MPI-M-MPI-ESM-LR	r2
SMHI-RCA4	CNRM-CERFACS-CNRM-CM5	r1
SMHI-RCA4	ICHEC-EC-EARTH	r12
SMHI-RCA4	ICHEC-EC-EARTH	r1
SMHI-RCA4	IPSL-IPSL-CM5A-MR	r1
SMHI-RCA4	MOHC-HadGEM2-ES	r1
SMHI-RCA4	MPI-M-MPI-ESM-LR	r1
SMHI-RCA4	MPI-M-MPI-ESM-LR	r3
SMHI-RCA4	NCC-NorESM1-M	r1
UHOH-WRF361H	ICHEC-EC-EARTH	r12

Table 2.8: Ensemble of models used for the CMIP5 Roff ensemble

GCM	**Realizations**
CNRM-CM5	r1
CanESM2	r1,r2,r3,r4,r5
MIROC-ESM	r1
MIROC5	r1
MPI-ESM-LR	r1,r2,r3
MPI-ESM-MR	r1
NorESM1-M	r1

Chapter 3

Impacts of High-Resolution Convection-Permitting Simulations on Hydrological Projections Under Climate Change

This chapter details the results of the high-resolution hydrological simulations described in Chapter 2. The analyses focus on evaluating the capacity of the CHyM hydrological model to model the river discharge in Italy and how the use of convection-permitting (CP) resolution as input, influences it. Projection ensembles under the RCP8.5 scenarios are used to assess the long-term evolution of average and extreme discharge behaviour under climate change. The main ensembles examined here are the CP TP and the CP Roff, which correspond to CP driven CHyM simulations using respectively the temperature and precipitation or the runoff configuration. Moreover, the lower resolution ensembles CORDEX Roff and CMIP5 Roff are both included for comparison.

Section 3.1 of this chapter presents the validation of CHyM simulations, through comparison of the different ensembles against observations. Subsequently, future projections are analysed in Section 3.2, and changes in average discharge, in the flood index (Q_{100}) and in the drought index ($Q_{7,10}$) are examined. Section 3.2.1 examines the change in seasonality through hydrological year indices and Section 3.2.2 refers to the model uncertainty obtained for the different ensembles. Finally, Section 3.3 discusses the main findings of this chapter and their relevance for future hydrological and climate modelling efforts.

Together, these analyses provide a comprehensive evaluation of how high-resolution CP simulations improve the representation of river discharge and influence hydrological projections for Italy under climate change.

3.1 Validation Period

The ensemble mean of the Kling–Gupta Efficiency (KGE) index for the CP TP and CP Roff simulation is shown in Figure 3.1, covering all validation points. Overall, both ensembles had satisfactory performances, with most points exhibiting positive KGE values. The CP TP simulations displayed a slightly better agreement with observations over the small catchments in mountainous areas (Swiss Alps), with one additional station with a positive result than for compared to the CP Roff ensemble. Across the main branch of the Po River (upper, central and delta regions), both configurations perform well, with nearly all stations presenting KGE values above 0.25, and some CP Roff points exceeding 0.50.

Figure 3.2 shows the individual components used in the KGE calculation: α, β and r. The values of α indicate an overestimation of discharge variability, particularly in higher altitudes. In contrast, results for β suggest an underestimation of average discharge, especially along the main branch of the Po. The correlation coefficient r generally lies between 0.25 and 0.75 for both ensembles. Only model simulations driven by reanalysis data are suitable for computing this index, and consequently the CORDEX Roff and CMIP5 Roff ensembles are not included in this analysis.

All ensembles can be used to construct the flow duration, peak discharge and low discharge curves. Figure 3.3 presents the flow duration curves of both simulated and observed river discharge in two sub-regions of the Po River basin: the Po delta and the Swiss Alps (shown in green and red in Figure 2.1). In the figure, each station is represented by a different colour, with observations plotted as solid lines. For the Swiss Alps, the range of outputs for each station is shaded using the corresponding colour, whereas in the Po Delta plots each subplot includes only two stations, one represented with a shaded area and one with a hatched area.

In the Po Delta plots (first column), all ensembles generally cover the observed flow duration curves within the range of simulation outputs. High and low frequencies flows (<10% and >95% exceedance) are more difficult to reproduce and and tend to be respectively underestimated and overestimated by all ensembles. The CP TP and CP Roff ensembles display the narrowest spread, with a slight tendency to underestimate average discharge. In contrast, the CORDEX Roff and CMIP5 Roff ensembles exhibit broader spreads. CMIP5 Roff mostly underestimates discharge, whereas CORDEX tends to overestimate it.

The second column corresponds to the Swiss Alps region, where the complex topography poses a bigger modelling challenge. Here, the benefits of kilometre scale resolution become more apparent. The CP ensembles closely reproduce the observed spread, whereas CORDEX and CMIP5 have spreads two to three times larger than observations. For instance, the CORDEX Roff simulations in the 50% exceedance range from between 10^{-2} to $10^{3} m^{3} s^{-1}$, while both observations and CP

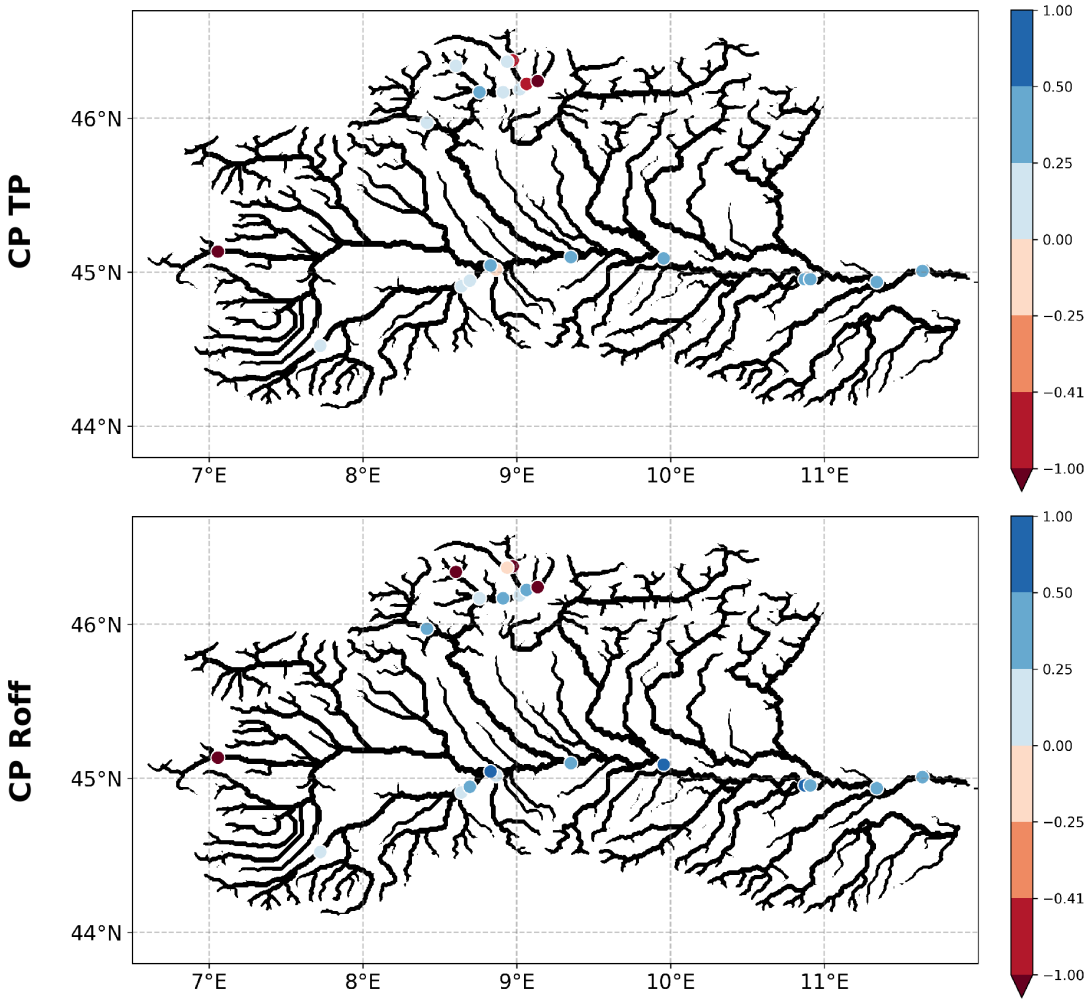

Figure 3.1: KGE index obtained for the validation points with the CP TP (top) and the CP Roff (bottom) ensembles. The river network of the CHyM model is represented in black.

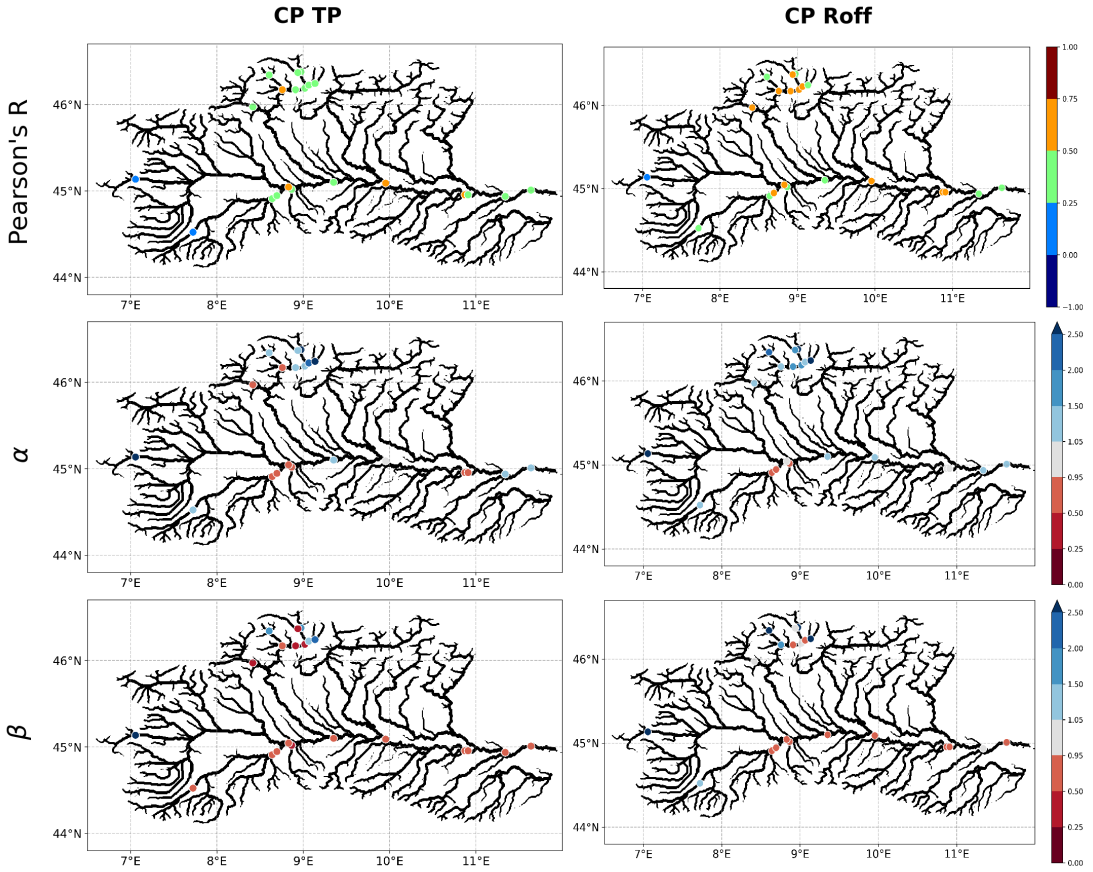

Figure 3.2: Pearson's coefficient r, α, and β values used in the KGE index calculation for the validation points with the CP TP (left) and the CP Roff (right) ensembles.

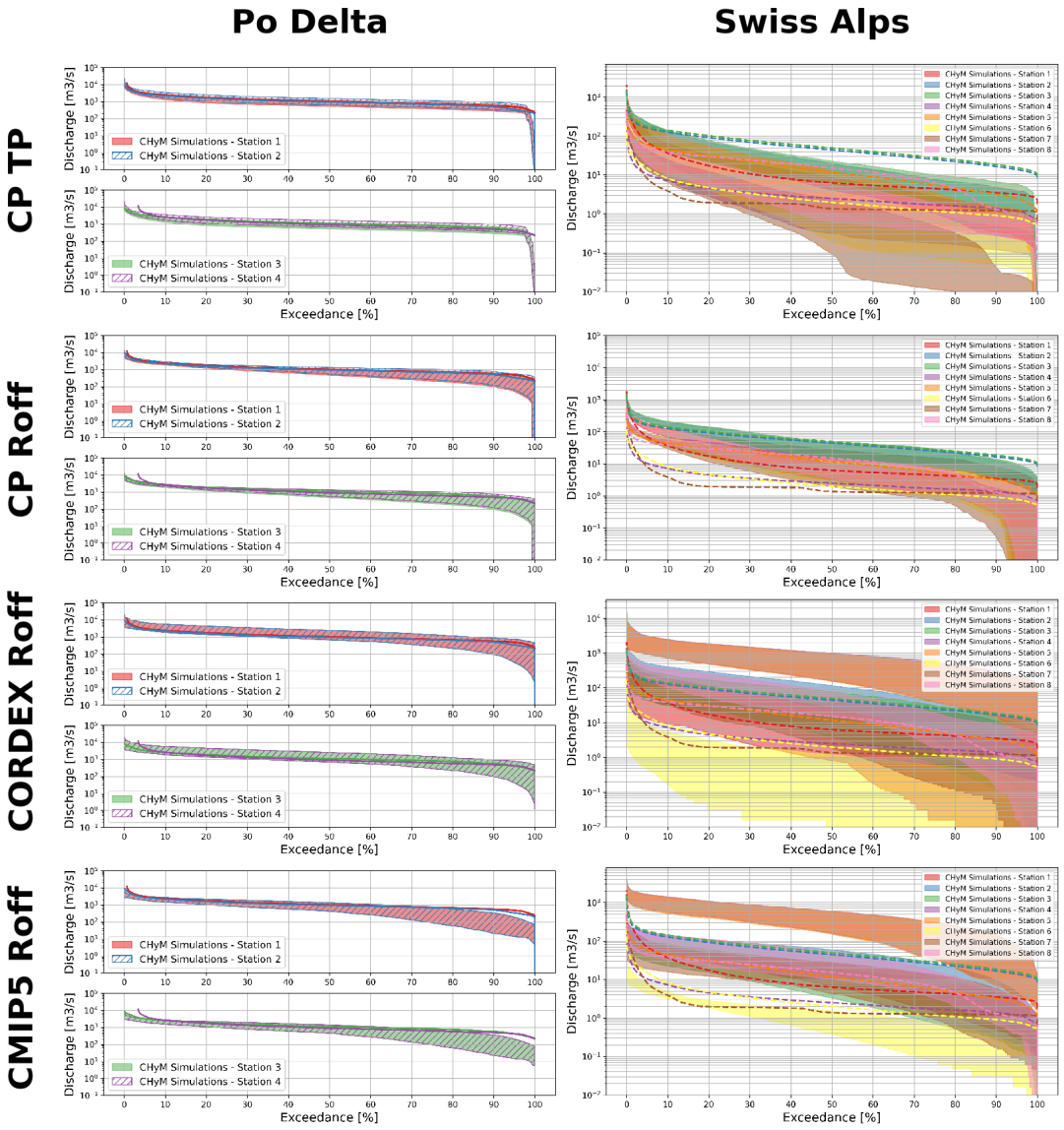

Figure 3.3: Flow duration curves for validation points located in the Po Delta (left) and Swiss Alps (right) region for the CP TP, CP Roff, CORDEX Roff and CMIP5 Roff ensembles. Each station is represented by a specific colour, with solid lines representing the observed values and shaded/hatched areas the range of the simulations.

ensembles remain between 1 and $10^2 m^3 s^{-1}$. CMIP5 Roff displays a slightly smaller spread than CORDEX Roff, but still considerably larger than the observed range. Across all four ensembles, low flows are underestimated: though observed values do not fall under $1 m^3 s^{-1}$, all ensembles produce values around $10^{-2} m^3 s^{-1}$ at certain points. CORDEX Roff shows the most pronounced low-flow underestimation. For the high discharge, the lower resolution ensembles (CORDEX and CMIP5) overestimate discharge magnitudes, whereas both CP TP and CP Roff reproduce them more accurately, with CP TP performing particularly well in this range of values.

To further analyse high flow behaviour, peak discharge curves were constructed (Figure 3.4) for both observations and simulations, following the same coloring scheme of the flow duration curves. Peak yearly flows for the two Po river sub-regions were fitted to a Gumbel distribution at each validation point, covering return periods from 2 to 100 years.

In the Po delta region, the CP and CORDEX ensembles overestimate high flows, specially in the CP TP configuration, which does not contain the observed values within its ensemble spread. CP Roff displays a more moderate overestimation, with observed values aligning closely with the lower part of the spread. The CORDEX Roff displays a smaller bias, with observed data lying close to its average value. In contrast, CMIP5 Roff underestimates the discharge by approximately $2 * 10^3 m^3 s^{-1}$. In the Swiss Alps region, both simulated and observed spreads are larger overall. While the CP ensembles' spreads remain comparable, CORDEX Roff and CMIP5 Roff exhibit greater variability, with simulated discharge values up to two orders magnitude lower than observed.

The analysis of the low flow discharges is displayed in Figure 3.5, with the colour scheme for stations and simulations consistent with that used in the previous figures. The yearly minimum of the seven-day average discharge was fitted to a Gumbel distribution for return times ranging from 2 to 30 years across the different clusters of validation points.

In the Po Delta region, the spreads of the CP TP, CP Roff and CORDEX Roff ensembles contain the observed values, although observations tended to be closer to the upper limit of the ensemble, indicating a tendency towards underestimation. In contrast, the CMIP5 Roff ensemble substantially underestimates low discharges and fails to capture observed values within its spread. These findings are consistent the results of the flow duration analysis (Figure 3.3). For the Swiss Alps validation points, the closest agreement with observations is found for CMIP5 Roff, which displays a comparable range of low discharge value. CORDEX Roff, however, exhibits the strongest overestimation of the low-flow behaviour, showing values well above observations.

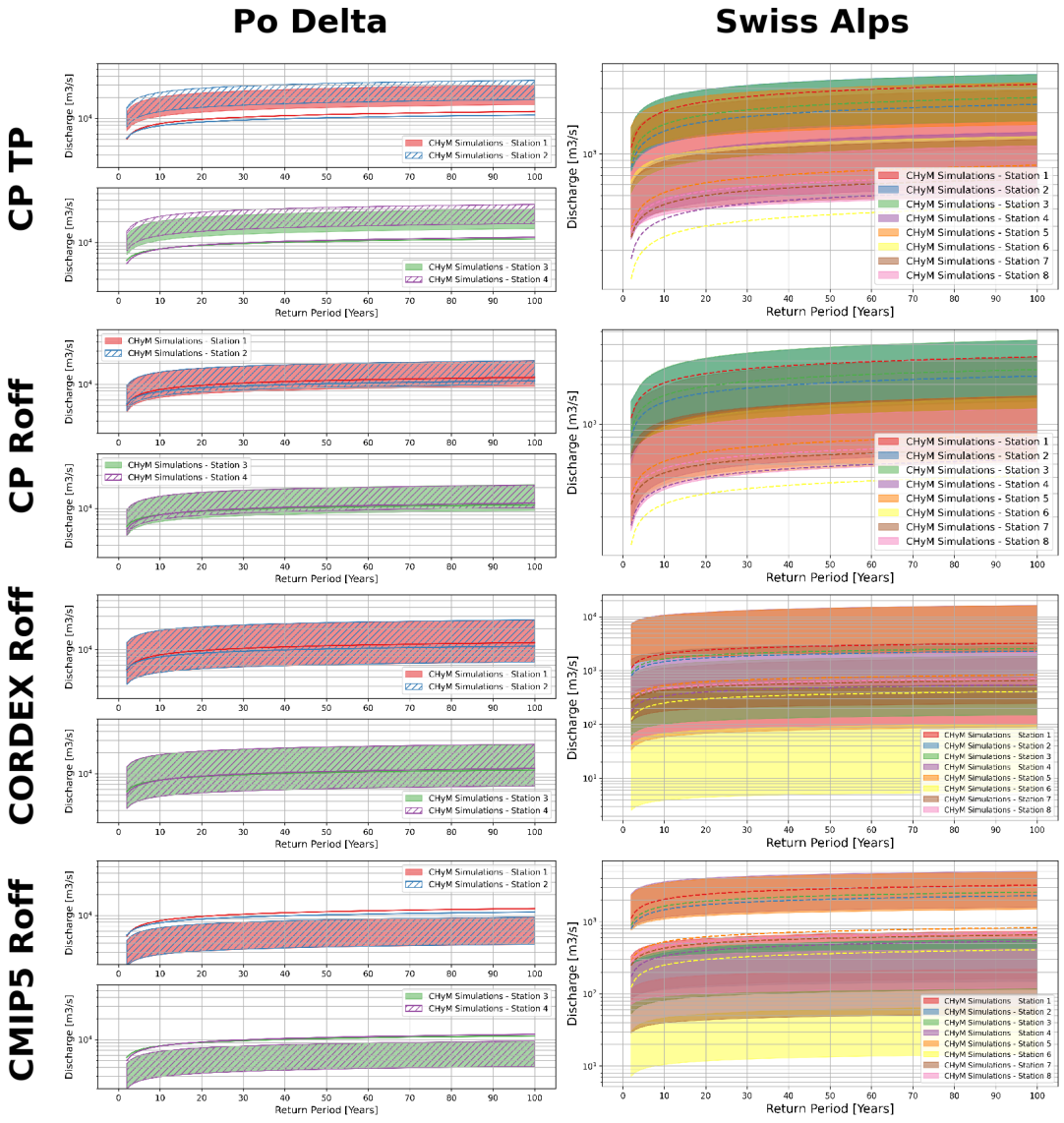

Figure 3.4: Peak discharge curves for validation points located on the Po Delta (left) and Swiss Alps (right) region for the CP TP, CP Roff, CORDEX Roff and CMIP5 Roff ensembles. Each station is represented by a specific colour, with solid lines representing the observed values and shaded/hatched areas the range of the simulations.

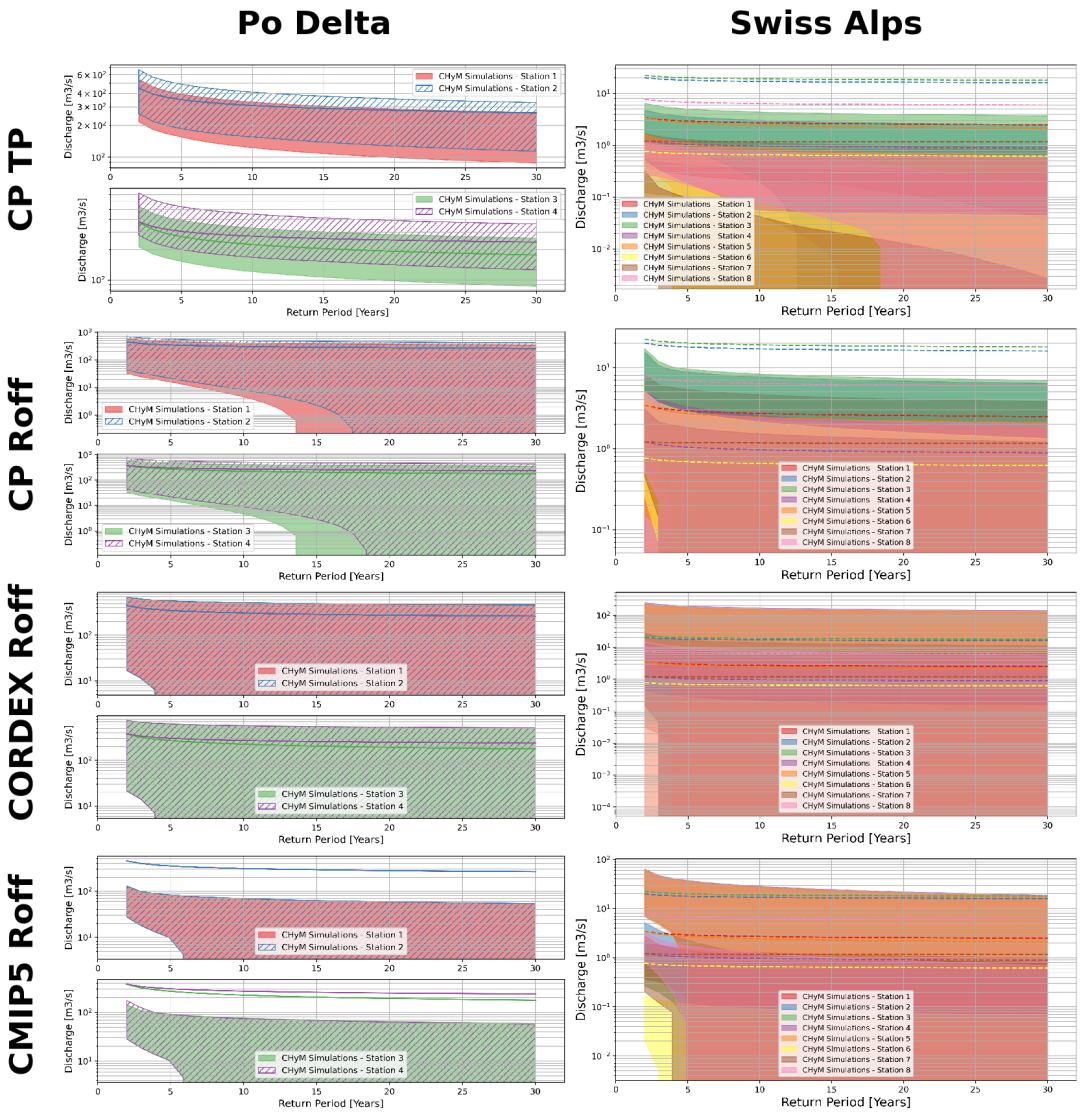

Figure 3.5: Low-discharge curves for validation points located on the Po Delta (left) and Swiss Alps (right) region for the CP TP, CP Roff, CORDEX Roff and CMIP5 Roff ensembles. Each station is represented by a specific colour, with solid lines representing the observed values and shaded/hatched areas the range of the simulations.

3.2 Climate Change Projection Results

Historical values for the Q_{mean}, Q_{100} and $Q_{7,10}$ are presented in Figure 3.6 and show consistent spatial pattern across all ensembles. Higher values of all three variables are found along the Po river and main contributing branches. The coarsening effect associated with lower spatial resolution is clearly visible in these maps: only the CP ensembles successfully reproduce the smaller tributaries and finer features in the river network.

Projected changes for the mid-century and end-of-century periods are shown in Figures 3.7 and 3.8, expressed as percentage of change relative to the historical period. In these figures, CP TP, CP Roff, CORDEX Roff and CMIP5 Roff are displayed in separate rows, while the first, second and third column correspond to Q_{mean}, Q_{100} and $Q_{7,10}$ respectively. The statistical significance of the projected changes, assessed using a Student t-test at the 0.05 significance level, is indicated for each panel in the box in the upper right corner. Throughout this chapter, any significant changes discussed was identified with this test. Areas in black or gray shading display statistically significant changes, whereas zones with no shading indicate non significant changes.

A larger higher fraction of results are significant in the end-of-century period compared to the mid-century period. In regions where significant change is observed, the primary difference between the two periods is an intensification of the signal by the end of the century. Variations in the signal of change between the two periods are concentrated in areas where change is not statistically significant. As such, this chapter focuses on the end-of-century change, where results are more significant and the magnitude of change is greater, while trends remain consistent with those observed at mid-century.

Figure 3.8 highlights the distinct responses of the ensembles to climate change. The CP TP ensemble shows a clearly topographically driven signal, with a significant increase in Q_{mean} in the northern half of the Po basin, as well as in Tuscany and parts of centre-eastern Italy. No comparable increase in average discharge is observed in other ensembles. CP TP simulations also display a decrease in average discharge of up 30% in Sardinia and of approximately 20% in the southernmost regions depicted. Furthermore, this ensemble exhibits increases in Q_{100} ranging from 20 to 60%, more intense than other ensembles, and decreases in $Q_{7,10}$ from 10 to 40% across the country. The remaining three ensembles show a consistent reduction in Q_{mean}, which is accentuated in lower resolution and reaches up to -40% decrease in the CMIP5 Roff models.

Changes in Q_{100} are positive for both CP Roff and CORDEX Roff, although they are generally less intense than those in CP TP ensemble. Higher flows are projected during flood events, with increases ranging from 5 to 60%. Not all increases are statistically significant, as with a large portion of southern Italy

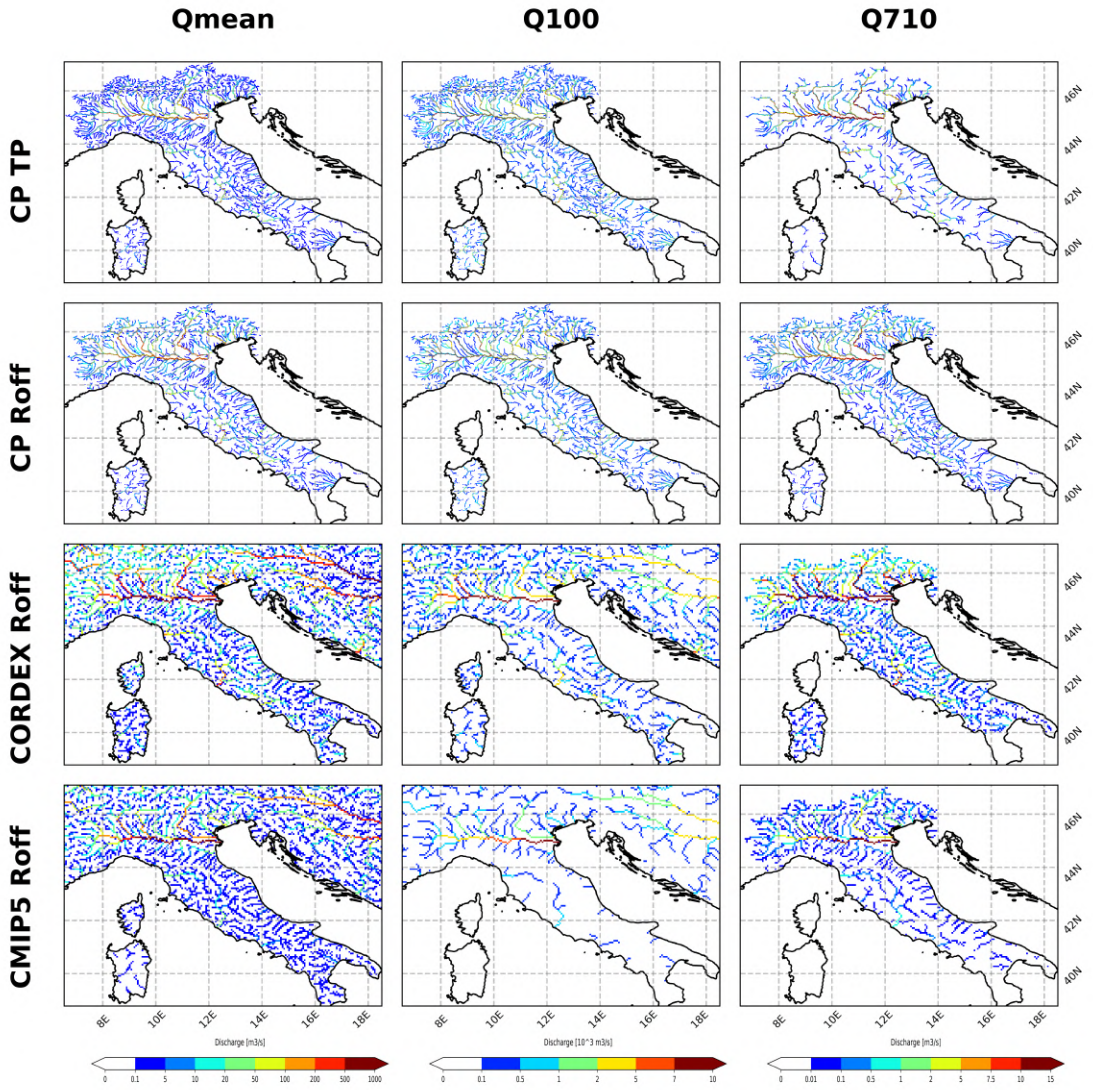

Figure 3.6: Q_{mean} $[m^3/s]$, Q_{100} $[1000m^3/s]$, and Q_{710} $[m^3/s]$ for the CP TP, CP Roff, CORDEX Roff, and CMIP5 Roff ensembles for the historical period.

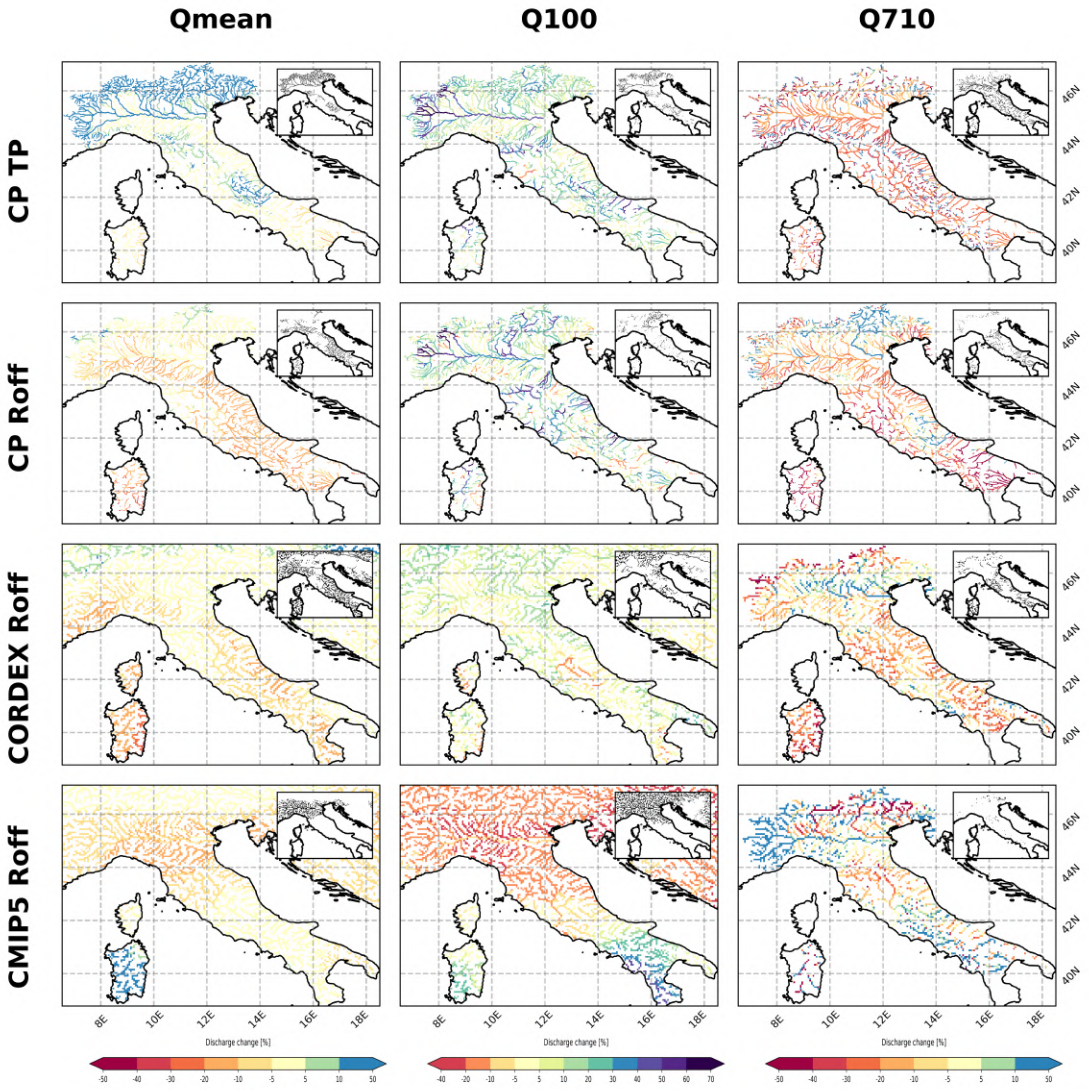

Figure 3.7: Q_{mean}, Q_{100} and Q_{710} change [%] for the CP TP, CP Roff, CORDEX Roff, and CMIP5 Roff ensembles for the mid-century period. Significance of change is indicated in upper right corner: only zones in gray have significant changes according to a t-test with a 0.05 significance level.

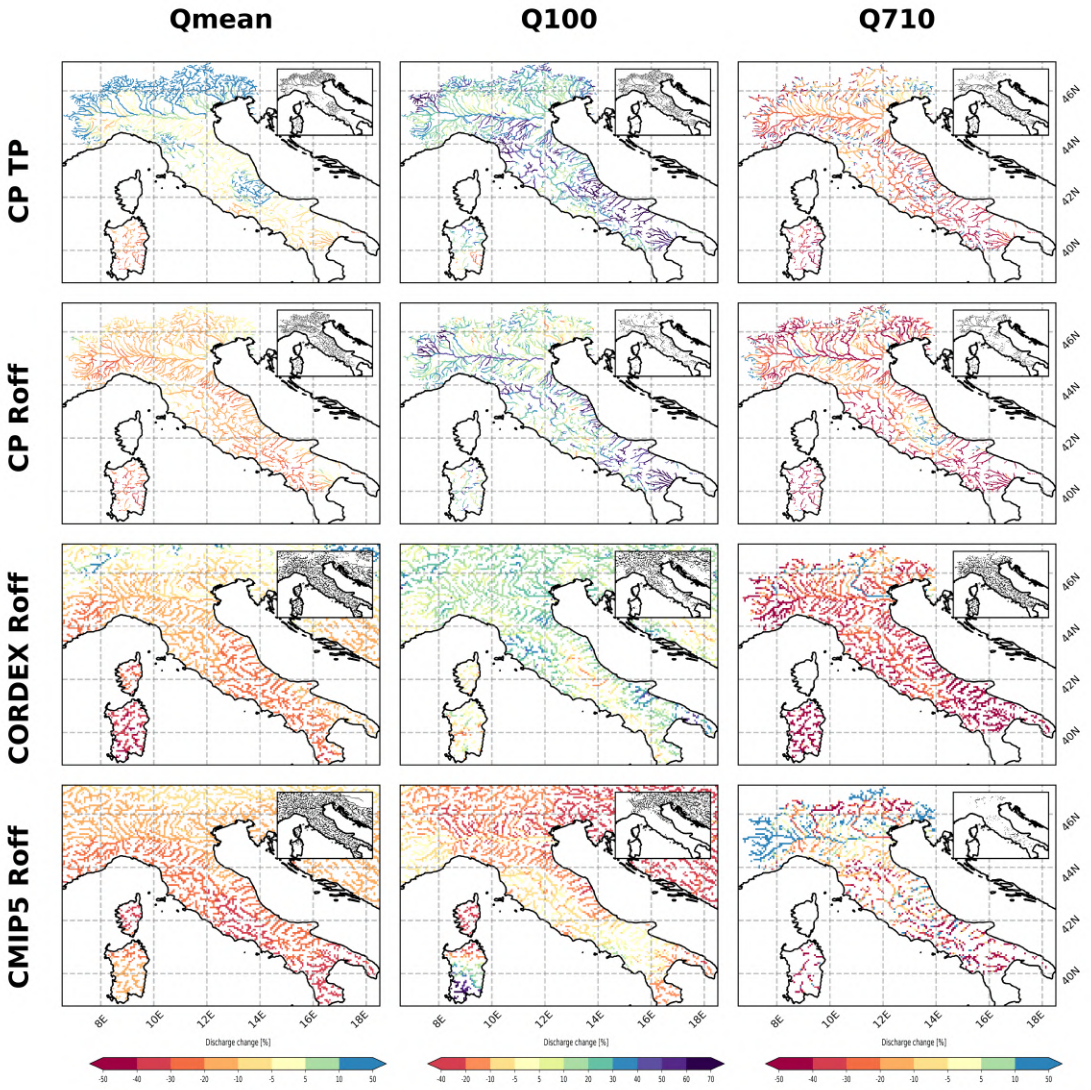

Figure 3.8: Q_{mean}, Q_{100} and $Q_{7,10}$ yearly change [%] for the CP TP, CP Roff, CORDEX Roff, and CMIP5 Roff ensembles for the end-of-century period. Significance of change is indicated in upper right corner: only zones in black have significant changes according to a t-test with a 0.05 significance level.

in CORDEX Roff displaying non-significant changes. In contrast, the CMIP5 Roff ensemble shows decreases in Q_{100} of over 40% in several regions, with the only increases appearing in Sardinia, none of which significant. An intensification pattern is observed with the CP ensembles analysed, relative to the lower resolution CORDEX and CMIP5 simulations.

The low flow analysis, done by means of the $Q_{7,10}$, shows a significant decreases for the CP and CORDEX ensembles in a large portion of the Italian river network. The CMIP5 Roff ensemble displays a more spatially heterogeneous signal, with very few areas exhibiting statistically significant changes.

Yearly average and extreme precipitation change were computed to help to interpret the hydrological behaviour of the four ensembles (Figure 3.9). Because of the distinct temporal resolution, extreme precipitation was calculated differently across ensembles: for the CP models, the 99.9^{th} percentile of hourly precipitation was used, whereas for CMIP5 and CORDEX, the 99^{th} percentile of daily precipitation was considered. Additionally, the average and extreme seasonal precipitation, together with seasonal mean discharge, were analysed and are presented in Figures 3.10 to 3.13. The differences in the precipitation signal between CP TP and CP Roff are due to the variation in ensemble size and members availability, as detailed in Tables 2.3 to 2.5.

In Figure 3.9, the ensembles show broadly consistent behaviour in average precipitation change for the end-of-century period. Most of Italy is expected to see a decrease of up to 25%, whereas an increase of 1% to 25% is visible north of the Alps . The extreme precipitation change of ensembles CP TP, CP Roff and CORDEX Roff indicate a widespread and significant intensification, reaching up to a 40% in many regions. This finding is consistent with those presented in [6] for CP models. The CMIP5 Roff ensemble, in contrast, displays a general decrease in extreme precipitation, with large areas showing no statistically significant changes.

For the winter season (DJF, Figure 3.10), the CP TP models indicate widespread increases of discharge, except over Sardinia and southern Italy. In the CP Roff and CORDEX Roff ensembles, the increases are concentrated in the northern half of the Po river basin, whereas the CMIP5 ensemble exhibits significant decreases south of the Po and little change elsewhere. Results for spring (MAM, Figure 3.11) display a similar pattern to DJF, although the area with positive discharge changes in northern Italy becomes smaller and decreases are more widespread. This same shift is observed in average precipitation change, where the drying area extends further north. Increases in extreme precipitation are less intense in compared to the winter months.

During summer (JJA, Figure 3.12), CP Roff, CORDEX Roff and CMIP5 Roff all show significant decreases in discharge across Italy, exceeding 40% in some areas, whereas CP TP exhibits milder drying. Moreover, the CP TP simulations

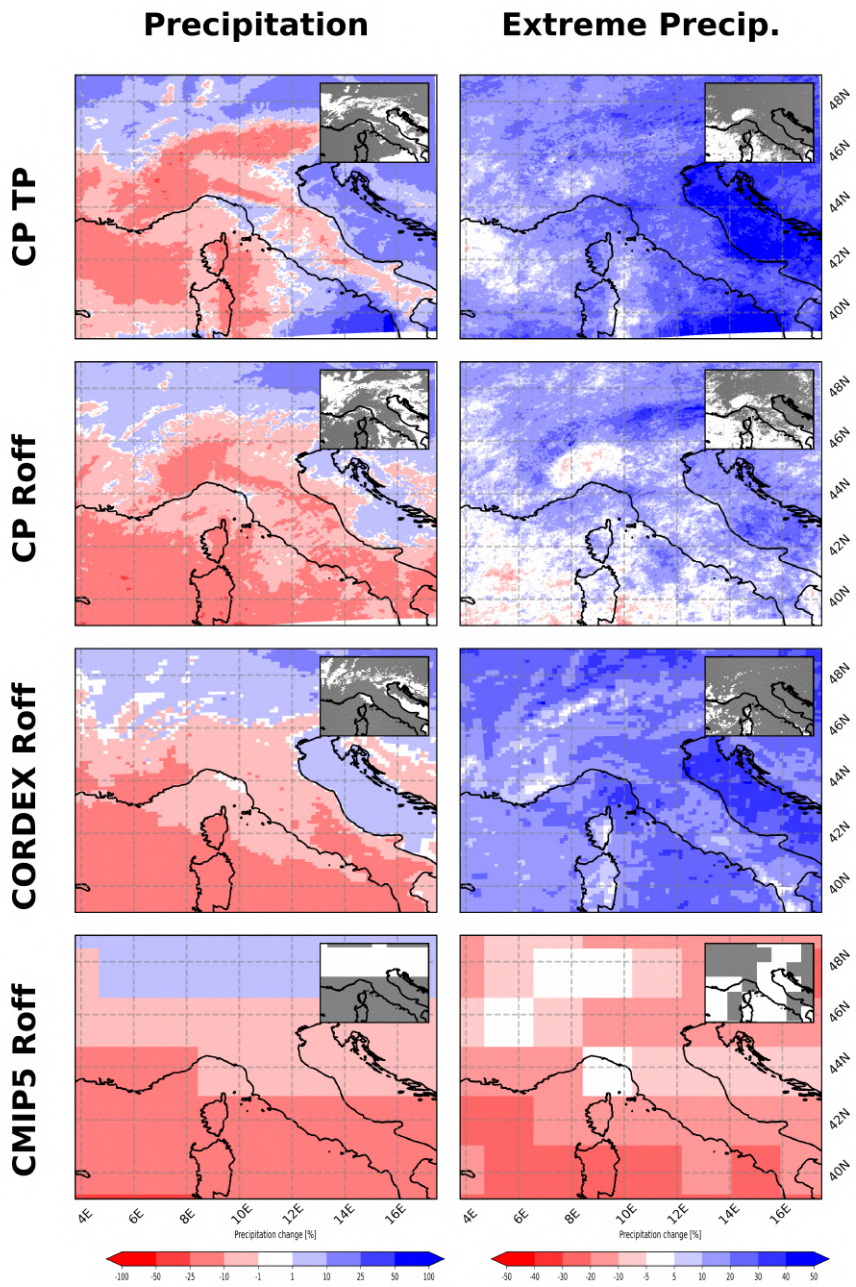

Figure 3.9: Average precipitation and extreme precipitation change [%] for the CP TP, CP Roff, CORDEX Roff and CMIP5 Roff ensembles for the end-of-century period. Significance of change is indicated in upper right corner: only zones in gray have significant changes according to a t-test with a 0.05 significance level.

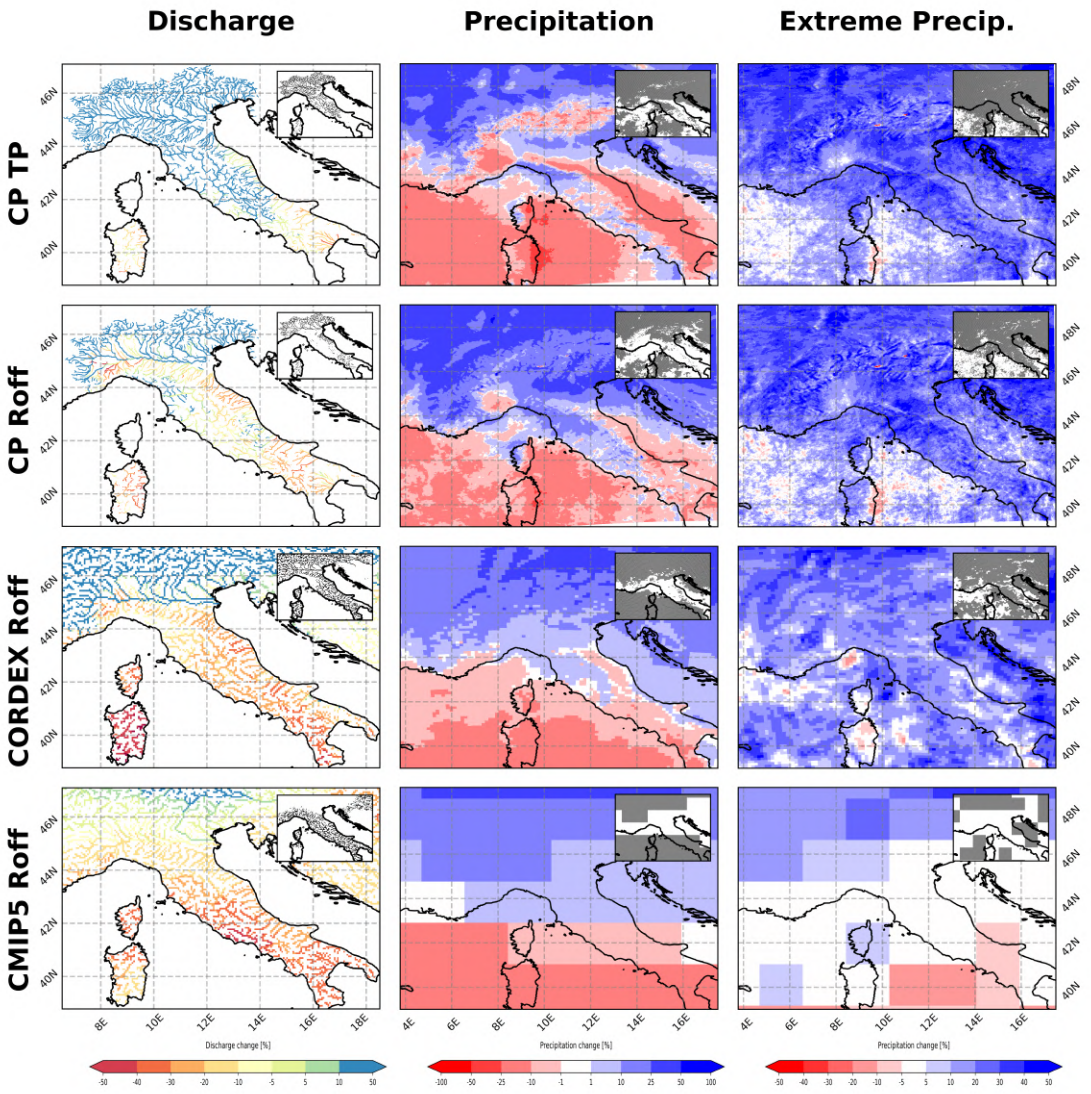

Figure 3.10: Average discharge, average precipitation and extreme precipitation change [%] for DJF in the CP TP, CP Roff, CORDEX Roff, and CMIP5 Roff ensembles for the end-of-century period. Significance of change is indicated in upper right corner: only zones in black/gray have significant changes according to a t-test with a 0.05 significance level.

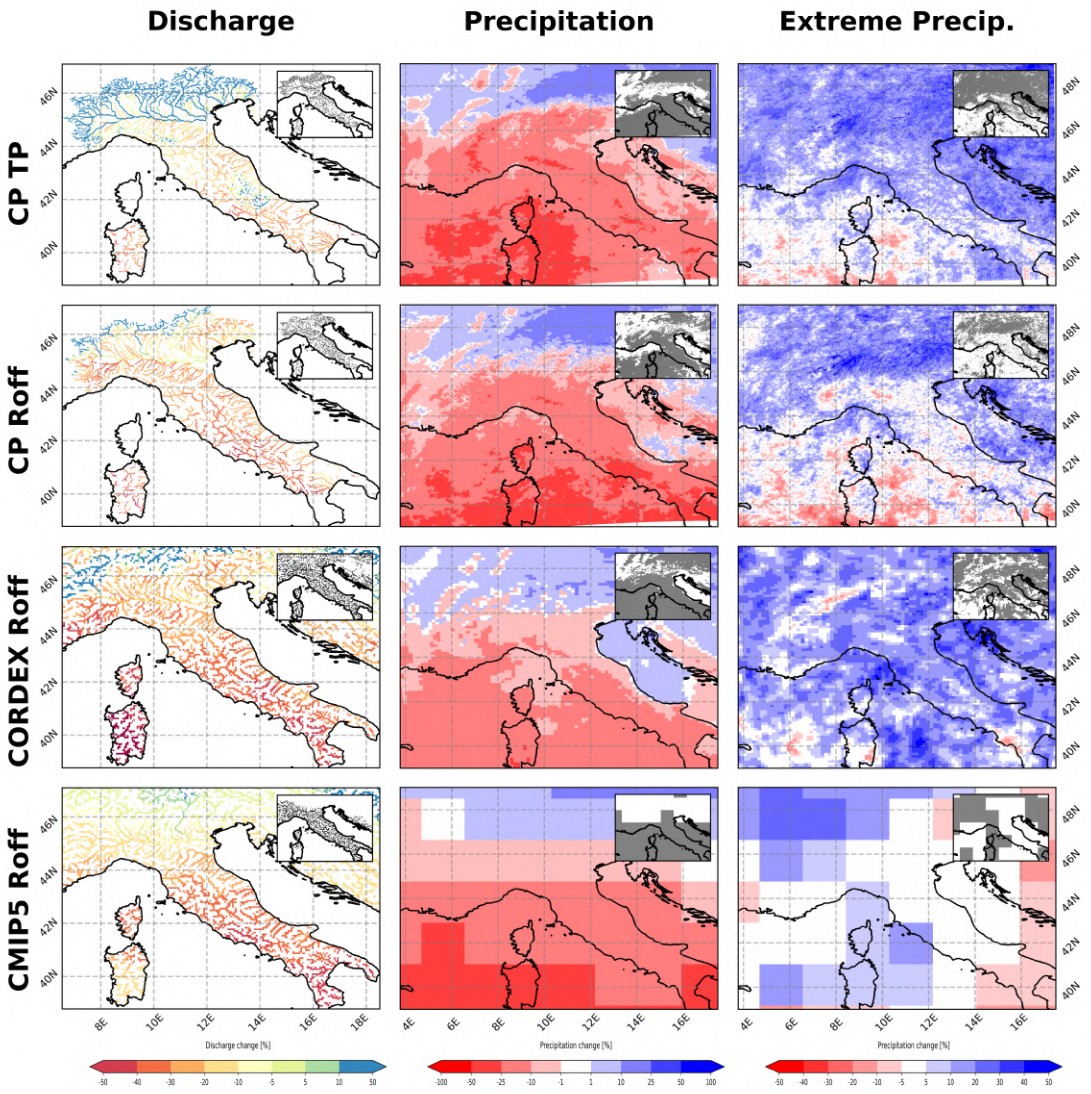

Figure 3.11: Average discharge, average precipitation and extreme precipitation change [%] for MAM for the CP TP, CP Roff, CORDEX Roff and CMIP5 Roff ensembles for the end-of-century period. Significance of change is indicated in upper right corner: only zones in black/gray have significant changes according to a t-test with a 0.05 significance level.

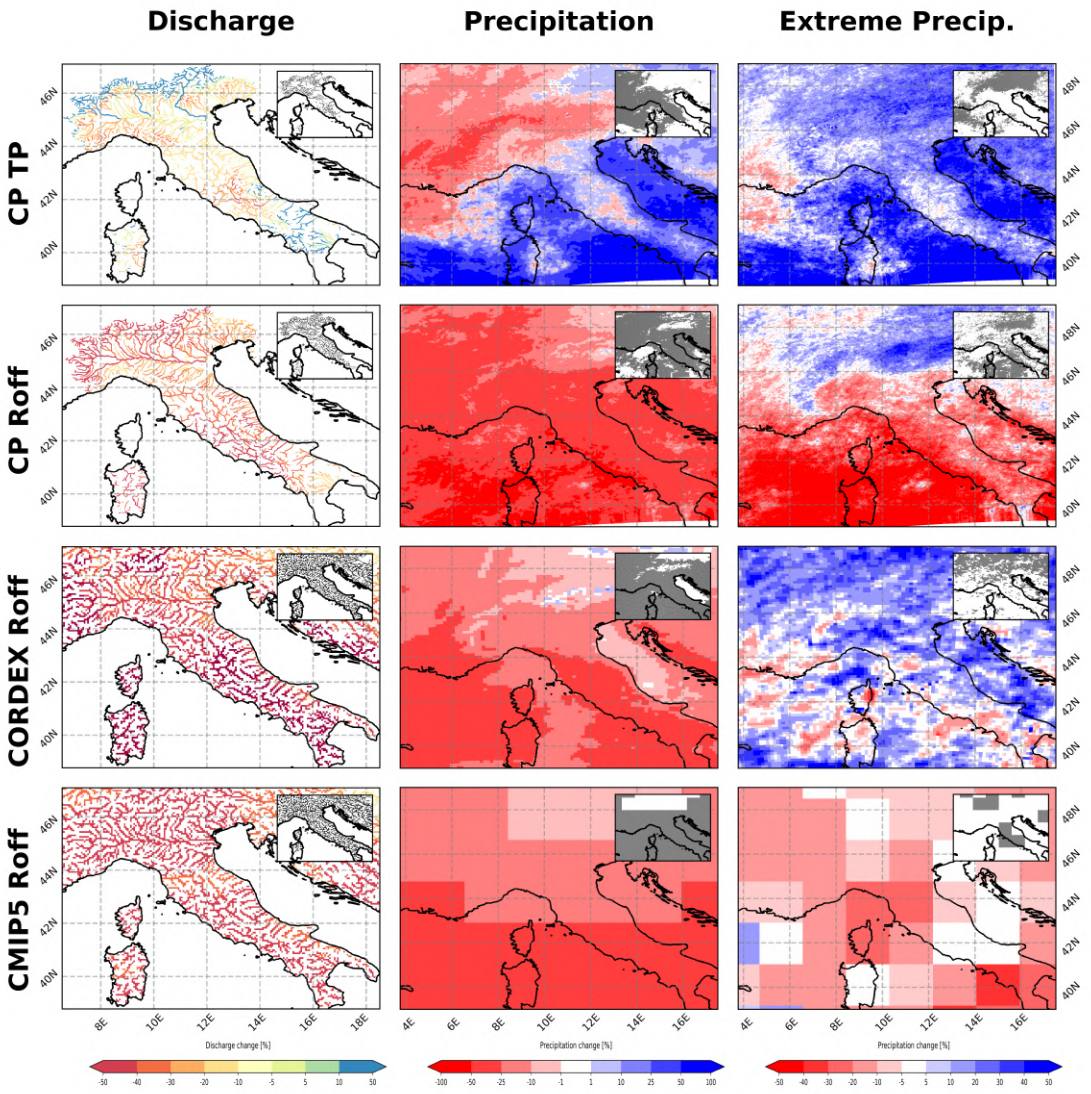

Figure 3.12: Average discharge, average precipitation, and the extreme precipitation change [%] for JJA for the CP TP, CP Roff, CORDEX Roff and CMIP5 Roff ensembles for the end-of-century period. Significance of change is indicated in upper right corner: only zones in black/gray have significant changes according to a t-test with a 0.05 significance level.

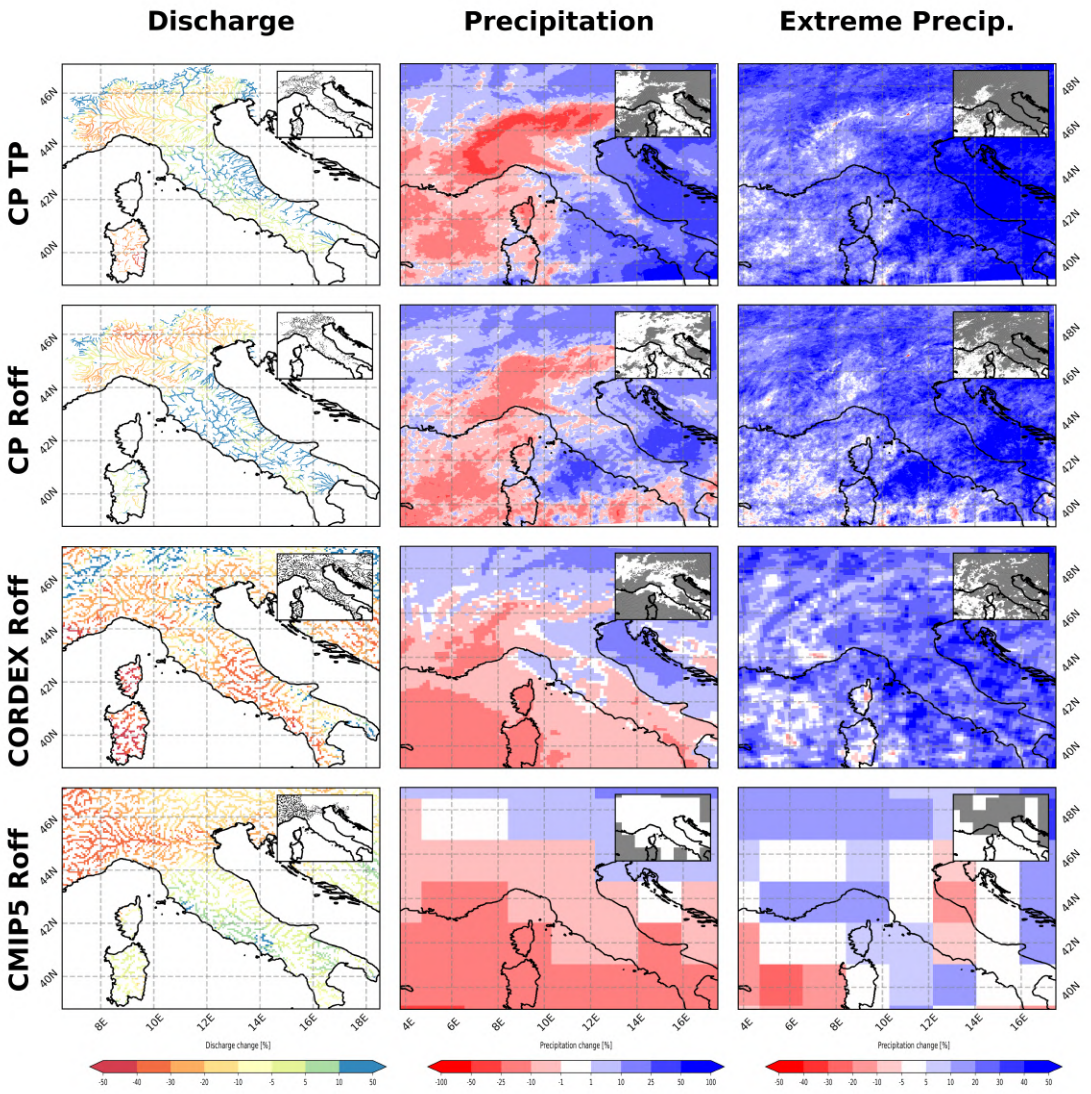

Figure 3.13: Average discharge, average precipitation and extreme precipitation change [%] for SON for the CP TP, CP Roff, CORDEX Roff and CMIP5 Roff ensembles for the end-of-century period. Significance of change is indicated in upper right corner: only zones in black/gray have significant changes according to a t-test with a 0.05 significance level.

display increases in discharge over the Alpine and southern Italy, not mirrored by other ensembles. The contrasting discharge patterns are consistent with differences in precipitation behaviour. While average precipitation decreases in CP Roff, CORDEX Roff and CMIP5 Roff, the CP TP models display increases south of the Po Valley. Additionally, extreme precipitation displays widespread intensification in the CP TP ensemble, whereas the CP Roff models show increases over the Alpine mountains and decreases elsewhere. The CORDEX simulations indicate increases in extreme precipitation and the CMIP5 ensemble decreases, though both ensembles display little significance over Italy. In autumn (SON, Figure 3.13), extreme precipitation increases across the domain, and, in the CP ensembles, average precipitation decreases over the Po Valley and increases over central and southern Italy. The spatial pattern of average precipitation change is similar to that of discharge.

The opposing changes of Q_{100} and $Q_{7,10}$ shown in Figure 3.8 are closely related to respectively the extreme and the average precipitation change illustrated in Figure 3.9. Mean discharge is primary influenced by changes in mean precipitation, but is modulated by extreme precipitation change. For example, in the CP TP ensemble, Figure 3.8 shows an increase in discharge over the Alps, Tuscany and Abruzzo, which is not reproduced by the other three ensembles. These increases are linked to the change in average precipitation in the months of DJF and SON, combined with a more intense increase of extreme precipitation during MAM and JJA over these regions. The remaining ensembles have a weaker increase in extreme precipitation, and the CMIP5 ensemble even shows decreases over large regions.

Positive changes in Q_{100} appear to be primarily driven by the increase in extreme precipitation across the different ensembles. When comparing CP TP and CP Roff, the former has more pronounced increases in extreme precipitation throughout the seasons, consistent with a stronger rise in extreme discharge shown in Figure 3.8. In contrast, the decrease in Q_{100} observed in the CMIP5 ensemble is consistent with the negative or zero change in extreme precipitation simulated by its models, though large regions of both variables are not statistically significant.

Drought discharge, represented by $Q_{7,10}$, decreases in the CP TP, CP Roff and CORDEX Roff ensembles, with no significant signal in CMIP5 Roff. The strongest reduction occurs in the CORDEX Roff simulations, driven by the decrease observed in both discharge and precipitation during JJA, which is more pronounced in this particular ensemble. The seasonal precipitation of JJA and MAM modulates the low-flow, with a stronger drying in CORDEX and CP Roff than in CP TP.

3.2.1 Hydrological Year

The historical values of the main variables characterizing the hydrological year are presented in Figure 3.14, with the hydrological year defined as beginning on

Table 3.1: Ensemble of models with available snow data (CPRCMs, driving intermediate RCMs and driving GCMs)

Institude	CPRCM	RCM	GCM	Timestep
Justus-Liebig-University Giessen	CCLM	-	MPI	6hr
KNMI The Royal Netherlands Meteorological Institute	HCLIM38-AROME	RACMO	EC-Earth	Daily
ICTP Abdus Salam Internatinal Centre for Theoretical Physicss	RegCM4	RegCM4	HadGEM	1hr
ETHZ Federal Institute of Technology	CCLM	CCLM	MPI	Daily

October 1^{st} and ending on September 30th. The figure displays the days on which cumulative discharge reaches 25%, 50% and 75% of the yearly total. Analysing the timing of these thresholds provides insights on how the seasonal distribution of streamflow, as well as the potential for floods and droughts, may change under climate change for each river segment ([91]). For example, if the number of days between d_{25} and d_{50} increases, the river segment will take a longer time to let the same volume of water through, indicating a decreased river flow. Therefore, there will be a higher likelihood of drought during this period. In contrast, a shorter interval suggests an increased discharge and higher potential for floods.

Relevant here is the snow cover and its evolution across future periods (Figure 3.15). Although snow data is only available for a portion of the CP models (3.1), results are consistent and indicate a significant decrease of snow cover. By the mid-century period, decreases between 1 to 75% are observed, and by the end-of-century, significant decreases occur across all regions with substantial snow presence. Over the highest parts of the Alps, decreases range between 25 and 50% and reach up to 100% in lower altitudes, with the presence of snow virtually disappearing. These changes in snow behaviour will affect the hydrological cycle of the region. Precipitation that previously fell as snow is expected to increasingly fall as liquid, altering surface runoff. Furthermore, the seasonal timing and quantity of snowmelt, which currently feeds into the river network, are expected to shift, leading to early spring snowmelt and reduced late spring streamflow.

The coloured dots in Figure 3.14 depict the station data, which can be directly compared to the historical simulations shown on the map. Overall, there is a good agreement for d_{50} and d_{75} between simulations and observations across all ensembles except for CMIP5 Roff, which underestimates values in the Alpine region. For d_{25}, the simulations align well with observations along the main branch of the Po, located in lower elevations, whereas values for high altitudes stations tends towards overestimated.

A clear dependency of CP TP and CP Roff simulations on terrain elevation is visible. CORDEX Roff also captures this orographic modulation, while CMIP5 Roff shows no visible relation between altitude and the hydrological indicators.

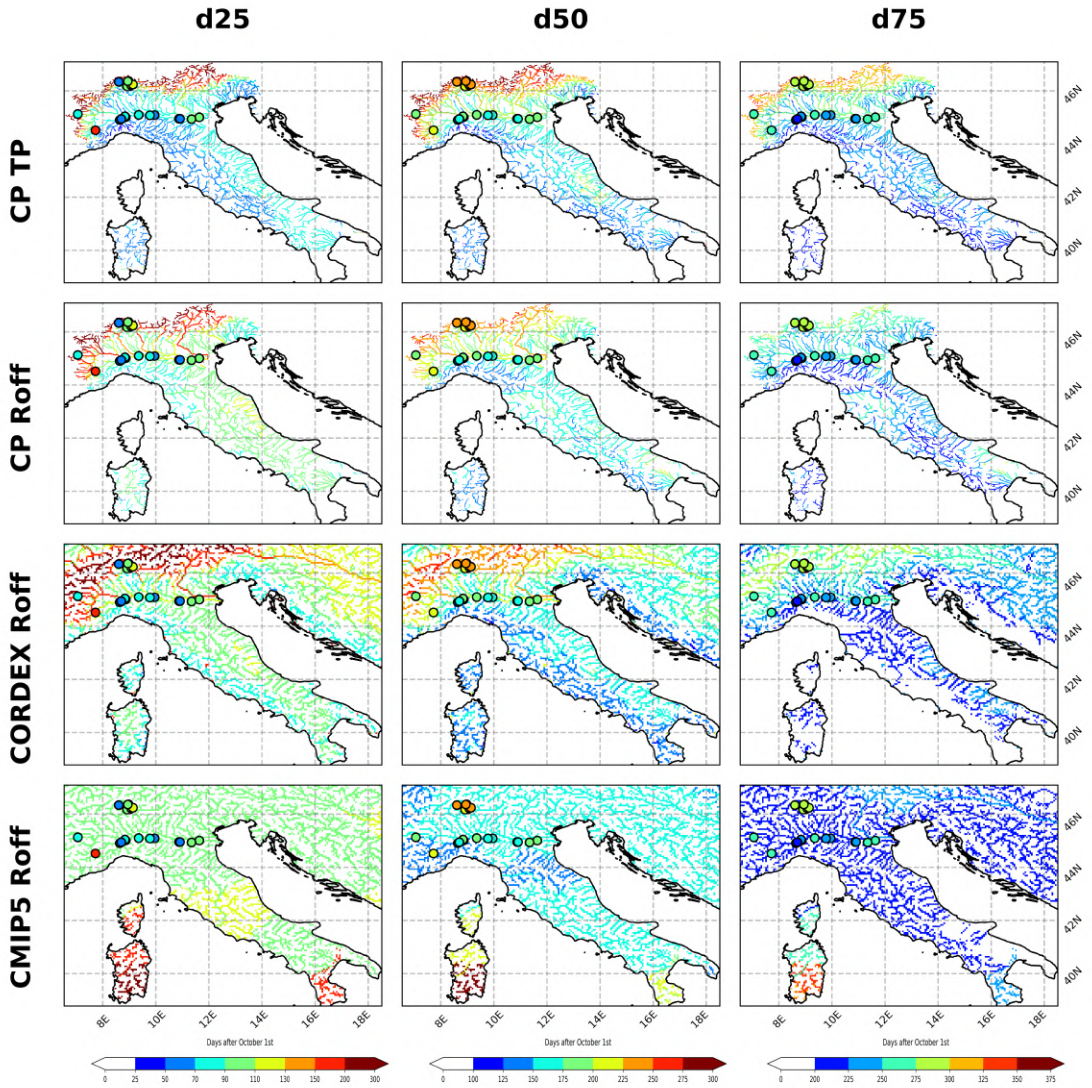

Figure 3.14: Average values for $d25$, $d50$, and $d75$ for CP TP, CP Roff, CORDEX Roff, and CMIP5 Roff ensembles for the historical period. The dots represent the values found for the station data.

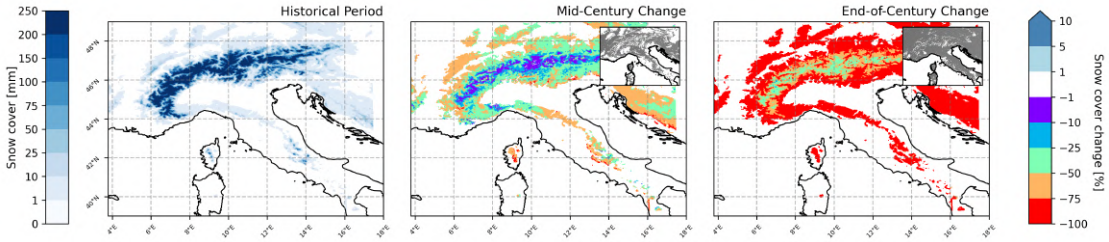

Figure 3.15: Snow cover [mm] in the ensemble of models in Table 3.1. The first figure represents the actual snow cover values for the historical period, whereas the second and third ones represent the percentage change of the values respectively for the mid-century and end-of-century period. Significance of change is indicated in upper right corner of the second and third figures: only zones in gray have significant changes according to a t-test with a 0.05 significance level.

This influence is physically expected, as snow accumulation and subsequent melt are orographically driven in the region, thus shaping the timing of the hydrological cycle.

To further investigate the relation with topography, the Po river basin was divided into six altitude categories: <250m, 250-500m, 500-1000m, 1000-1500m, 1500-2000m, and >2000m. The values for d_{25}, d_{50} and d_{75} for each altitude class are reported in Figure 3.16 for the three projection periods (his, mid and end).

The CP TP ensemble shows a strong topologically dependent behaviour. Categories below 1000m display similar dynamics, with d_{50} and d_{75} shifting up to one month earlier in the hydrological year. This change in timing could lead to reduced discharge later in the year and worsened summer drought conditions. Above 1000m, however, the hydrological behaviour is noticeably distinct. The d_{25} shows a shifts towards the earlier months of the year, by up to two months by the end of the century for the elevations $>$ 2000m , whereas d_{50} shifts by roughly 2 weeks in this same category. These changes are larger at higher altitudes and by the end-of-century period. These changes imply an increased likelihood of higher flow rates (proxy for floods) in winter and early spring, due to the earlier d_{25}, and lower flow rates (proxy for droughts) in late spring, as the distance between d_{25} and d_{50} increases. The snow related changes (shown in Figure 3.15) are the driver of these shifts: more liquid precipitation during winter and earlier snowmelt in spring, producing higher earlier peak flows and lower discharge in late spring.

Similar altitude dependent behaviour is observed in the CP Roff and CORDEX Roff ensembles, which are able to capture the distinct timing shifts across different elevation bands. In both, d_{25} occurs up to two months earlier in the year, while d_{50} and d_{75} also shift earlier, but only up to a month. In contrast, CMIP5 Roff simulations display no altitudinal dependent behaviour, showing its limited ability

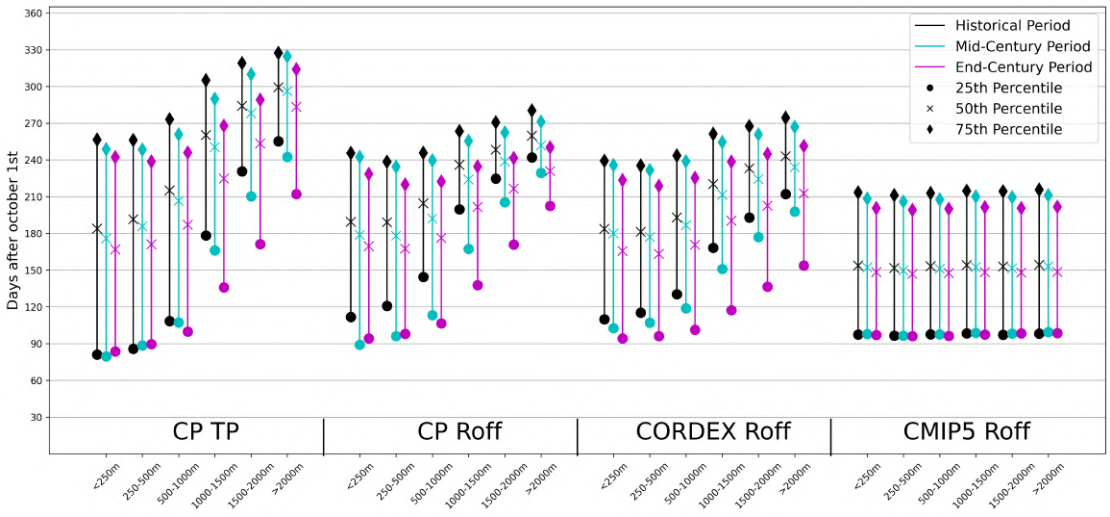

Figure 3.16: Representation of the hydrological year and its main percentiles (25^{th}, 50^{th} and 75^{th}) for different altitudes in Po Valley basin. Markers represent the days when the different percentiles were reached in each period for all ensembles: circle for d_{25}, cross for d_{50} and diamond for d_{75}. Black lines represent the historical period, blue lines the mid-century period and magenta lines the end-of-century period.

to resolve the topographically driven processes. The only consistent signal is the shift of d_{75} of two weeks towards the beginning of the year across all elevation bands.

The end-of-century changes in the three hydrological year percentiles are illustrated in Figure 3.17. A clear influence of the Alps is visible in d_{25} for CP TP, CP Roff and CORDEX Roff, while the d_{50} and d_{75} display consistent shifts across different altitudes. Figure 3.17 also confirms the lack of topographic driven signal in CMIP5 Roff results.

The altitude dependence of the hydrological year timing is clearly more pronounced in the higher resolution ensembles and intensifies by the end-of-century period. This result is consistent with the projected decreases in snow cover (Figure 3.15), where high altitude regions experience substantial reductions. These decreases affect the timing of snowmelt processes, leading it to occur earlier in the year. These shifts can impact water resources management in the Alps, as extremes become more likely to occur in the region.

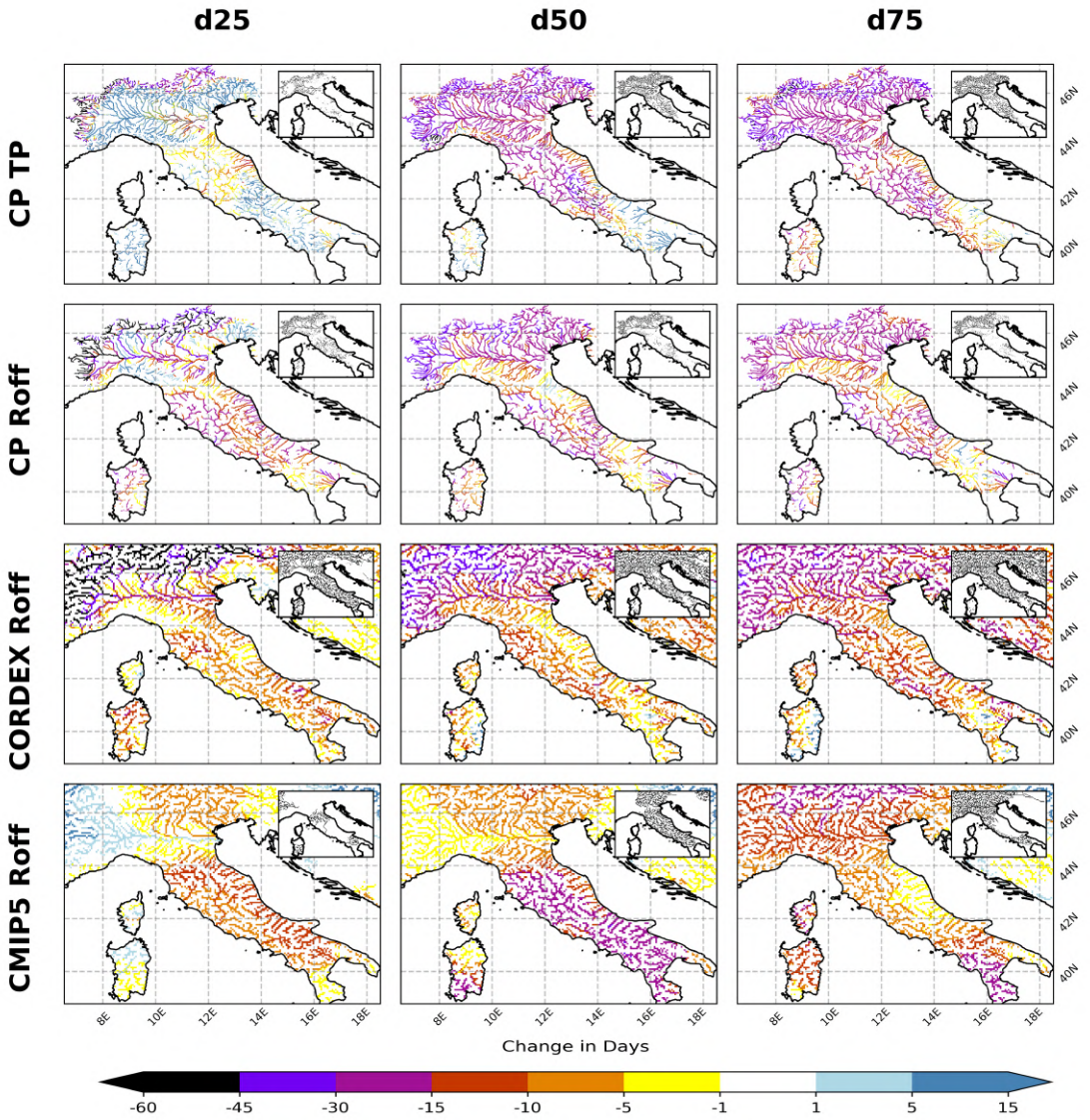

Figure 3.17: Average values for $d25$, $d50$ and $d75$ change in days for CP TP, CP Roff, CORDEX Roff and CMIP5 Roff ensembles for the end-of-century period. Significance of change is indicated in upper right corner: only zones in black/gray have significant changes according to a t-test with a 0.05 significance level.

3.2.2 Model uncertainty

The uncertainty of change of the different model ensembles was calculated for both Q_{mean} and Q_{100} at the end-of-century period (Figure 3.18). The use of convection permitting models is expected to decrease model uncertainty and produce lower uncertainty levels in CP ensembles.

The three ensembles using the same CHyM configuration, CP Roff, CORDEX Roff and CMIP5 Roff, show a decrease in model uncertainty with increasing resolution. For Q_{mean}, uncertainty falls below 0.15 across most of the CP Roff domain, reaching values under 0.05 in some regions. In contrast, CORDEX Roff maintains uncertainty values of around 0.2 and CMIP5 Roff ranges more widely from 0.1 to over 0.5. The uncertainty for Q_{100}, which represents variability in projected streamflows, is less straightforward. CMIP5 Roff exhibits a broad range of 0.2 to 0.7, and CORDEX varies from 0.2 to 0.5. CP Roff has the widest spread, from below 0.2 to over 0.7, though most of the domain hovers around 0.3-0.4.

For Q_{mean}, the CP TP ensemble display uncertainty levels comparable to, though slightly higher than, CP Roff, and is clearly lower than the two lower-resolution ensembles. For Q_{100}, however, the CP TP shows uncertainty levels more comparable to CORDEX Roff and CMIP5 Roff. Overall, the lowest uncertainty was found thus in the CP Roff ensemble.

3.3 Discussion

Throughout this chapter, the impact of climate change on the river network of Italy was investigated using high-resolution climate and hydrological modelling, based on the methodology described in Chapter 2. Recent developments allow regional climate models to simulate the climate evolution at the kilometre scale, enabling a detailed study of the hydrological cycle in the region. Outputs of the CORDEX-FPS convection project, consisting of various convection permitting (CP) models, were used to drive the hydrological model CHyM, which simulate river discharge for different time periods. The study examined the effects of fine spatial and temporal resolution and the removal of convection parametrization on hydrological representation. For comparison, previously published hydrological simulations, driven by the CORDEX-CORE and CMIP5 model outputs, were analysed to assess potential improvements in model performance. The CP driven CHyM simulations used RCMs forced by either Era-Interim reanalysis or GCMs. The former allowed for validation against discharge, whereas the latter provided climate projections for three decade-long time slices under the RCP8.5 scenario: historical, mid-century and end-of-century. The chapter also compared the two CHyM configurations, forced by either the temperature and precipitation (TP) or

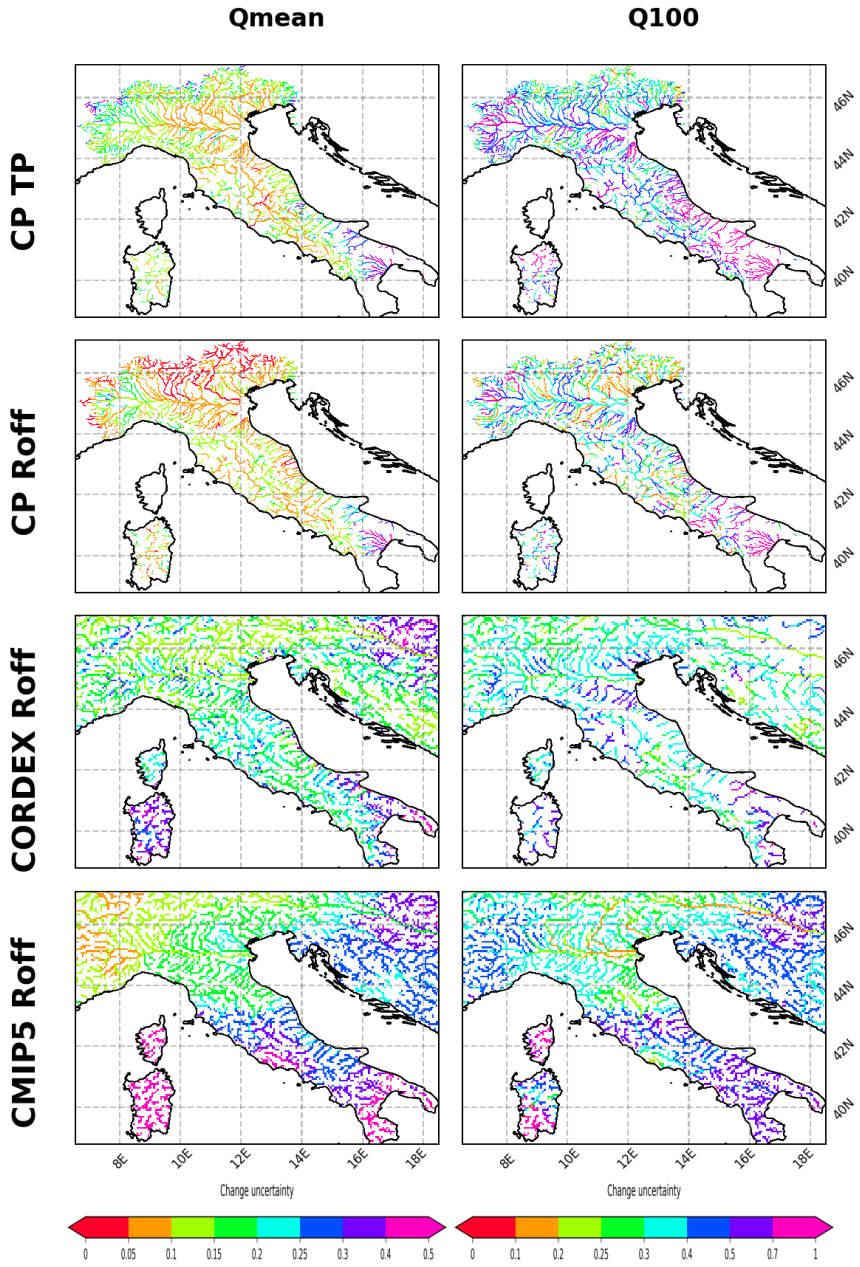

Figure 3.18: Uncertainty of the Q_{mean} and Q_{100} signal [-] for the CP TP, CP Roff, CORDEX Roff and CMIP5 Roff ensembles for the end-of-century Period.

the runoff (Roff) from CP models.

Using the Era-Interim driven simulations, the methodology presented in Chapter 2 was validated, and both CHyM configurations were considered suitable for this study, performing comparably in simulating river discharge. CHyM satisfactorily reproduced discharge behaviour across sub-regions with distinct hydrological regimes. The validation also confirmed the expected improvements achieved by higher resolution simulations, particularly over mountainous areas.

Spatial resolution was found to strongly influence how climate change affects river discharge. This finding was particularly evident in the interplay of mean and extreme precipitation on the average, the peak and low discharge signal. Seasonal precipitation also played a key role. The mean discharge change across the studied domain was mainly influenced by the average change in precipitation during winter and autumn, and modulated by extreme precipitation intensity in spring and summer. The high flow rates were linked to increased extreme precipitation throughout the year, whereas low flow were primarily driven by average precipitation change of JJA and MAM.

The analysis of the hydrological year highlights an influence of topography in the seasonality. The higher resolution ensembles (CP and CORDEX) capture the altitude dependent behaviour, absent in CMIP5 simulations, showing distinct behaviours in regions above and below 1000m. Above 1000m, shifts were observed for the 25^{th}, 50^{th}, and 75^{th} percentile of cumulative discharge, with d_{25} occurring up to two months earlier in the year. The increased interval between d_{25} and d_{50} indicates more drought prone conditions in the area during late spring/summer. This shift can be attributed to a rise in the proportion of liquid precipitation during winter and an earlier snowmelt process.

Across all the analyses, resolution of the climate input had a key role in representing river discharge. For instance, the influence of the Alps is clearly evident in all CP simulations and remains present, though less pronounced, in CORDEX simulations. CMIP5 models, however, fail to capture these interactions, which are important aspects of the hydrological cycle. As topography is known to be a relevant driver of hydrological processes, coarser resolution simulations cannot be expected to fully capture discharge signals. For example, the CMIP5 ensemble projected a decrease in flood discharges for much of Italy, which is opposite compared to the trends projected by higher resolution models.

The CHyM model was capable of describing river discharge over Italy and was employed to assess projected changes from the historical period to the mid-century and end-of-century periods. Both drought and flood events are expected to become more intense, and the average discharge to decrease across most of the country. The decrease in snow cover in mountainous regions and an increase in extreme precipitation are more effectively captured by the high temporal and

spatial resolution of CP models and are important factors in modulating the river discharge change, emphasizing the added value of CP simulations in hydrological studies.

In contrast, the use of CP models entails substantial computational and storage cost that should be considered when designing similar studies. Within the CORDEX-FPS convection project, not all models provided the necessary variables, and some were available for only one time slice. These constraints limited the number of members for the CP ensembles presented in this work (varying from 5 for the CP Roff projections up to 17 for CP TP validation), compared to the 44 members available in the CORDEX ensemble. While larger ensembles and longer time slices would be desirable, the challenges posed by CP models must be taken into account and a caveat is needed when analysing and generalising the results displayed in this chapter.

The direct comparison between CHyM TP and CHyM Roff relies on the assumption that the description of hydrological processes present only in the former is equivalent to those employed by LSMs when calculating the runoff later used by CHyM Roff later on. This hypothesis was considered acceptable given the similar performance of both configurations in simulating observed river discharge. Nonetheless, it is possible that an ensemble with enhanced LSM descriptions could influence the results and make CHyM Roff a more reliable configuration than its counterpart. If an LSM were to include in its modules human forcing on water resources and have a more comprehensive description of groundwater and surface water interaction, subsequent river discharge calculations would be expected to improve. Given the increasing complexity of current LSMs, interactions between hydrological variables and other components can be represented, with potential influences ranging from glacier to urban modules and affecting the simulated runoff.

The methodology described in Chapter 2 whose results were displayed in this chapter can be extended to other regions. Areas where convective precipitation is observed and/or regions of complex topography can particularly benefit from CP modelling. Though currently only the Greater Alpine region has a large CP ensemble available, similar efforts are planned for other domains, such as the Caribbean ([92]) and the South American regions ([93]). Moreover, this study can be further extended inside the Greater Alpine Domain into regions north of the Alps, providing that validation data becomes available.

One limitation of the present approach is that hydrological and climate models were run offline, with no way to feedback the hydrological model results into the atmospheric model. To incorporate these interactions, the climate model should have a physically based hydrological component inside its land-surface scheme, able to simulate local hydrological processes. This integration would allow direct feedback between hydrological and climate or land surface variables, and directly

produce reliable discharge information, streamlining works on the topic and improving physical consistency.

Moreover, a better description of soil moisture and groundwater interactions could greatly benefit the simulation of discharge values, especially in a coupled modelling system. Groundwater can not only directly recharge rivers, which is not possible in the CHyM model, and affect soil moisture, but it can also be directly modulated by other hydrological variables. [94] showed a link between the snowmelt and groundwater recharge that notably impacts summertime river flow. The snowmelt process becomes a key driver of discharge changes in the projections explored in this chapter, particularly over the Alpine mountain range. Nonetheless, this feedback chain has not been explored here and could be implemented in future studies to improve the reliability of results, as could the inclusion of an explicit groundwater module.

Overall, the results presented in this chapter highlight the advantages of kilometre-scale CP simulations in representing the river discharge of Italian rivers. The explicit treatment of convection and fine topographic representation lead to improved discharge dynamics, reduced model uncertainty, and physically consistent responses to snow and precipitation changes. These findings emphasize the growing importance of high-resolution modelling for projecting hydrological extremes and guiding future climate adaptation strategies.

Chapter 4

Integrating eCLM into RegCM5: online hydrological coupling at high resolutions.

There are several advantages to coupling climate models with hydrological ones, as the integration allows for a more comprehensive investigation of the impact of climate change on the water cycle. In the previous chapter, an offline approach was presented, in which outputs from climate simulations were used as forcing for the hydrological model CHyM. Because these simulations were offline, the hydrological processes simulated could not influence the climate model through feedbacks, limiting interaction between the hydrological quantities and the atmosphere. For example, when using total runoff as an input to CHyM, there is no distinction between surface and subsurface runoff, even though their behaviour and residence time are different.

The current iteration of the Community Land Model (CLM5.0, [9]) directly tackles this issue. The new land scheme includes a physically based hydrological module, the Model for Scale Adaptive River Transport (MOSART), which interacts directly with runoff and differentiates between surface and subsurface components. In addition to the hydrological improvements, CLM5.0 exhibits several advances in the land use description and the vegetation scheme, both of which can indirectly affect river flow representation.

RegCM5.0 currently uses CLM4.5 as its default land-surface scheme. Although CLM4.5 remains a robust LSM, it lacks the improvements developed for CLM5.0. The RegCM community has demonstrated a strong interest in incorporating CLM5.0. The improved physical representations are specially relevant as the regional modelling communities moves towards kilometre scale CP simulations, where local hydrological feedbacks become increasingly significant and larger number of processes must be resolved.

Moreover, the climate modelling community has developed increasingly complex Earth System Models (ESMs). More than 55 GCMs contributed to CMIP6 ([1]), which were developed by independent institutions worldwide. The scope of current ESMs includes robust components for aerosols, carbon cycle, sea and land ice, among others. Often, the separate components are independently developed, posing greater challenges for integration. Different approaches can be explored for integrating them, with the framework know as "multiple-executable" perceived as facilitating coupling between independently developed models. This approach, which will be further explore in this chapter, minimizes code modification and does not require extensive alteration when the models will be updated.

However, the RegCM5.0 model is based on a rigid coupling structure. Incorporating external models into its framework currently requires considerable and labour intensive adaptation, which has discouraged implementation of CLM5.0 so far. Nevertheless, the advent of eCLM, an adaptation of CLM5.0 with more flexible coupling efforts, offers a new less intrusive alternative. This framework allows eCLM to be coupled with RegCM5.0 while preserving the independent development of each model and facilitating the inclusion of future CLM updates with minimal effort.

This Chapter presents the development of a couple system combining RegCM5.0 and eCLM through the OASIS3-MCT coupler. It evaluates the hydrological performance of both offline and coupled simulations of eCLM, validating them against CHyM simulations forced by RegCM, to assess possible improvements with the updated land-surface scheme and coupling framework.

Section 4.1 describes the models and the OASIS3-MCT coupling framework. Section 4.2 introduces the evaluation simulations performed both offline and online. Section **??** presents the preliminary results, and Section 4.4 discusses the main findings and outlines future directions for this ongoing effort.

4.1 Modelling and coupling framework

Coupling different models within Earth System Models (ESM) typically follows one of two different frameworks. ESMs combine different numerical components representing atmosphere, land surface, ocean, and others, which must be able to effectively exchange information during model simulations. Different components of the global system, such as the atmosphere, the land surface and the ocean, are often represented by different models that come together to simulate the Earth's climate. The choice of coupling approach depends on the specific needs of the model system.

The first framework is the single-executable approach, where all model components inside a ESM are compiled and executed together under a single executable

file (`.exe`). In this configuration, the exchanges are done inside of this executable and the different components are present as sets of subroutines within it. The Earth System Model Framework (ESMF) is a commonly used architecture for developing and assembling climate models implementing this approach ([95]). The ESMF library provides a standardized and efficient way of exchanging information among components of an ESM. Although it offers efficiency and consistency, this format has reduced flexibility when integrating independently developed codes.

The second approach is the multi-executable framework, in which the different model components are represented by different executables. The exchanges of variables are performed by an external coupler, which manages all inter-model communication. In this framework, models only interact directly with the coupler rather than to other components, facilitating the integration of climate models created by independent institutions.

4.1.1 The OASIS3-MCT coupler

The Ocean Atmosphere Sea Ice Soil (OASIS) coupler in its version 3, together with the Model Coupling Toolkit (OASIS3-MCT) implements a multi-executable configuration in which the different models are simulated through distinct executables. This feature facilitates the coupling of independently developed models, as it minimizes modifications inside each components, maintaining their individual structure. The coupler manages the interpolation and exchange of fluxes between models, permitting, for instance, the use of a land-surface model at a different spatial resolution than its atmospheric counterpart.

The OASIS software is widely used in the climate modelling community, particularly across European research groups, and is notable for its low implementation and performance costs ([11]). It currently employs the MCT library for parallel data transfer from source to destination, which also provides interpolation and remapping techniques for exchanging fields. Since OASIS3-MCT3.0, the user is also allowed to use pre-defined mapping files for mapping weights. The coupler permits exchanges of 1D, 2D and 3D fields, and provides different options for time operations.

OASIS3-MCT works based on a *put-get approach*, which means subroutines from each component should include a *put* (send) and a *get* (receive) call for each exchanged fields, requiring consistency between models. The configuration file `namcouple` indicates which fields are exchanged between models, the frequency of exchange and any spatial or temporal operations to be performed. Each field can be processed individually or multiple fields can be exchanged within the same step. The current version of the coupler provides a lot of flexibility to model developers, in which different grids and components are allowed inside a single executable. OASIS3-MCT can handle large numbers of exchanged fields, many

processing cores, and high-resolution simulations ([11]).

The multi-executable approach of OASIS3-MCT requires minimal changes to each component's code compared to an integrated framework such as ESMF. Each individual model uses a selected set of cores and MPI communication tools are responsible for the inter-model exchanges, no longer done inside the computing cores. The gain in minimizing intrusiveness to the code is counterbalanced by a small loss in computational efficiency in variable communication. Nevertheless, the increase in flexibility remains very advantageous when dealing with independently developed models.

4.1.2 RegCM5

The Regional Community Model (RegCM) was the first Regional Climate Model (RCM) to be developed, aiming to dynamically downscaling the coarse fields of Global Climate Models (GCMs) by providing large-scale forcings to the RCM and resolving processes at the GCM sub-grid scale. Since its early versions, when RegCM1 had a 50-60km spatial grid, to its recent developments (RegCM5.0, [3]), the model has evolved to include a vast game of physical schemes and support kilometre scale simulations.

RegCM5.0 provides several new distinct configurations (see Table 1 in[3]), according to the different physical schemes available, and its outputs are sensitive to choices of representation, often requiring region specific optimizations ([3]). Furthermore, one of the main advancements of the current version is the possibility of using a non-hydrostatical dynamical core derived from the weather prediction model MOLOCH. The traditional hydrostatic core is still available, with now MOLOCH as an added option.

RegCM5 uses a hybrid terrain with a uniform vertical coordinate ζ defined between the surface and a top rigid lid of the atmosphere (Z_t). The resolution is given by $\partial\zeta = \frac{Z_{top}}{kz}$, where kz is the number vertical levels. This scheme increases the numerical stability of RegCM and allows up to five times longer time step than in previous versions. The longer steps are particularly important for the convection permitting (CP) simulations, which require a spatial grid of 1 - 3 km .

Horizontal and vertical derivatives are calculated through a second-order centred finite difference scheme. The time integration uses a three time step explicit scheme: an implicit Euler-backward scheme for the vertical sound wave propagation (dt_s); a second order total variation method for advection terms (dt_a); and, for physical parametrizations, a longer user-configured time step (dt_p)([3]).

RegCM5 currently uses the Community Land Model 4.5 (CLM4.5, [96]) as its default land-surface scheme, integrated through the ESMF in a single executable configuration. Other less current LSMs are available for use inside RegCM: CLM3.5 ([97]) and BATS ([98]). The current architecture of RegCM creates an

obstacle to updating the LSM with ease as new versions of CLM become available. New LSMs need to be manually translated inside of the RegCM code, a challeging and laborious task given that CLM and RegCM are maintained by different research groups. This limitation has encourage the development of a new coupling configuration for RegCM, exploring a more flexible multi-executable framework and allowing for easier future updates to the system.

4.1.3 eCLM

The Community Land Model (CLM) is the land component of the Community Earth System Model (CESM). Its latest version CLM5.0 is the default for CESM2 and different iterations of CLM are used as the LSMs of other GCMs and RCMs. CLM5.0 introduced significant updates compared to CLM4.5 and CLM4 (see Table 1 of [9], [99]). Lawrence et al. [9] cites as key parts of the progress made with CLM5 *"a push toward more mechanistic treatment of key hydrologic and ecological processes and more comprehensive and explicit representation of anthropogenic land management"*. Major improvements include new crop types and parametrizations, transient land units, an enhanced glacier description, and a physically based river routing scheme. These developments improved the model in comparison to earlier versions ([9]).

While CLM5 was originally designed for single-executable integration within CESM via ESMF, Shrestha, Sulis, Masbou, Kollet, and Simmer [10] introduced an alternative multi-executable structure compatible with the OASIS3 coupler. This approach enables coupling CLM with independently developed models, such as ICON or ParFlow, through the Terrestrial Systems Modeling Platform (TerrSysMP). The adapted version of CLM5 used in TerrSysMP—referred to here as eCLM—retains all physical representations of CLM5 but replaces its coupling interface, making it compatible with any model system using OASIS3-MCT.

CLM5.0 was originally developed inside a integrated single-executable approach using the ESMF libraries, which is considered suitable inside a controlled development environment. Nonetheless, Shrestha, Sulis, Masbou, Kollet, and Simmer [10] present an alternative multi-executable structure for CLM, using the OASIS3 coupler. Since CLM3.5, CLM has been included in the Terrestrial Systems Modeling Platform (TerrSysMP, [10]) as the LSM, exchanging through OASIS3 with the atmospheric model ICON and the hydrological ParFlow. The current iteration, TerrSysMP2 ([100]), includes CLM5.0 in its configuration, referred to here as eCLM. This fork of CLM5.0 maintains all physical representations of the original model, but replaces the coupling approach to make it functional with OASIS3-MCT. This version of CLM5.0 can be thus more easily incorporated to any systems using OASIS3-MCT.

Model for Scale Adaptive River Transport (MOSART)

One of the major improvements in the hydrological description of CLM5.0 was the introduction of the Model for Scale Adaptive River Transport (MOSART), which substituted the River Transport Model (RTM) available in previous versions ([101], [**gmd-7-947-2014**]). Whereas RTM employed simple linear reservoir method, MOSART uses a physically-based kinematic wave method.

MOSART divides each grid-cell into three categories for river routing: hillslope, tributaries and main channels. Hillslope routing transfer runoff from the spatial unit into a tributary channel. Surface runoff is treated as overland flow entering into the sub-network channel, with its residence time accounted for in the kinematic equations, whereas sub-surface runoff directly enters the sub-network channel. Different tributary channels within a single cell are treated as a single equivalent channel, which routes the received hillslope runoff into a main-channel. In turn, the main channel receives inflow from both upstream cells and tributaries, and routes water downstream or into ocean cells.

MOSART uses an equation similar to Equation 2.2.1 to define the velocity of river flow. The main differences are that here n represents directly Manning's coefficient without any adjustment and S is defined as the friction slope, which can be approximated by the channel slope if it is sufficiently steep. The hydraulic radius is approximated for both hillslope and tributary/sub-network routing (respectively R_h and R_t) as equal to the water depth (h).

$$R_h = h_h \tag{4.1.1}$$
$$R_t = h_t \tag{4.1.2}$$

For main channels, the hydraulic radius R_r is given by Equation 4.1.3, where A_r and P_r represent the wetted area (i.e. the river cross-section area) and the wetted perimeter.

$$R_r = \frac{A_r}{P_r} \tag{4.1.3}$$

Finally, the continuity equation is given by 4.1.4, which is equivalent to Equation 2.2.5. In Equation 4.1.4, ν represents the water volume within a grid cell, while Q_{in} and Q_{out} are respectively the inflow from upstream and the outflown downstream or to the ocean. Q_s represents sources and sinks within the cell. Q_{in} is always be zero for hillslope and tributary routing, whereas Q_s equals the runoff generation rate for hillslope, lateral inflow for tributaries and zero for main channels. In theory, Q_s could represent also other fluxes, such as infiltration and

evaporation, although these are not used in the version of MOSART used in this work.

$$\frac{d\nu}{dt} = Q_{in} - Q_{out} + Q_s \tag{4.1.4}$$

MOSART has a widely available global hydrography dataset at 0.5°resolution, which was not was not fine enough for the experiments conducted in this study. Therefore, preprocessing steps were adapted from the CHyM structure to create the input data required for constructing a coherent river network. More details are provided in Appendix A. The dataset used here combines downscaled information from the 0.5° global product and outputs from the CHyM preprocessing routine, which employs a eight flow-direction network derived from a DEM, as previously discussed in Section 2.2.

4.1.4 RegCM5.0 and eCLM coupled system

As discussed, the eCLM fork of the Community Land Model is an adaptation of CLM5.0 for use with the OASIS3-MCT coupler, without altering its physics. This configuration enables its integration to atmospheric components beyond CESM, providing a modular less-intrusive alternative to the ESMF based coupling. Furthermore, it facilitates future updates (e.g. CLM5.5 or CLM6) with minimal code changes. Therefore,a new framework was developed to couple eCLM and RegCM5.0 through OASIS3-MCT.

The integration only required minimal changes to the eCLM code. The eCLM fork was created first for coupling with the atmospheric model ICON and already is setup for working with and exchanging fields through OASIS3-MCT. Therefore, changes were primarily directed at exporting additional variables required by RegCM and not by ICON. RegCM, in contrast, required more significant adaptations. Although the model already included routines for interacting with OASIS3-MCT from previous coupling efforts with the SYMPHONIE ocean model ([102], https://github.com/DesmetQuentin/RegCM), those routines needed to be adapted to support land-atmosphere exchanges and not ocean-atmosphere ones.

The new coupling scheme disables RegCM's internal land-surface subroutines, responsible for incorporating CLM4.5 and other LSMs to the model, and redirects the surface flux calls to pass through OASIS3-MCT towards eCLM. The initialization procedure was updated, and new exchanges fields were incorporated in the OASIS3-MCT subroutines. The resulting system successfully allows RegCM5.0 and eCLM to operate as distinct executables within a single coupled workflow, maintaining their independent codebases while enabling two-way flux exchange.

4.2 Preliminary Simulations

4.2.1 Offline simulations

To assess whether the eCLM scheme, together with the MOSART hydrological module, can satisfactorily represent the hydrological cycle, a series of offline simulations were first completed. In these simulations, input variables from CP simulations of RegCM were used as forcing for a stand-alone version of eCLM. The following variables were derived from the RegCM5 climate model: precipitation, downward shortwave surface radiation, surface temperature, wind and near surface specific humidity. Wind, provided at the lowest level, is not a directly available in RegCM, but can be obtained by combining its *uas* and *vas* variables, which represent the eastward and northward wind components respectively.

According to the eCLM documentation ([99]), other variables can also be used as forcing. For instance, specific humidity may be replaced by dew point temperature or relative humidity. Additional optional variables, such as surface pressure, observational height and incident longwave radiation, were not employed in this study. In their absence, the model assumes standard pressure, a constant observational height of 30 meters, calculates the longwave radiation with temperature, pressure and humidity. In a coupled configuration, all these variables would be obtained from the atmospheric component, with eCLM providing feedbacks back to the atmosphere. This interaction is expected to improve the final output obtained by the combination of the atmospheric and the land surface coupled components.

Pre-processing for these simulations followed the protocol of the eCLM documentation ([103]), with additional steps to enable the use of the MOSART component. To build a consistent river network within the studied domain, MOSART requires a set of inputs, including flow direction, drainage area and channel width. However, the dataset provided with MOSART's documentation does not include high resolution files and the finest globally available grid reaches only 0.125°. Typically, eCLM and its precursor CLM5.0 are used either with the MOSART module deactivated or at coarser resolutions than those targeted in this study. Given the goal of exploring high-resolution modelling and coupling climate models with improved land surface schemes, using lower resolution MOSART grid would represent a set back. Therefore, we combined the CHyM protocol for constructing high-resolution river networks ([82]) with information from the HydroSHEDS global database and existing lower-resolution MOSART input files available. The complete protocol is provided on Appendix A and is expected to be refined in the future.

Using these inputs, we successfully ran eCLM in stand-alone offline mode driven by RegCM forcings. Two simulations were performed. For the first one, forcing were obtained from CP RegCM 4.7 simulations that contributed to the CORDEX-

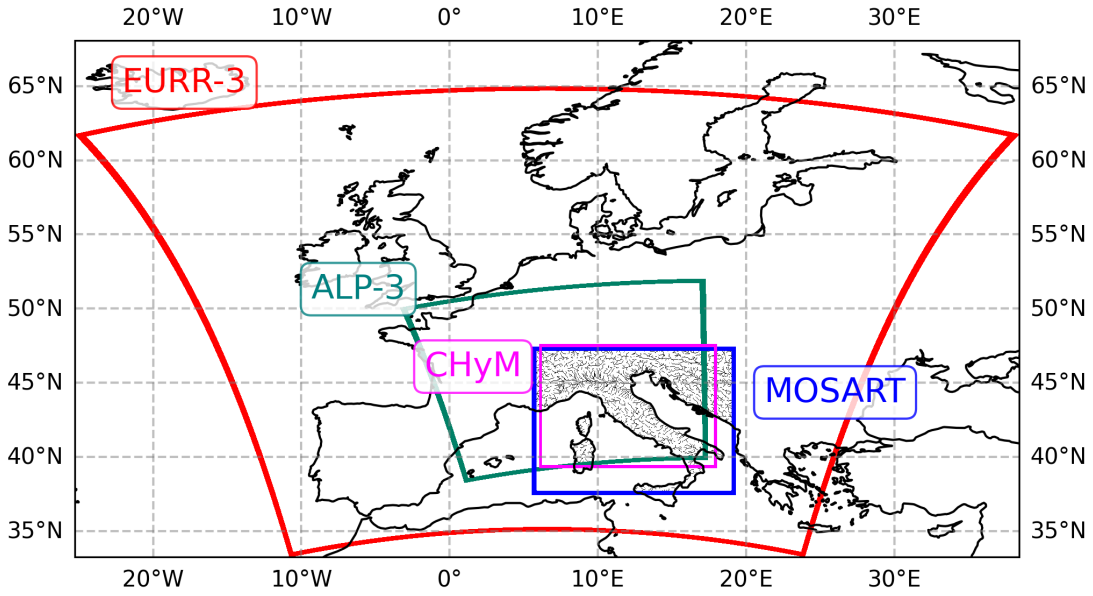

Figure 4.1: Domains used in the different RegCM and hydrological simulations: EURR-3 in red, ALP-3 in green, MOSART in blue and CHyM in magenta. The river network inside the MOSART module is depicted in black.

FPS convection project, covering the Greater Alpine Domain (ALP-3), allowing direct comparison with the RegCM-driven CHyM results presented in Chapter 3. The second simulation used forcing from RegCM5.0 simulations for the Reduced European Domain (EURR-3) ([3]), as part of the CMIP6 downscaling effort. Although the full projections are not completed yet, the available ERA5-driven evaluation simulation provided a suitable counterpart to the CORDEX-FPS validation ensemble. All hydrological simulations were performed over a smaller domain compared to both the EURR-3 and the Great Alpine domain, encompassing only Italy and neighbouring regions (Figure 4.1). Simulations performed with eCLM-MOSART covered the domain titled MOSART, and the forcing for its offline simulations were remapped from either the EURR-3 or the ALP-3 regions. The domain utilized for the CHyM simulations was also included in Figure 4.1.

4.2.2 Coupled simulations

A short test simulation of three months was performed with the newly developed eCLM-RegCM5.0 coupled system. The span of the simulation was from September to November 2001 to ensure comparability with the previous outputs. Data from the offline simulation were used as restart information to minimize spin-

up time. The atmosphere configuration matched that of the EURR-3 RegCM5.0 simulations, and the spatial domain was similarly limited to Italy and adjacent territories. All preprocessing for eCLM and MOSART followed the same sequence of steps described in Section 4.2.1.

The two models exchanged variables every 360s, consistent with the frequency previously used between CLM4.5 and RegCM, and eCLM communicated with MOSART at an hourly interval, comparable to the CP forced CHyM simulations. The following variables were passed from RegCM to eCLM: temperature [K], wind speed in the northwards and eastwards directions [m/s], specific water vapour content [-], thickness of the lowest atmosphere level [m], surface pressure [Pa], direct and diffuse shortwave downward radiation [W/m^2], longwave downward radiation [W/m^2], and rain and snow precipitation [kg/m^{2}s]. In turn, RegCM received from eCLM the following: temperature at 2m [K], surface specific humidity at 2m [kg/kg], wind speed at 10m [m/s], evapotranspiration [kg/(m^{2}s)], aero-dynamical resistance [s/m], thermal resistance [s/m], snow water [mm H_2O], momentum flux [N/m^2], radiation temperature [K], surface roughness length [m], short and longwave direct and diffuse albedo [%], vegetation temperature [K], surface runoff [kg/(m^{2}s)], total runoff [kg/(m^{2}s)], surface temperature [K]. Additional variables will be included in future configurations to guarantee RegCM fully satisfies the output standards of the CORDEX-CORE protocol, which required land-surface information.

4.2.3 Evaluation methodology

The methodology used to evaluate the performance of the different simulations in representing the hydrological cycle followed closely the approach described in Section 2.3. Five simulations were included in the analysis: RegCM4.7 with CHyM-Roff (CHyMRoff47), RegCM4.7 with CHyM-TP (CHyMTP47), RegCM4.7 with offline eCLM (off47), RegCM5.0 with offline eCLM (off50) and RegCM5.0 with coupled eCLM (couple50). All these simulations were forced by a reanalysis driven RCM, and are therefore directly comparable to observations. Since no ensembles were employed, each simulation was evaluated separately, without ensemble statistics.

To assess model performance, flow duration, peak discharge and low discharge curves were constructed, and the KGE index was computed for all simulations. The observational dataset is the same as described in Section 2.1.1. The evaluation period covers 2001 to 2009, as one full spin-up year to ensure that eCLM created a suitable river network over the region. This spin-up period was discarded in the evaluation. Not all analysis include the coupled simulation, given its short duration.

4.3 Results

Figure 4.2 display the results for offline RegCM driven hydrological simulations. Panels (a) and (b) represent the CHyM outputs, whereas (c) and (d) display eCLM-MOSART simulations. The overall skill of the two models is similar. A small number of stations in panel (d) have negative KGE values, while in (c) they are positive. These stations are located in mountainous regions and have small drainage basins. The KGE index was not calculated for the coupled simulation given its reduced time series.

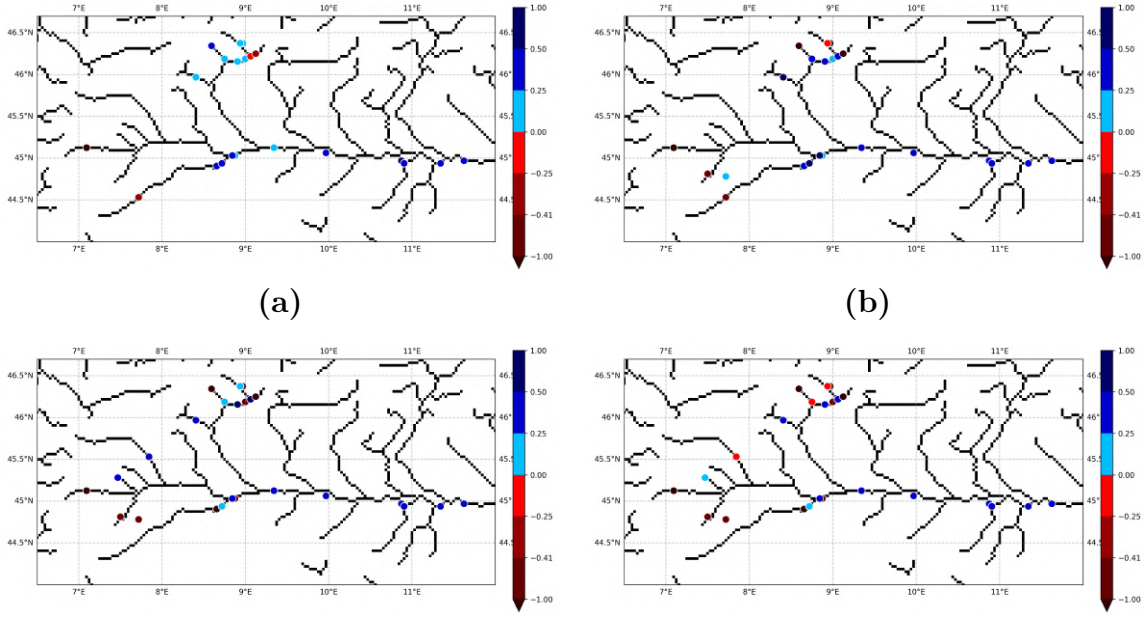

Figure 4.2: KGE index obtained for the validation points with the following simulations :**(a)** CHyMTP47 **(b)** CHyMRoff47 **(c)** off47 and **(d)** off50. The river network constructed by MOSART is depicted in black.

Additionally, flow durations curves are displayed in Figure 4.3 for the Po Delta and Swiss Alps regions of the Po Valley (see Figure 2.1). All simulations describe accurately the shape of the curve of the Po Delta region, though CHyM outputs tend to underestimate low flow magnitudes. For the Swiss Alps, the spread of observations is approximately mirrored by simulations, though one station of MOSART simulations clearly underestimates observed values.

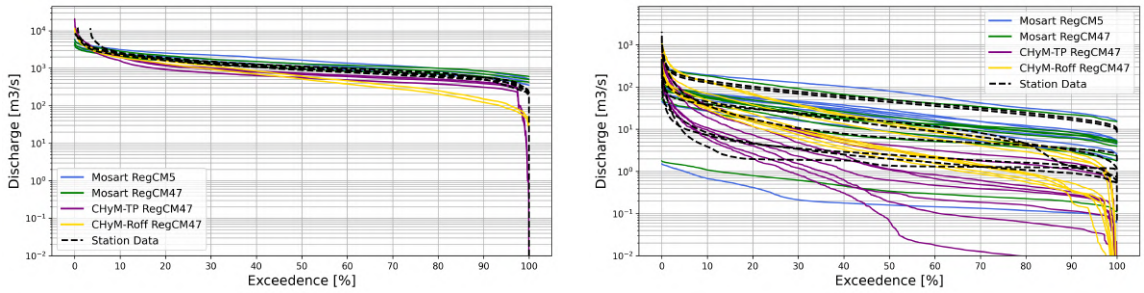

(a) **(b)**

Figure 4.3: Flow duration curves for validation points located on the **(a)** Po Delta and **(b)** Swiss Alps for the CHyM47Roff, CHyMTP, off47 and off50 simulations. Station data is plotted with black dotted lines and simulated data is plotted in continuous lines

Figure 4.4 displays the peak discharge curve for observed and simulated values. For the delta region, CHyM overestimates the peak discharge and MOSART underestimates it. Though the analysis done in Chapter 3 was done for the ensemble of CP models and not individually for RegCM, the same overestimation tendency by CHyM was present. For the Swiss Alps, however, CHyM captures very well the range of observed values, with MOSART exhibiting clear underestimations, as already seen in Figure 4.3.

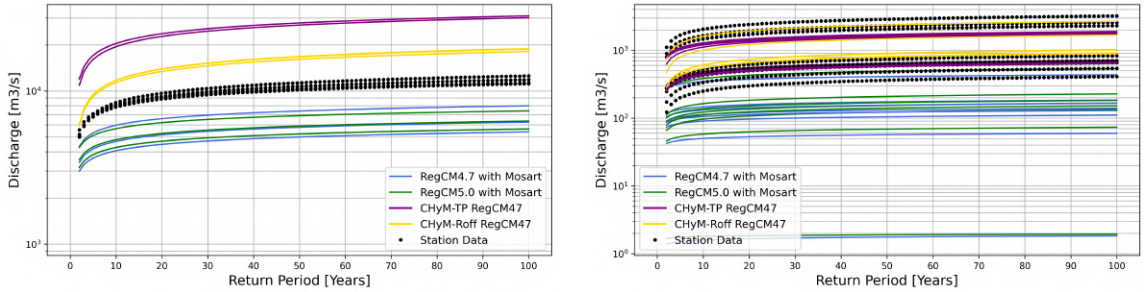

(a) **(b)**

Figure 4.4: Peak discharge curves for validation points located on the **(a)** Po Delta and **(b)** Swiss Alps for the CHyM47Roff, CHyMTP, off47 and off50 simulations. Station data is plotted with black dotted lines and simulated data is plotted in continuous lines

In Figure 4.5, the Po Delta exhibits an underestimation of low flow values by CHyM and an overestimation by MOSART. Over the Swiss Alps, MOSART captures quite well the range of observations, and CHyM underestimates it. Across the

three constructed curves, CHyM tends to underestimate low-flow values and overestimate high-flow values, whereas MOSART has the opposite behaviour. These results are nevertheless comparable with the performances of the hydrological ensemble in Chapter 3 and are therefore within the model uncertainty range.

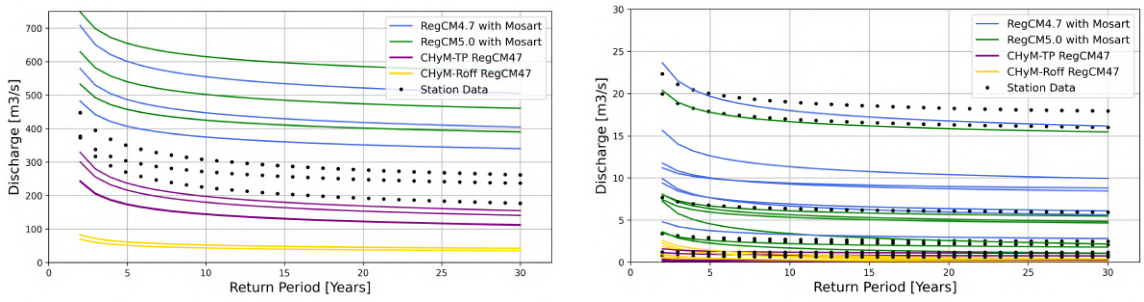

Figure 4.5: Low discharge curves for validation points located on the **(a)** Po Delta and **(b)** Swiss Alps for the CHyM47Roff, CHyMTP, off47 and off50 simulations. Station data is plotted with black dotted lines and simulated data is plotted in continuous lines

Coupled results are preliminary, and Figures 4.6 to 4.8 display the discharge (in blue) response to precipitation (in red) input of RegCM at three different locations for CHyM47Roff, off50, couple50 and observations. Two of the selected locations correspond to observational stations in the Central Po region (Pontespessa and Piacenza), whereas the third is located in the Po Delta area (Pontelagoscuro). The plotted precipitation time series corresponds to the total precipitation contributing to the contributing basin of each station. Observed precipitation data was obtained from GRIPHO ([104]). Only small differences are observed between the precipitation signal among the different RegCM simulations.

The coupled discharge signal initially exhibits a similar range of values to that of the eCLM offline simulation. However, as the simulation progresses, a notable drying effect appears in discharge, which seems not directly correlated to a reduction in precipitation. Precipitation remains broadly similar to the offline results, with only a small reduction in couple50. This inconsistency needs further investigation and could indicate an issue in the fluxes exchanged between models. In the time series, a precipitation peak within the contributing basin is generally followed by an increase in discharge, a behaviour clearly visible in offline50 and CHyM47Roff around day 50. In contrast, the coupled simulation (couple50) shows only a very small discharge response, suggesting a damped hydrological reaction to the driving precipitation. This aspect will be further explored in the continuation of this work. Nevertheless, both couple50 and offline50 simulations display a

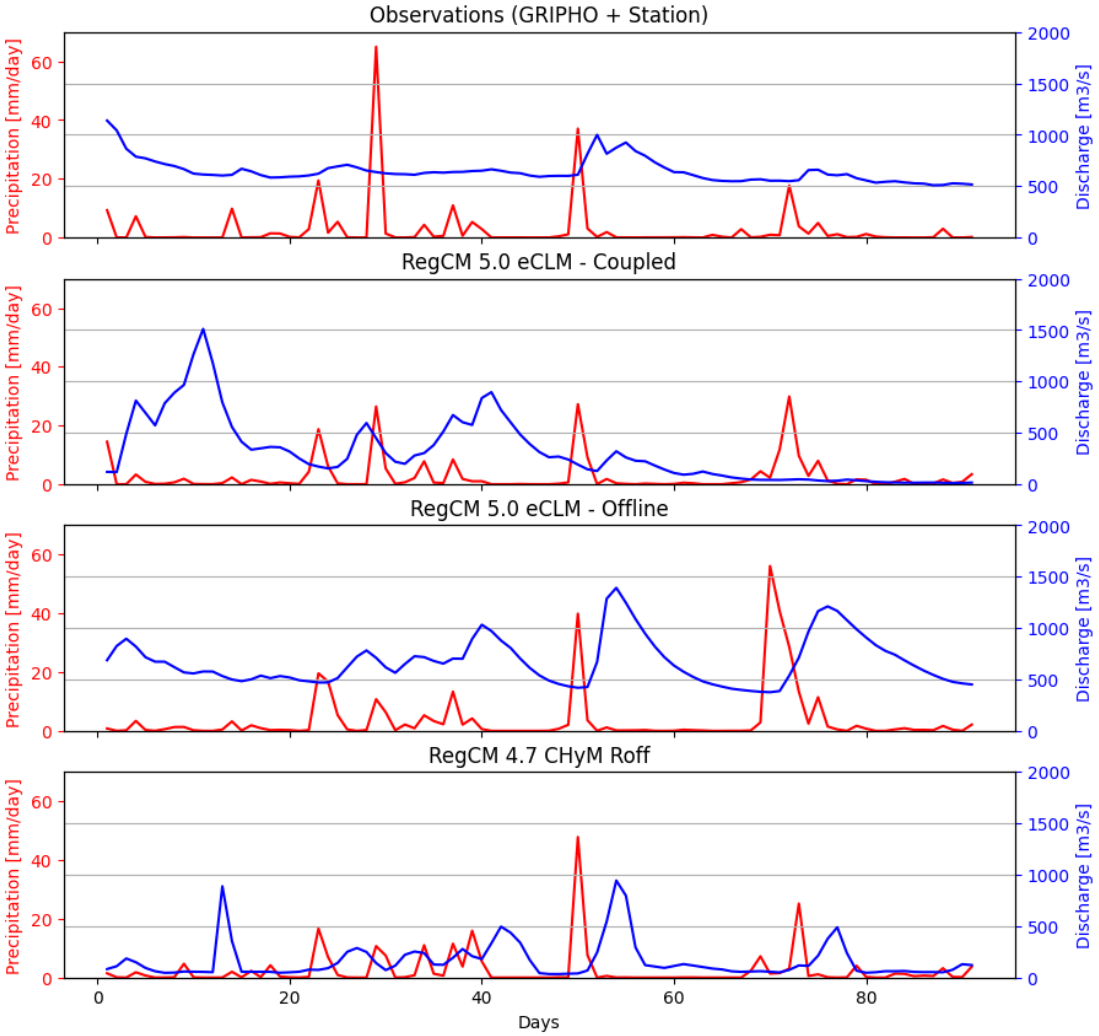

Figure 4.6: Time series of discharge (m^3/s, in blue) and precipitation (mm/day, in red) for different RegCM simulations in validation point located in Pontespessa.

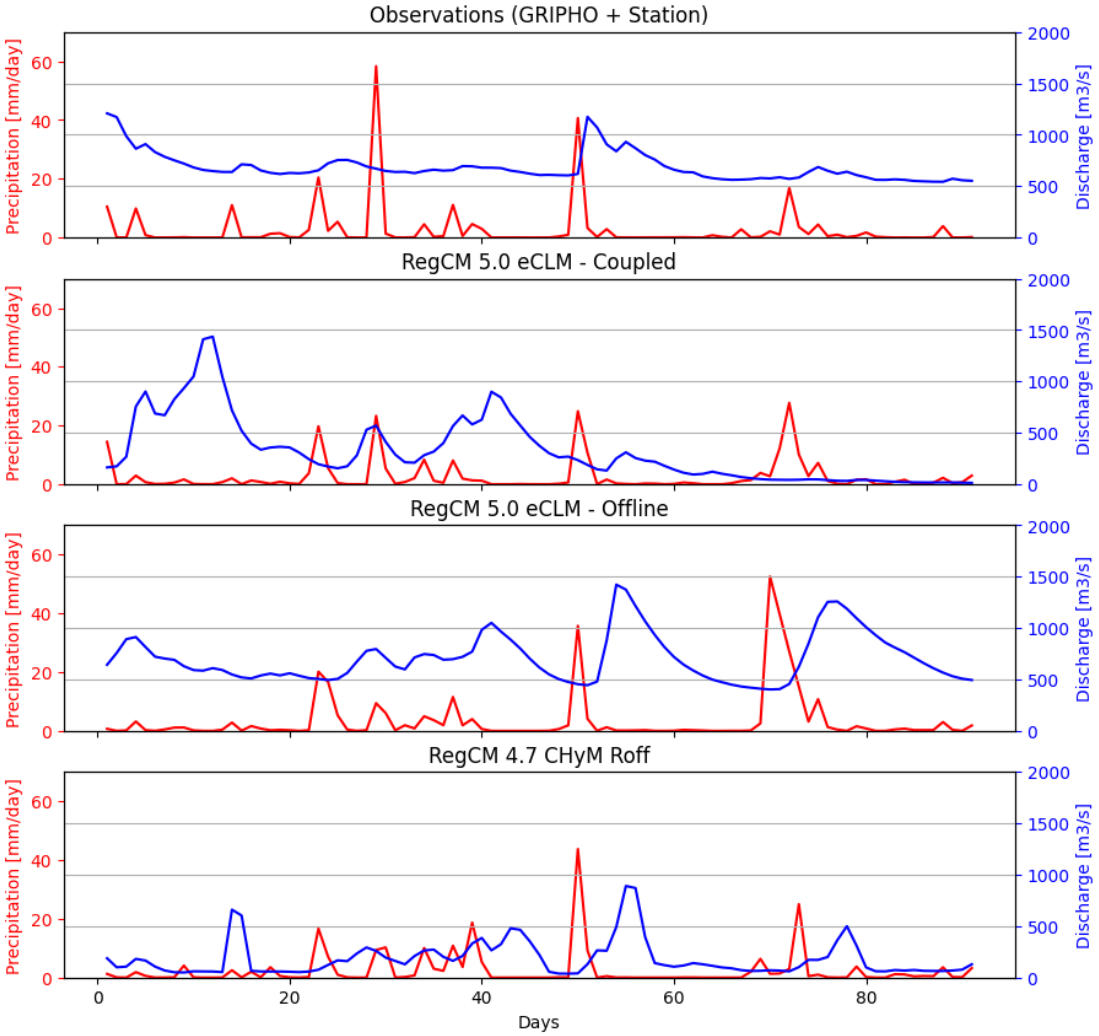

Figure 4.7: Time series of discharge (m^3/s, in blue) and precipitation (mm/day, in red) for different RegCM simulations in validation point located in Piacenza

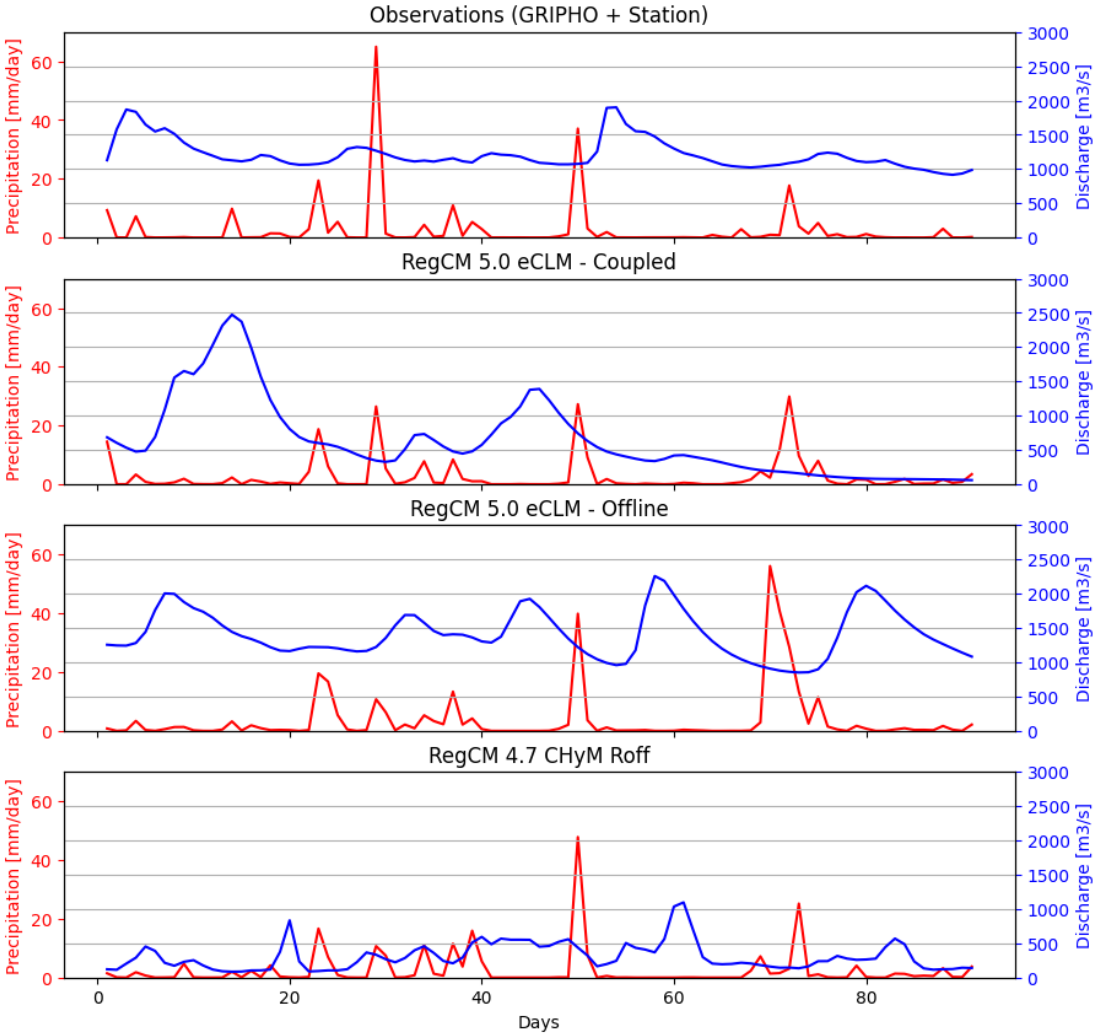

Figure 4.8: Time series of discharge (m^3/s, in blue) and precipitation (mm/day, in red) for different RegCM simulations in validation point located in Pontelagoscuro

higher base flow than CHyM47Roff. This finding is consistent with the pronounced underestimation of low-flow magnitudes by CHyM exhibited in Figure 4.5. These preliminary results outline both the potential and the current limitations of the newly coupled system, setting the stage for its continued development and a more comprehensive evaluation in future work.

4.4 Discussion

In this chapter, an updated land-surface scheme was implemented within the regional climate model RegCM, with the goal of creating a new two-way coupled system between RegCM5.0 and eCLM, a fork of the Community Land Model version 5.0. The two models and the adopted coupling framework were described in Section 4.1, outlining the scientific motivation behind the modelling choices made in this development. By adopting a multiple-executable scheme coupled through OASIS3-MCT, a flexible and modular approach was achieved, requiring minimal code alterations and facilitating future updates.

To ensure eCLM could adequately represent local river discharge, offline simulations over Italy were first conducted, using atmospheric forcing from reanalysis driven RegCM4.7 and RegCM5.0 simulations. These experiments covered the period 2000 to 2009, with the first year excluded from analysis and used as a spin up period. The MOSART module available inside eCLM was activated, and a pre-processing protocol was developed to ensure that MOSART could generate a coherent river network across any chosen domain. This protocol will be refined in future stages of the project.

The two offline simulations directly produced river discharge as an output variable. The simulate discharge was evaluated against both previous RegCM driven CHyM simulations and local observations. The eCLM-MOSART outputs showed comparable performance to CHyM in reproducing observed discharge. CHyM has a tendency to produce more intense extremes, whereas eCLM-MOSART underestimates peak flows. Observed discharge values generally fell between the two model behaviours.

Preliminary coupled simulations were also performed to evaluate the system's performance. However, the short timeseries obtained prevents us from drawing broad conclusions. The three months simulated showed similar precipitation patterns compared to offline results, but exhibited a drying trend in discharge towards the end of the period that was not consistent with the precipitation pattern. This discrepancy will be further investigated to better understand its origin. Possible causes include issues in flux exchange between the coupling scheme or insufficient spin up information provided to the model. Future work will extend these simulations over longer time periods and a more thorough evaluation of outputs will be

performed.

Nevertheless, the offline simulations demonstrated that eCLM can successfully simulate river discharge through its internal MOSART module, with no need for an external hydrological model. This integration streamlines the process and enhances our ability to depict hydrological processes in the region. Although fully coupled long term simulation is not available yet, future research could extend this framework beyond evaluation periods, and investigate how the RegCM-eCLM system, with its improved land-surface scheme, influences climate change projections. Though this part of the work is still in progress, the results obtained so far are providing a promising foundation for future development. Moreover, the inclusion of eCLM in the RegCM system will benefit other applications, as its advancements over CLM4.5 extend well beyond hydrological representation.

The improvements achieved with advanced land-surface schemes and convection permitting simulations presented so far in this thesis have a clear impact on simulated river discharge. Enhanced model performance supports a better understanding of regional discharge patterns and strengthens the reliability of climate change projections. A more accurate comprehension of future drought and flood behaviour is evidently valuable to society, as human activities heavily depend on river networks. Furthermore, hydrological modelling can have direct and practical applications beyond scientific research. The following chapter presents such an example: a case study of an extreme flood event that hit southern Brazil in 2024. In that work, hydrological modelling and river discharge information were incorporated into an climate change attribution analysis of the event. The inclusion of this data expanded the scope of the study and improved the understanding of the record breaking floods, highlighting the potential of hydro-climate modelling in real-world applications.

Chapter 5

Application of regional hydrological projections in real world events: attribution of a flood event in Southern Brazil in 2024.

Though there is solid scientific interest to studying the capacity of climate and hydrological models to mimic the water cycle from a purely theoretical perspective, the outcome of this kind of research can also have direct applicability on real world issues. Studying long term trends of hydrological variables under climate change already has an important role in planning, for example, adaptation measures in a specific region, but to study how a specific disastrous event observed in present day climate will evolve in future scenarios is also very much needed. This could help not only to answer the question how much is climate change already influencing today's climate, but also to have a more clear information on how this influence could evolve in relation to the hazardous event in future climates.

The world of extreme event attribution has gain importance in recent years, as a need to understand whether climate change is playing a role in so called natural disasters has grown. With a scientific consensus on the existence of anthropogenic global warming, the research community has shown there is also a trend of increase in intensity and frequency of extreme events ([20]). The inherent low-frequency of extreme events creates a challenge when studying them and analysing their long term evolution under a changing climate. Moreover, we may be interested to know if a specific event is attributable to climate change and whether it will become more frequent in the following decades. In terms of policy making and regional adaptation strategies, there is often an interest in knowing about one type of event that may occur in a specific region.

In this context, different frameworks have been develop to assess whether or

not climate change attribution is possible for a given case. Often the division has been made into probabilistic approaches and "risk-based" story line analysis ([105], [106]), but recently a third category of analogue methods has also been used in research works ([15]). An additional burden on existing attribution efforts is the use of hydrological variables in those studies, such as using river discharge directly and not only precipitation to study flood events. Long-term time series of observations are needed for these frameworks to have a solid understanding of the average behaviour of the river network and its variability and to capture as many previous extreme events as possible. River discharge observations are harder to obtain than precipitation. Indeed, they are not, for example, available in large-scale reanalysis such as ERA5 ([16]). Thus, few studies have been successful in attribution of specific streamflow flood events to global warming (e.g. [107]).

In late April and early May of 2024, the southern-most state of Brazil, Rio Grande do Sul, saw floods of massive record-breaking proportions. The large network of observation stations in the region's river network manage to capture the discharge during the event, although not all stations were properly working since several were damaged due to the violence of the flows. This extensive observation network has been present for decades, as the fluvial network plays a key role in the region, and a dataset of these observations, which begin in the mid 20^{th} century, is widely available. Therefore, this flood event meets the requirement for attempting an extreme event attribution study based on river discharge. Two different attribution methods will be use to analyse the event: an analogue attribution assessment based on the ClimaMeter protocol ([15]) and a statistical attribution study based on the World Weather Attribution protocol ([14]). These two attribution analysis will include the river discharge variable, based on the extensive station observation network and, in the case of the analogue framework, by the use of climate and hydrological modelling.

5.1 Event Description

The extreme flood event studied occurred between late April and early May 2024, when unprecedented rainfall affected the southernmost state of Brazil, Rio Grande do Sul (RS). The extreme and prolonged precipitation caused record-breaking floods across the region, inundating several major cities.

According to [108] the large-scale drivers of the event were linked to an anomalous heating in the western Indian Ocean. This warming generated an anomalous barotropic high-pressure system over south-eastern Brazil and strengthened the subtropical jet to its south. The enhanced jet stream induced an uplift over the region, leading to the development of a mesoscale convective system. Moreover, a strengthened low-level jet east of the Andes transported warm and moist air into

the RS, helping to stablish the heavy precipitation. Additionally, the passage of a cold front in April 28 further intensified rainfall over the region.

The peak of the precipitation event happened between April 29 and May 5, with a secondary burst of extreme precipitation on May 11 and 12. The highest daily rainfall amount was recorded in the municipality of Segredo, reaching 386.2mm, while several other stations reported over 300mm in 24 hours ([13]). The resulting flood affected around 15,000 km^2, much of it inside the Guaiba river basin. River levels increased dramatically: in the town of Muçum, on the Taquari river, water levels rose by more than 21 meters in just 24 hours, reaching discharges of over 13,000 $m^3.s^{-1}$ ([109]). In Porto Alegre, the state capital, peak discharge is estimated to have surpassed 300,000 $m^3.s^{-1}$ [13], and the Guaiba river exceeded its 3m flood level, reaching 5.37m at the height of the event.

A recent study has identified the Taquari and Jacuí rivers as the main contributors to the catastrophic flood levels experienced in Porto Alegre ([110]). The Taquari river was primarly responsible for the peak discharge, whereas the Jacuí river determined the long duration of the high water levels. Additionally, the above average precipitation seen throughout April ([109]) potentially worsened the draining conditions of the soil, aggravating the flood severity.

Notably, a similar but les extreme flood event occurred in the state in September 2023, about eight months earlier. During that event, intense rainfall over the Taquari basin caused severe floods that broke historical records in several towns ([111]). The occurrence of two record-breaking floods within such short interval has raised concern about the influence of global warming and natural variability in increasing the frequency and intensity of these events. Prior to the 2023 and 2024 floods, the most severe event on record had happened in 1941, referred to a "once-in-a-lifetime" flood. The recurrence of even more intense floods in recent years emphasized the need for flood management, and, should climate change be found to intensify such events, adaptation and mitigation strategies for the coming decades.

5.2 Methodology

5.2.1 Observations

To better understand the role of climate change on this extreme flood event, local observations, reanalysis data and model simulations were analysed. Local data was obtained from observation stations measuring both river discharge and precipitation, provided respectively by the Instituto Nacional de Meteorologia (INMET) and the Agência Nacional de Águas (ANA). Prior to the analysis, two groups of stations were selected: one long-term dataset and another representing the ex-

treme event. The former includes all stations which less than 10% missing daily data between 1960 and 2023, and the latter comprises all locations that captured the flood event without data gaps. To maximize observational coverage, the two groups do not contain the same stations. A preliminary analysis confirmed their comparability, and they are thus treated as equivalent for the purposes of this study.

5.2.2 Statistical Attribution of the Event

To assess the influence of anthropogenic warming on the 2024 flood event, the first framework applied was the World Weather Attribution (WWA) protocol, which follows a statistical attribution methodology ([14]). The analysis was performed using the long-term discharge and precipitation records of local observation stations, excluding data from 2024 to avoid bias from the event itself.

The WWA framework compares the distribution of observed extremes under two distinct climate conditions: a Counterfactual (CF) world and a Factual (F) world. The CF world represents a climate with little to moderate influence of anthropogenic emissions, whereas the F world reflects a climate strongly influenced by global warming. The two distributions are then analysed to assess if the return period of extreme events, of the same or greater magnitude, has any statistically significant difference.

For each variable, the yearly maximum value of the daily series was fitted to a Generalized Extreme Value (GEV) distribution, using the global mean surface temperature (GMST) as a covariate. Both the mean value and the standard deviation of the two periods are assumed to vary with GMST, whole the ratio remains constant. Two separated distributions are obtained: one representing present-day conditions (F) and one representing a cooler climate (CF). In the F world, the GMST anomaly for 2024 is plugged into the distribution, whereas a temperature 1.2°C lower is assumed for the CF world. Following the methodology described in section 4.3.2 of [14], both precipitation and discharge are assumed to scale exponentially with the smoothed global mean temperature. The maximum daily values of precipitation and discharge observed during the event were then computed and used to obtain the return period of events of the same or greater magnitude in both distributions.

Given the availability of observations several different stations, annual peaks from all locations were pooled together, treating each station's maxima as independent samples and assuming a homogenous distribution. Additional steps have been proposed in literature to ensure the validity of this assumptions ([112]) which have not been executed for this study, as the focus of this analysis is on assessing the relative shift occurring in event likelihood with global warming, rather than deriving precise return periods.

Table 5.1: Ensemble of models used from the CORDEX-CORE project and their respective ensemble member

GCM	Ensemble	RCM
MOHC-HadGEM2-ES	r1i1p1f1	GERICS-REMO2015
MOHC-HadGEM2-ES	r1i1p1f1	ICTP-RegCM4-7
MPI-M-MPI-ESM-LR	r1i1p1f1	GERICS-REMO2015
MPI-M-MPI-ESM-MR	r1i1p1f1	ICTP-RegCM4-7
NCC-NorESM1-M	r1i1p1f1	GERICS-REMO2015
NCC-NorESM1-M	r1i1p1f1	ICTP-RegCM4-7

Table 5.2: Ensemble of models used from the CMIP5 project and their respective ensemble member

GCM	Ensemble
BCC-CSM1-1-M	r1i1p1f1
CanESM2	r1i1p1f1
GFDL-ESM2M	r1i1p1f1
MIROC-ESM	r1i1p1f1
CNRM-CM5	r1i1p1f1
MPI-ESM-LR	r1i1p1f1
INMCM4	r1i1p1f1
CSIRO-Mk3-6-0	r1i1p1f1
MIROC5	r1i1p1f1
MPI-ESM-MR	r1i1p1f1
NorESM1-M	r1i1p1f1
CMCC-CMS	r1i1p1f1

5.2.3 Discharge Modelling

The hydrological model CHyM, described in Chapter 2, was also used in this study by having different climate model data as input. The CHyM runoff configuration was used to perform simulations forced by six RCMs from the CORDEX-CORE ensemble and twelve GCMs from CMIP5 (see Tables 5.1 and 5.2).

Daily runoff data from each model was routed through the entire South America domain for both a historical period (1970-2005) and a future projection under the RCP8.5 scenario (2006-2100). River discharge outputs were produced with at a daily timestep and a 6km spatial resolution. Given the spatial focus of the attribution study, only the domain covering southern Brazil and neighbouring regions (65°W to 40°W and 20°S to 55°S) was analysed in this chapter.

Model performance in representing the regional river discharge was assessed

Table 5.3: Ensemble of models used from the CMIP6 project and their respective ensemble member

GCM	Ensemble
CESM2	r4i1p1f1
CNRM-CM6-1-HR	r1i1p1f2
FGOALS-g3	r1i1p1f1
KACE-1-0-G	r1i1p1f1
MPI-ESM1-2-LR	r1i1p1f1
TaiESM1	r1i1p1f1
ACCESS-ESM1-5	r1i1p1f1
CESM2-WACCM	r1i1p1f1
CNRM-ESM2-1	r1i1p1f2
GFDL-CM4	r1i1p1f1
INM-CM4-8	r1i1p1f1
MIROC6	r1i1p1f1
MRI-ESM2-0	r1i1p1f1
UKESM1-0-LL	r1i1p1f2
CMCC-CM2-SR5	r1i1p1f1
EC-Earth3	r1i1p1f1
GFDL-ESM4	r1i1p1f1
INM-CM5-0	r1i1p1f1
NESM3	r1i1p1f1
CanESM5	r1i1p1f1
CNRM-CM6-1	r1i1p1f2
EC-Earth3-Veg	r1i1p1f1
HadGEM3-GC31-LL	r1i1p1f3
IPSL-CM6A-LR	r1i1p1f1

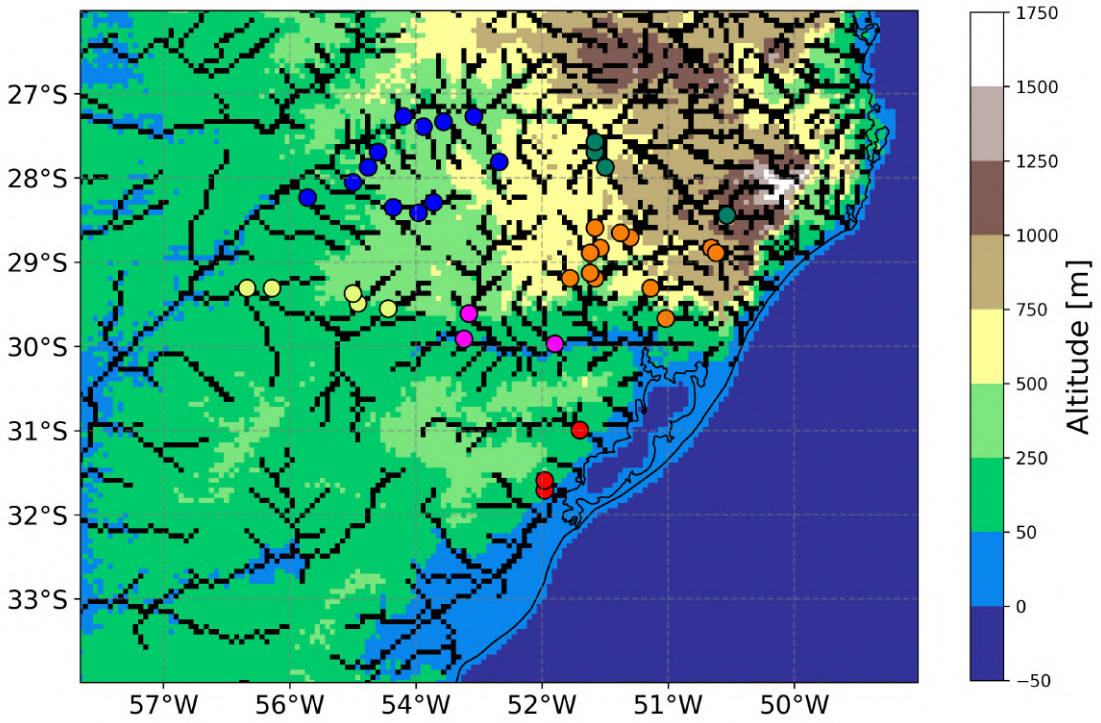

Figure 5.1: Altitude map of the Rio Grande do Sul region, with its river network shown in black. Coloured dots represent discharge stations used in the model validation. Stations were grouped together based on their hydrological characteristics: Serra Gaúcha (orange), Upper Uruguay and tributaries (green), Central Uruguay and tributaries (blue), Lower Uruguay and tributaries (yellow), Jacuí basin (pink) and South of Patos Lagoon (red)

by comparing the simulated discharge from the historical period against local observations. The validation followed the methodology described in Chapter 2, by extracting from CHyM's network the grid points corresponding to each observation station. The ensemble of stations were grouped into six hydrological sub-regions according to their drainage areas and the elevation of the topography (see Figure 5.1), to facilitate the analysis.

As described in Section 2.3, flow duration and peak discharge curves were constructed for each of the six clusters selected to evaluate the model's ability to reproduce observed river discharge. For both observed and simulated data, the yearly maximum discharge at each point was fitted to a Gumbel distribution, computing analytical discharge values for return periods (RP) ranging from 2 to 100 years.

5.2.4 Attribution of the event with the analogue method

The ClimaMeter attribution protocol ([15]) was also applied to analyse the 2024 extreme flood event. This framework is based on the analogue method, and has been used to provide rapid attributions of extreme events. It has been used for attributing several types of extreme event, including a preliminary analysis of the same extreme precipitation event that occurred in early May 2024 ([113]). The methodology identifies events with a similar synoptic patter to the one under investigation, also referred to in this chapter as the **target event**, within a selected time period. These similar cases, known as analogues, are then assessed in terms of their associated variables. For example, we can analyse whether the precipitation linked to the analogues of the factual (F) period has changed compared to those of the counterfactual (CF) period.

The event investigated in this chapter was defined by the nine-day average between April 26 and May 4 2024 for the relevant variables. Analogue identification was based on the 9-day average mean sea level pressure (msl) anomaly, which represents the signal of the **target event**. This pattern was compared to the 9-day daily running mean of the msl anomaly for all days within the time periods analysed. The Euclidean distance was computed between the **target event** and the running mean, and the dates for which this distance is under a selected threshold were selected as analogue events. These present a synoptic pattern considered most similar to the extreme event investigated.

This procedure was performed separately for the F and CF periods, and, for each, the average of the associated variables from the respective analogues was computed. The evolution of the composite patterns and associated variables of the analogues between the two time periods was evaluated. This study focuses on the three main associated variables: precipitation (pr), temperature (tas) and river discharge (dis). By comparing the analogue composites between CF and F periods, we can assess if any substantial changes occur with global warming.

The ClimaMeter provides a conditional analysis framework for attributing the event to climate change, distinct from the WWA protocol. Together they provide distinct but valuable perspectives on the effect of anthropogenic emissions on extreme hydrological events, such as the 2024 floods.

ERA5

The attribution framework was firstly applied to the ERA5 reanalysis dataset ([16]). The analogue events were determined for "past" (CF, 1960-1985) and "present" (F, 1986-2023) periods. The signal of the **target event** was also obtained from ERA5, using the average values between April 26^{th} and May 5^{th}, and represented by the msl anomaly in order to describe the synoptic pattern. The

spatial domain of the study (65°W to 40°W and 20°S to 55°S) captured both the msl anomaly responsible for the event and the region most severely affected by the floods. The associated variables precipitation and temperature were directly retrieved from ERA5, and complemented with long-term observations from local stations. These stations provided daily records of precipitation and discharge, which were also averaged across the analogue events and served as additional associated variables in the ERA5 attribution analysis.

Within the ClimaMeter protocol ([15]), indices were also computed to assess the influence of three natural variability modes on the event: the El Niño–Southern Oscillation (ENSO), the Atlantic Multidecadal Oscillation (AMO) and the Pacific Decadal Oscillation (PDO). The distributions of these indices in the analogues of both the CF and F periods, and statistically significant differences between them, were evaluated to identify the potential contribution of natural variability to the floods.

Climate models

The second part of the analogue analysis focused on climate model simulations, using the extended ClimaMeter protocol to assess analogue events under climate projections ([114]). For this purpose, simulations from the CORDEX-CORE, CMIP5 and CMIP6 projects were used (Tables 5.1 to 5.3). As in the ERA5 analysis, the analogues were identified using the msl anomaly, while precipitation and temperature were studied as associated variables.

Because of the major role of river flooding took in the 2024 event, an additional associated variable was included in the analysis, river discharge. Since discharge is not a standard output available in climate models, it was obtained from the CHyM hydrological simulations (see Section 2.2), which were individually forced by different CORDEX and CMIP5 models. This approach integrated river discharge into the analogue analysis of these two ensembles. CHyM simulations were not available for CMIP6 and their analogue analysis included only focus on precipitation and temperature as associated variables.

To evaluate the models' capability of reproducing the local climate, the CORDEX, CMIP5 and CMIP6 ensembles were compared against the ERA5 reanalysis dataset. The annual cycle and a time series of msl, pr and tas were plotted for both the models and ERA5. Since discharge is not available in ERA5, its validation was performed separately, as described in Section 5.2.3. For each model the correlation coefficient between its analogue events and the **target event** was computed to assess whether it should be included in the ensemble. The coefficient was compared to the correlation coefficient between ERA5's own analogue events and the **target event**, and only models exceeding a chosen threshold were selected. The ClimaMeter protocol also includes a bias-correction step, in which the each model's

msl anomalies are adjusted based on ERA5 data, while other variables are not corrected.

The CF period was defined as 1976 to 2005 for all model based analyses. The initial F period represents the present/near-future interval (2006 and 2035), for which their analogue events associated variables were examined. To extend the analysis further into the future, different Global Warming Levels (GWLs 1.5, 2.0, 3.0 and 4.0 °C) were considered as F periods. A GWL is characterized by the change in the GMST in comparison to pre-industrial conditions ([17]). Each GWL thus represents the climate state when the GMST reached a certain temperature above pre-industrial conditions (e.g. 1.5°C for GWL1.5). For CMIP5 and CMIP6, the GWL of each model were defined directly from GCMs simulations with climatology between 1850-1880. In contrast, the CORDEX simulations start in 1970 and, due to their limited spatial domain, cannot directly provide GMST values. Therefore, the GWLs of the driving GCMs of each RCM were used to determine the warming levels of the CORDEX ensemble.

The analogue analysis described above allows for the assessment of the link between climate change and extreme events similar to the 2024 floods. In the following section, we present the results obtained from both the ERA5 and climate model analogue analysis, outlining how precipitation, temperature, and river discharge respond to anthropogenic warming at different global warming levels.

5.3 Results

5.3.1 Event definition

As discussed previously, the average values for the event were calculated over the period between April 26 and May 4, although high flood levels in many locations persisted for several weeks afterwards. The variables of interest were obtained from both ERA5 data (msl anomaly, temperature anomaly and precipitation) and local stations (precipitation and discharge). The nine-day averages for these datasets are shown in Figure 5.2, with in panels A to C corresponding to ERA5 variables and D to E to local observations. A strong msl anomaly is visible south of the state of Rio Grande do Sul, while ERA precipitation displays very high nine-day average precipitation values, exceeding 30mm/day in some areas.

Some local stations experienced difficulties recording the event due to its severity, resulting in data gaps during the most intense days and unreliable averages for the whole event. Stations that successfully capture the event were manually selected for analysis and are shown in Figure 5.2. Several stations measured precipitation totals greater than those in ERA5, with several locations presenting 9-day averages over 50mm/day. Local reports confirm cumulative precipitation

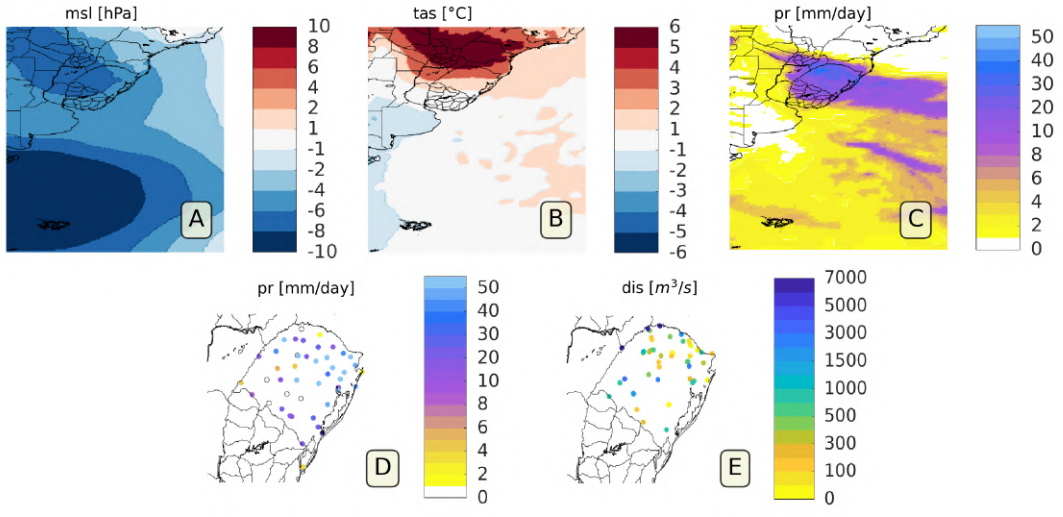

Figure 5.2: Definition of the target event in ERA5 (panels A to C), showing the nine-day average between 26/04/24 and 04/05/24 of mean sea level pressure anomaly [hPa], the temperature anomaly [°C], and precipitation [mm/day]. Panels D and E show the nine-day average for the same period from station data of precipitation [mm/day] and river discharge [$m^3.s^{-1}$].

surpassing 450mm during the event ([115]), suggesting a smoothing of spatial extremes in ERA5 and underestimated localized precipitation. The most intense precipitation recorded in stations occurred over the north-east of Rio Grande do Sul, while ERA5 indicated the most intense rainfall broadly over northern half of the state.

Observed discharge during the event reached thousands of $m^3.s^{-1}$ at several stations. The largest recorded flow occurred along the Uruguay River, the largest in the region. Nonetheless, even small basins experienced extremely intense flows in the 9 days. Moreover, extreme and localized downpours were concentrated in a single day in many smaller catchments, suggesting that the actual event intensity was much higher than suggested by the nine-day mean.

5.3.2 Statistical Attribution

The statistical attribution analysis was conducted using local observations. In Figure 5.3, the variable of interest (either discharge or precipitation) is shown in the y-axis, while the corresponding return time (RT) is displayed the x-axis. The fitted GEV distributions for the CF (in blue) and F (in red) periods are visibly distinct for both cases, and are intersected by the dashed black line, which represents the magnitude of the **target event**.

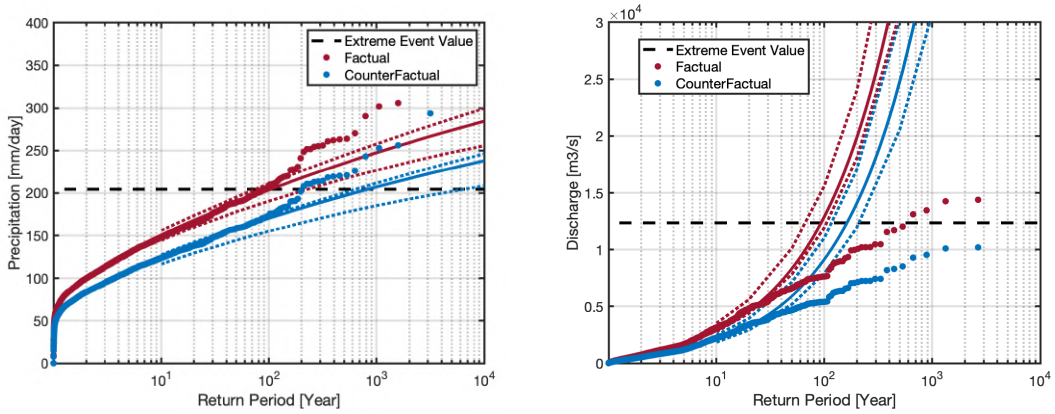

Precipitation Discharge

Figure 5.3: Fitted distributions of local observations for the CF and F periods following the WWA protocol ([14]), respectively in blue and red. The fitting used the yearly maxima of all stations in the region with more than 90% data present between 1960-2023, and the maximum daily value observed during the event was used as the target event magnitude (dashed black lines). Solid lines represent the fitted distribution and dashed lines represent the confidence intervals. Circles represent observed values.

Table 5.4 summarizes the results of the fitted distributions. Both variables display a statistically significant reduction (p-value < 0.05) in RT from the CF to the F period, indicating an increase in frequency of events of similar or greater magnitude under global warming. The probability of occurrence for discharge increased by approximately 1.7 times, whereas for precipitation, the rise was of approximately 8 times. This finding corresponds to a decrease in RT from over 800 years in the CF world to around 100 in the F world, indicating a very strong climate change influence in the frequency of extreme precipitation.

Table 5.4: Statistical attribution results for precipitation and discharge. The return time obtained and its confidence interval is displayed for both the Counterfactual and Factual Period, as well as the probability ratio between the two periods. The p-value attests whether the two distributions are significant different.

Variable	**Return time (CI) CF**	**Return time (CI) F**	**Probability ratio (CI)**	**p-value for ratio $\neq 1$ (one-sided)**
Precipitation	826.46 (639.64 - 6347.2)	103.20 (73.738 - 228.64)	8.0086 (5.1826 - 48.476)	0.0010
Discharge	161.60 (119.19- 211.25)	93.056 (68.663 - 105.60)	1.7366 (1.2861 - 2.7694)	0.0010

According to the WWA protocol ([14]), this results confirms the 2024 flood has become significantly more likely/frequent with the current levels of global warming. However, it is important to note that discharge extremes are more directly influenced by human intervention than precipitation. The studied domain includes several sources of human forcing, such as dams, irrigation withdrawal and reservoirs, which could modify streamflow. Human activity could modulate the observed discharge extremes, introducing additional uncertainty into the fitting and decoupling from a purely climate-driven signal.

These results will be complemented by the analogue-based attribution analyses presented in the following section, which explore how similar synoptic events have evolved under a warming climate.

5.3.3 Model validation

Hydrological validation

One sub-region of the Rio Grande do Sul state (stations highlighted in orange in Figure 5.1), which was strongly affected by the floods, was selected to assess CHyM's performance in reproducing river discharge (Figure 5.4). The sub-region is characterized by higher altitudes compared to the rest of the state and by steep terrain, conditions that contributed to the intense flash floods observed there during the event.

Figure 5.4 presents the validation results. The first column displays the flow duration curves, where simulation output is depicted in blue and observations in red. In both ensembles, CHyM successfully reproduces the shape of observations, although the simulated ensemble spread is larger than the observed. The CMIP5 ensemble presents the larger spread and tends to underestimate the observations, whereas CORDEX remains closer to observations, though both capture observations within their range.

The peak discharge curves (second column) display an underestimation of ob-

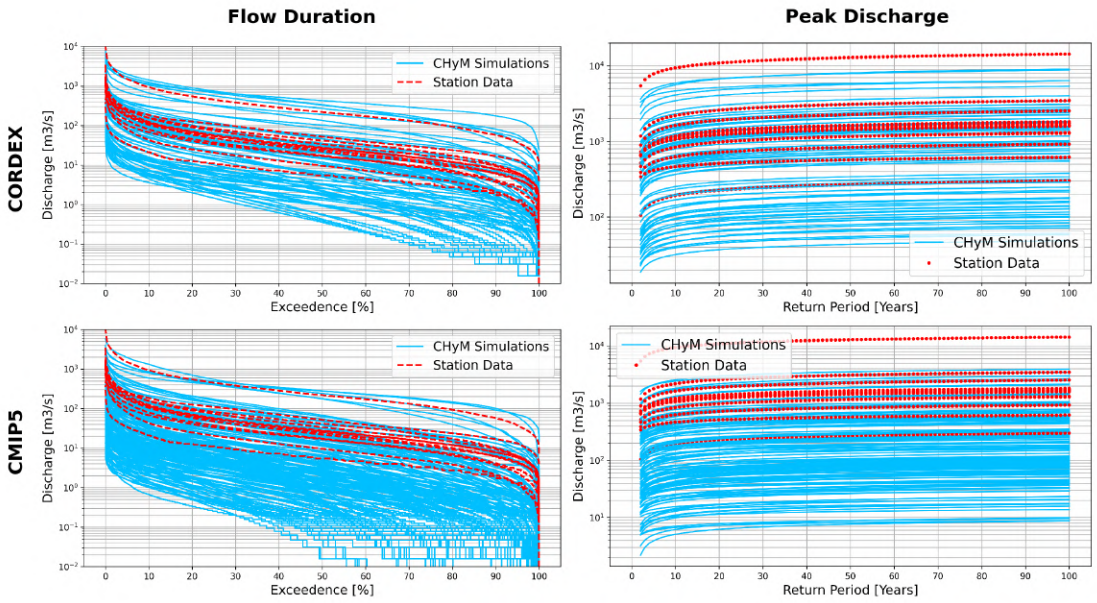

Figure 5.4: Flow duration curves (left) and peak discharge curves (right) for a subregion strongly affected by the flood (shown in orange in Figure 5.1). Observed data is compared to simulated discharge from the CHyM model forced by the CORDEX ensemble (top row) and the CMIP5 ensemble (bottom row). CHyM Simulations are shown as solid blue lines and observations as dashed red lines.

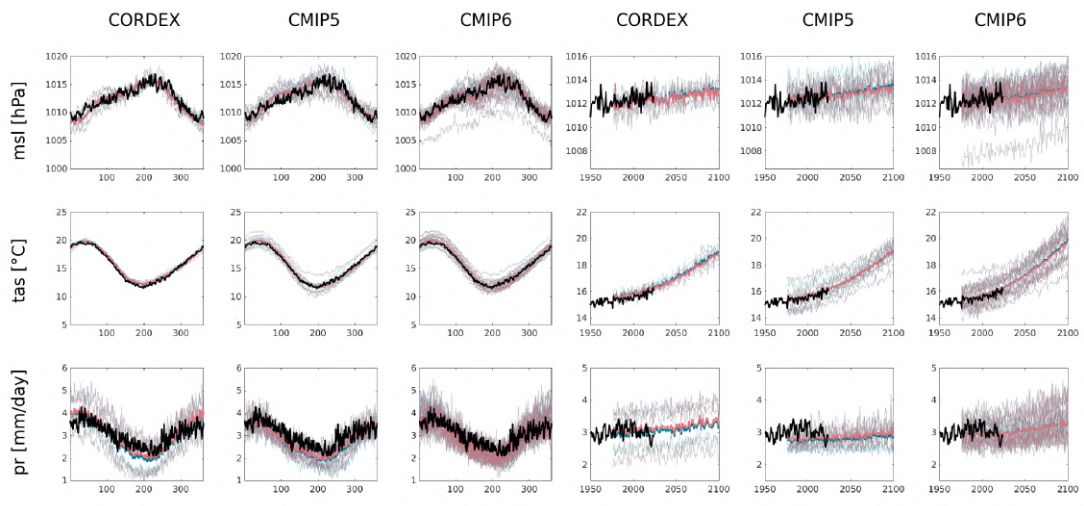

Figure 5.5: Annual cycles (first three columns) and time series (last three columns) of msl [hPa], tas [°C] and pr [mm/day] for non-bias corrected models in CORDEX, CMIP5 and CMIP6 ensembles during the reference period (1976-2005). ERA5 data are shown in black. Thick blue and red lines represent, respectively, the mean of all ensemble members and the mean of the selected models only. Thin lines indicate the individual models, with gray lines for selected models and blue lines for non-selected ones. The x-axis in the annual cycle represents days of the year, while in the time series it corresponds to the year of the data.

served extremes from both ensembles. CMIP5 models, in particular, have the strongest bias and a much larger spread than observations. Despite these issues, both CMIP5 and CORDEX driven CHyM ensembles have a satisfactory performance in reproducing the local river flow, validating their use for the attribution analysis conducted in this chapter.

Model Validation for the Analogue Attribution

The models included in each ensemble were evaluated against ERA5 to guarantee an adequate representation of the local climate (Figure 5.5). The annual cycles and the time series of msl, pr and tas were plotted, with ERA5 displayed in thick black lines. Thick blue and red lines respectively represent the ensemble mean of all available models and of the subset of selected models. Thin gray and blue lines represent respectively the individual selected and non-selected models. Overall, the models represent well observations, with precipitation exhibiting a larger inter-model variability than msl and tas.

Model selection (described in Section 5.2.4) resulted in including 5 out of 6

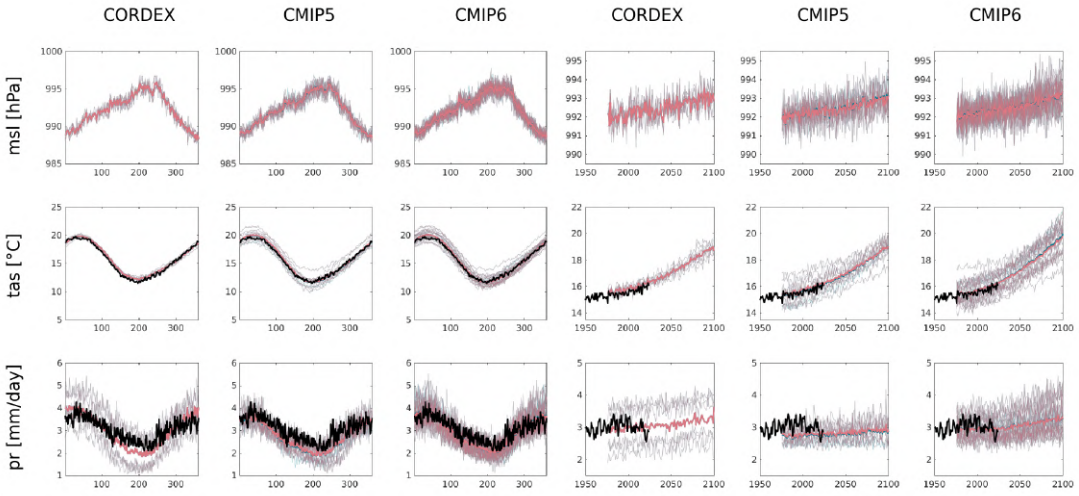

Figure 5.6: Annual cycles (first three columns) and time series (last three columns) of msl [hPa], tas [°C] and pr [mm/day] for bias corrected models in CORDEX, CMIP5 and CMIP6 ensembles during the reference period (1976-2005). ERA5 data are shown in black. Thick blue and red lines represent, respectively, the mean of all ensemble members and the mean of the selected models only. Thin lines indicate the individual models, with gray lines for selected models and blue lines for non-selected ones. The x-axis in the annual cycle represents days of the year, while in the time series it corresponds to the year of the data.

CORDEX models, 10 out of 12 CMIP5 models and 22 out of 24 CMIP6 models. A bias-correction step was then applied to the msl variable, and the selection procedure was repeated (Figure 5.6). No substantial increase of models selected after bias-correcting was obtained, increasing the CORDEX and CMIP5 ensembles by only one additional model each and leaving CMIP6 ensemble unchanged. Given the minimal improvements observed and the potential of introducing additional uncertainties in the analysis, the attribution study was continued with only the non-bias-corrected ensembles. These models already showed satisfactory representation of the studied variables

Once verified that the climate models successfully reproduce key variables, we proceeded to conduct the analogue attribution analysis and investigate how similar extreme events might evolve under climate change.

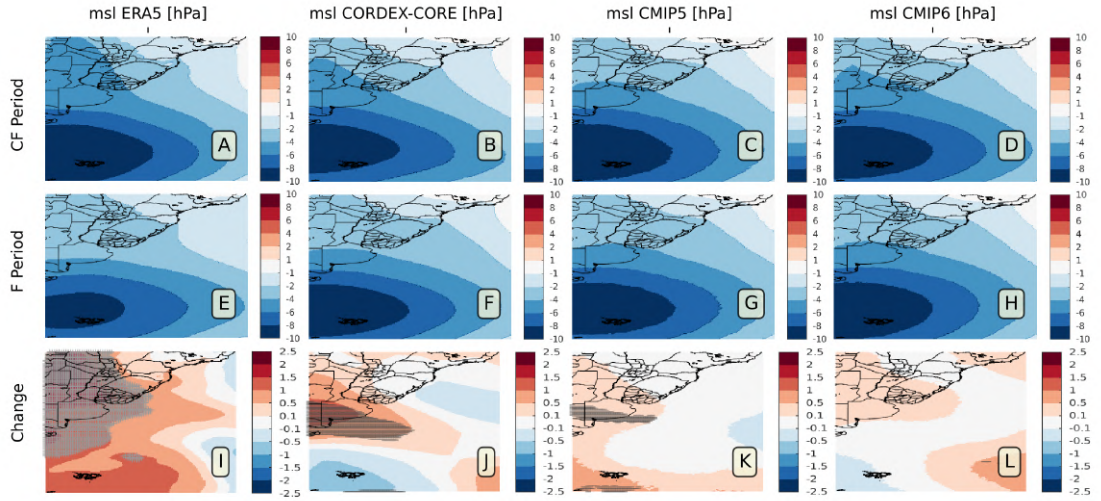

Figure 5.7: Composite of msl anomaly [hPa] of analogue events for the CF period (1976-2005, panels A-D), the F period (2006-2035, panels E-H) and their difference (panels I-L) for ERA5, CORDEX, CMIP5 and CMIP6. In the change panels of climate models, horizontal hatching indicates a consistent signal among at least 80% of models, and vertical hatching indicates significance at the 95% confidence level. For ERA5, crosses indicate significance at the 95% confidence level.

5.3.4 Analogue Method

ERA5

In Figure 5.7, the msl anomaly for the CF and F period of ERA5 are compared (panels A, E and I). The synoptic pattern is similar between the two periods, although the F period shows a weaker negative anomaly west of the Brazilian border, resulting in a significant increase of over 2hPa in msl. For ERA5 variables, crosses indicate the statistical significance of change at the 95% confidence level calculated with a bootstrap technique with a Student T test. Figure 5.8 shows the changes in associated variables between the same CF and F periods. The temperature anomaly (panel B) decreases significantly over most of the state, with overall variations between -0.1 and -1 °C. The precipitation from ERA5 (panel A) showed decrease in the central areas and an increase along the southern and northern borders, with variations between -4 to +4mm/day. Statistical significance was found for the regions with most intense precipitation change. The northern part of Rio Grande do Sul, which was most severely affected by the event, coincides with the strongest precipitation increase displayed.

Changes obtained from local stations for precipitation and discharge are exhibited in panels C and D of Figure 5.8. The spatial pattern of precipitation change

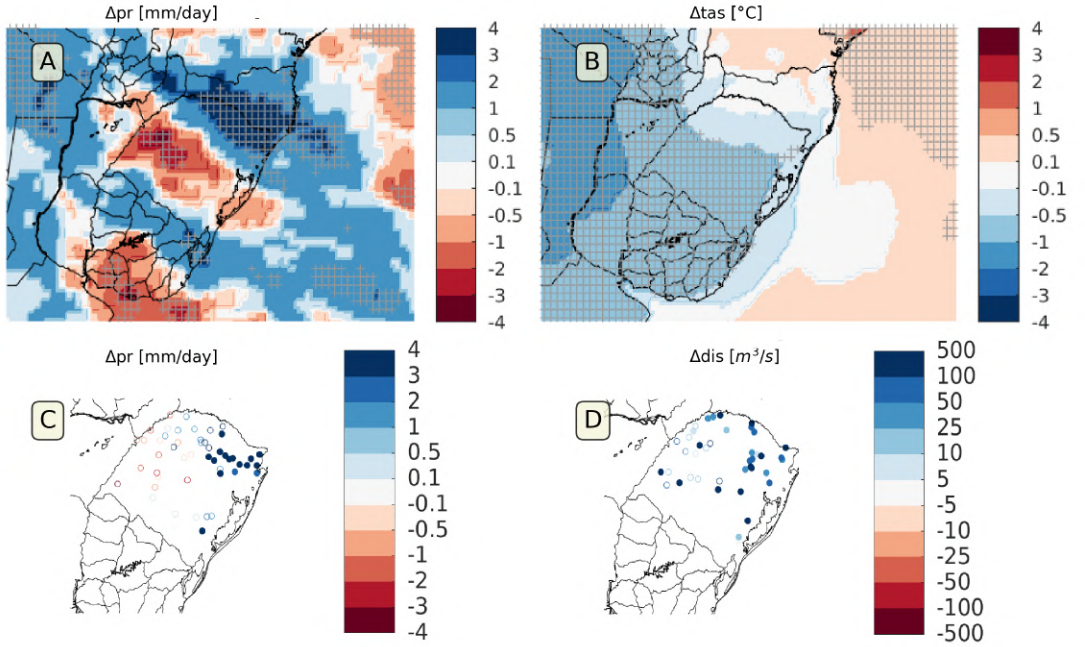

Figure 5.8: Composite change of variables associated with analogue events for ERA5 (A,B) and station observation (C,D). Changes are computed between the "past" (1950-1986) and "present" (1987-2022) for : (A) precipitation [mm/day]; (B) temperature anomaly [°C]; (C) observed precipitation [mm/day]; and (D) observed river discharge [$m^3.s^{-1}$]. In panels A and B, crosses represent statistically significant changes at the 95% confidence level. In panels C and D, filled circles represent significant changes at the 95% confidence level, whereas empty circles represent non-significant ones.

matches that of ERA5, with both showing the dipole of increased and decreased intensity. The station data indicated a stronger increase, with a larger proportion of the state displaying rises above 3mm/day. Filled dots represent stations with statistically significant changes, whereas open dots refer to non-significant changes. All precipitation stations with a significant signal showed positive changes of at least +2mm/day, located mostly in the northern-eastern part of the state, with one outlier in the southern Patos Lagoon region.

Discharge stations displayed only positive changes in the analogues, often exceeding $+100m^3s^{-1}$. Several stations showed statistically significant increases, largely concentrated in the northeastern region. Furthermore, whenever a station with significant precipitation increase was nearby, corresponding discharge stations also consistently exhibited a significant rise.

To investigate the role of natural variability in the extreme event, the distributions of indices representing three natural variability modes were compared for the CF and F periods (Figure 5.9) of the ERA5 analogue study, following the ClimaMeter protocol. No significant change was found for the AMO index in-between periods (p-value = 0.05783), while both ENSO and PDO indices have significantly distinct distributions for the two periods (p-values respectively 0.0092 and 0.01816). Therefore, we cannot statistically discard a possible effect of natural variability in the analogue changes, although this finding does not guarantee its impact. ENSO is known to modulate precipitation in the region, increasing precipitation during its positive El Niño phase. During the **target event**, however, the ENSO index used in the ClimaMeter protocol indicates a weak El Niño phase in April and neutral conditions in May (0.89 and 0.35, respectively) of 2024. These anomalies are insufficient to explain the exeptional intensity of the extreme precipitation observed. According to the ClimaMeter protocol, **natural variability alone cannot explain the increases in precipitation and discharge found over the region**.

Global and regional climate models changes

The analysis of analogue change was extended to climate projections to assess the evolution between F and CF periods in different model ensembles. The discharge variable present in this section for the CORDEX and CMIP5 ensembles was obtained from the CHyM hydrological model, which used the ensemble members as forcing and was validated in Section 5.3.3.

In Figure 5.7, the msl anomalies corresponding the analogue events are displayed for the following periods: CF from 1976 to 2005, and F from 2006 to 2035. This comparison represents the "past" versus "present" or near-future. Across all ensembles, the msl anomaly remains comparable between periods, showing a slight decrease in intensity but maintaining a similar synoptic pattern. The magnitude

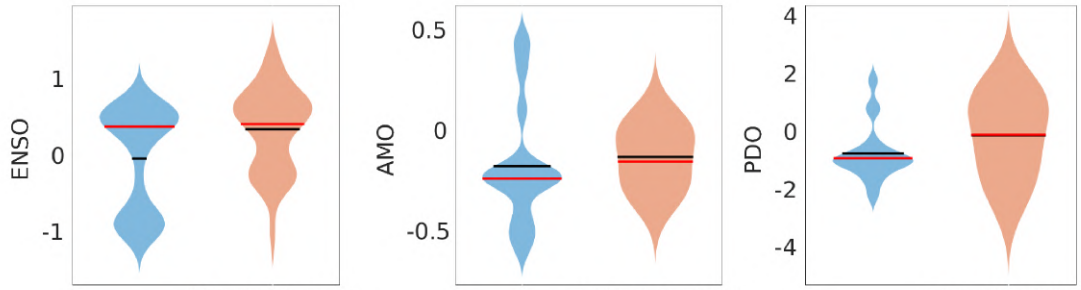

Figure 5.9: Distributions of natural variability indices (ENSO, AMO and PDO) during analogue events for the F (in orange, 1985-2023) and CF (in blue, 1960-1985) periods in the ERA5 analogue attribution analysis. The two distributions are statistically indistinguishable for AMO (p-value>0.05), but different significantly for ENSO and PDO (p-values<0.05).

of change remained under 1.5hPa in all ensembles, although a consistent change appears over the Buenos Aires province in northern Argentina for the CMIP5 and CORDEX models. In the model's change panels, horizontal hatching indicates a consistent signal among at least 80% of ensemble members, whereas vertical hatching translates to a statistically significant change at the 95% confidence level calculated with a Student T test and controlled for the false discovery rate using the Benjamini–Hochberg method ([116]).

The changes in the composite of analogue events are displayed in Figure 5.10. An overall increase of temperature between 0.1 and 2 °C is found in the three ensembles in the F period, with the signal being most consistent and significant for the CMIP6 ensemble and least for the CORDEX. The change in precipitation of CORDEX models display the greatest spatial variability of the three ensembles, with most of the state showing increases of up to 4mm/day and localized decreases of up to 1mm/day. For CORDEX, the change in discharge has a negative sign corresponding to the location of the maximum observed discharge during the event and varying in signs partially matching the direction of precipitation change. CMIP5 models, in contrast, show increases in precipitation and discharge of respectively up to 2mm/day and over $100 m^3 s^{-1}$ in almost all locations. The CMIP6 ensemble does not include the discharge variable, but displays a widespread precipitation increase, which is slightly more intense than that of CMIP5.

GWLs Projections

To assess changes further into the future, periods corresponding to different GWLs were used as F periods, while keeping the same years (1976-2005) as the CF reference. The msl anomaly for the CORDEX ensemble cross the different F periods

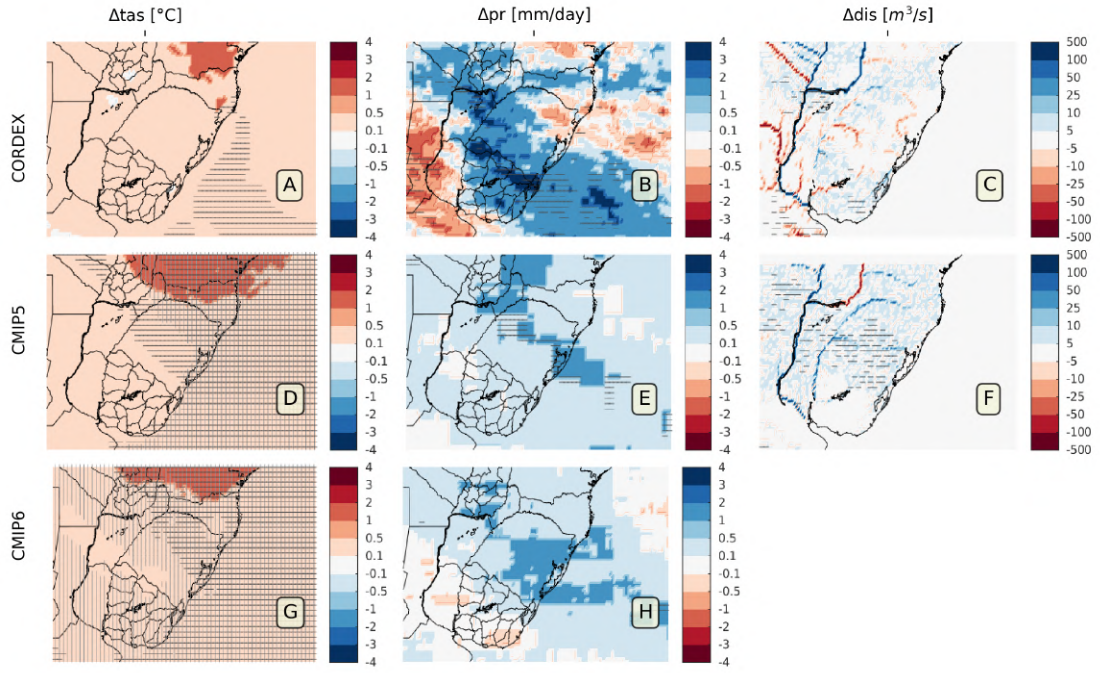

Figure 5.10: Composite change in variables associated with analogue events for the CORDEX, CMIP5 and CMIP6 ensembles, including CHyM model outputs (used only with CORDEX and CMIP5). Columns display changes between the F (2006-2035) and CF (1976-2005) periods in: (A,D,G) temperature anomaly [°C]; (B,E,H) precipitation [mm/day]; (C,F) river discharge [$m^3.s^{-1}$]. In the change panels, horizontal hatching indicates a consistent signal between at least 80% of models and vertical hatching indicates significance at the 95% confidence level.

(Figure 5.11) remains similar, with the CF period showing a slightly more intense anomaly. As expected, increasing global warming leads to a larger positive temperature change by GWL 4°C, with all regions showing statistical significance.

Precipitation tends to increase with climate change, although with considerable spatial variability, remaining around 3mm/day on average. Consistency among models is highest in regions of most intense change for precipitation. River discharge increases in the region, with large rivers often showing consistent increases of over $100m^3s^{-1}$. Although the general trend shows greater changes at higher GWLs, the increase is not monotone. For instance, several rivers display a higher discharge increase at GWLs 2°C and 4°C than at GWL 3°C. The enhanced spatial variability observed here, compared to the next two ensembles, aligns with expectations for RCMs, which typically exhibit more variability than GCMs due to the higher spatial resolution. Similar variations are also found in the average change seen for the different GWLs, compute across the whole MAMJ period rather than only for extreme events (Figure 5.12).

For the CMIP5 ensemble, the results are broadly similar to the CORDEX composite, though represented at a coarser resolution. A small weakening of the msl anomaly with rising GWLs is observed, leading to a a -2hPa change over the Buenos Aires province. Temperature increases are similar to those of CORDEX models, becoming more consistent and statistically significant at higher GWLs, with fully significant changes by GWL 4°C. Precipitation increases across the majority of the region, although this increase is consistent only in small patches. The intensity of the increase is lower than in CORDEX, not surpassing 2mm/day.

The synoptic pattern of msl investigated for the extreme event appears to generate precipitation responses that vary spatially in the CMIP5 ensemble. At GWL 3°C, the region of increased precipitation shifts northward along the coastline and, at GWL 4°C, it moves offshore (not shown). When examining the average changes across the whole period (Figure 5.14), rather than only the analogue events, a wettening trend occurs over the domain in both the discharge and precipitation, with a localized drying patch in the northwestern corner. No precipitation peak is observed at GWL 2°C, reinforcing the hypothesis that the apparent maximum in Figure 5.13 reflects a spatial shift in precipitation linked to the msl anomaly characterising of the **target event**.

In CMIP5 models, discharge increases at all the GWLs, with limited variation between periods. The highest consistency is found at GWL 2°C, and the changes remain below $+100m^3s^{-1}$ in the Rio Grande do Sul region. Because the resolution of CMIP5 GCMs forcing the CHyM simulations is coarser than that of CORDEX RCMs, the simulations are less likely to capture localized hydrological responses, leading to give a more spatially uniform signal.

The composite of analogue changes in the CMIP6 ensemble (Figure 5.15)

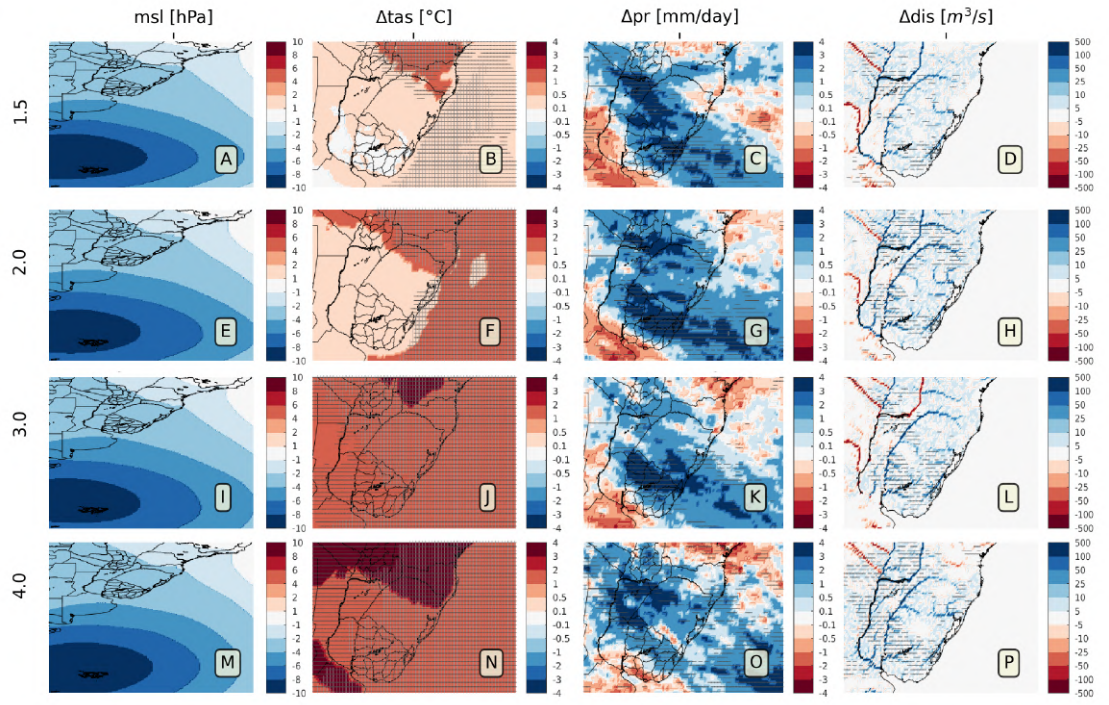

Figure 5.11: Composite of variables associated with analogue events in the CORDEX ensemble combined with the CHyM model, for different Global Warming Levels serving as F periods, relative to the reference period (CF, 1976-2005). Columns represent: (A,E,I,M) msl during the F period [hPa]; (B,F,J,N) change in temperature anomaly [°C]; (C,G,K,O) change in precipitation [mm/day]; and (D,H,L,P) change in river discharge [$m^3.s^{-1}$]. Changes are calculated relative to the reference period (1976-2005) and, in the change panels, horizontal hatching indicates a consistent signal between at least 80% of models and vertical hatching indicates significance at the 95% confidence level.

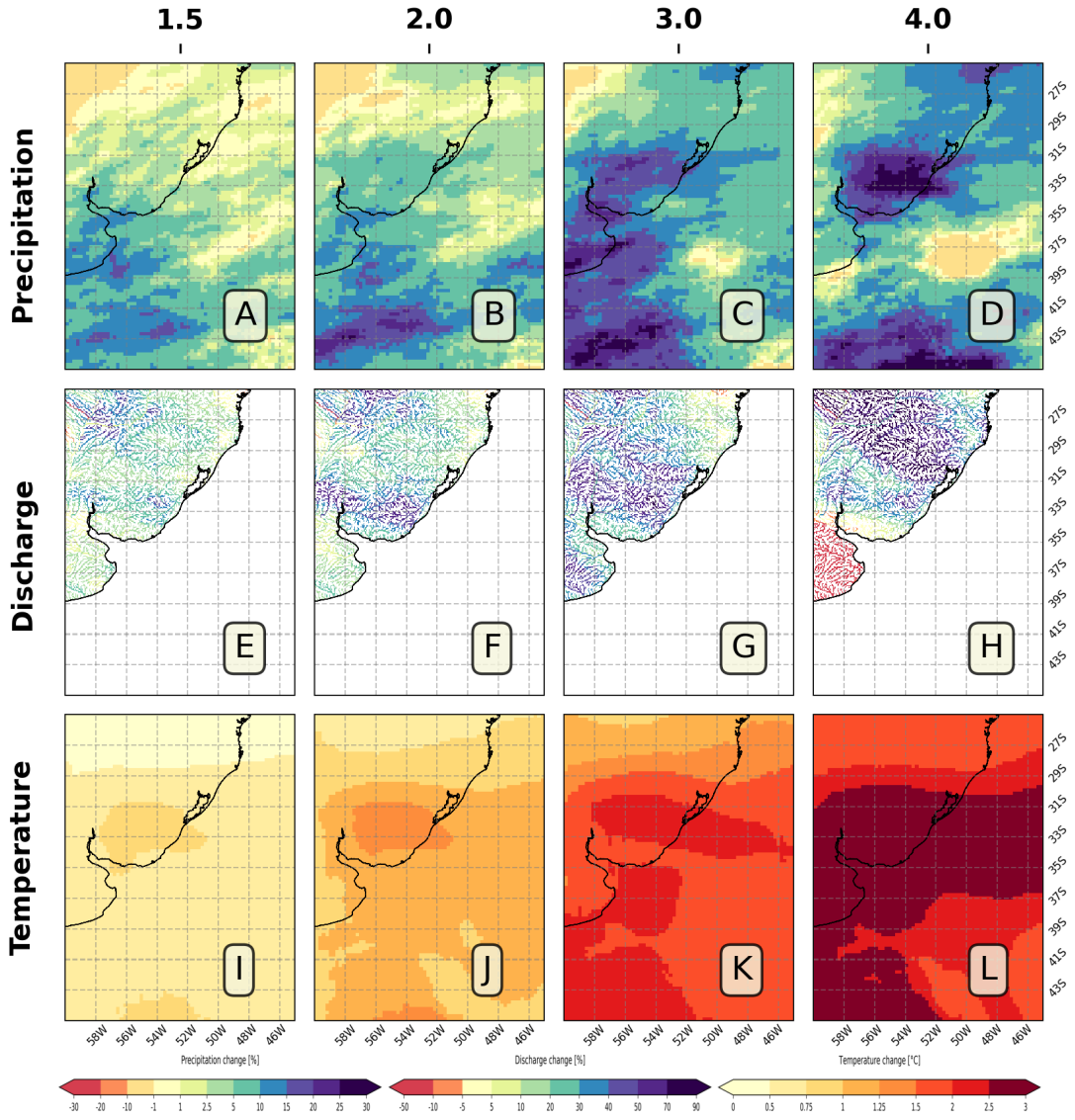

Figure 5.12: Average change for MAMJ period for different GWLs, relative to the reference period (1976-2005) for the CORDEX ensemble combined with CHyM model outputs. Rows represent: (A-D) change in precipitation [mm/day]; (E-H) change in river discharge $[m^3.s^{-1}]$; and (I-L) change in temperature [°C].

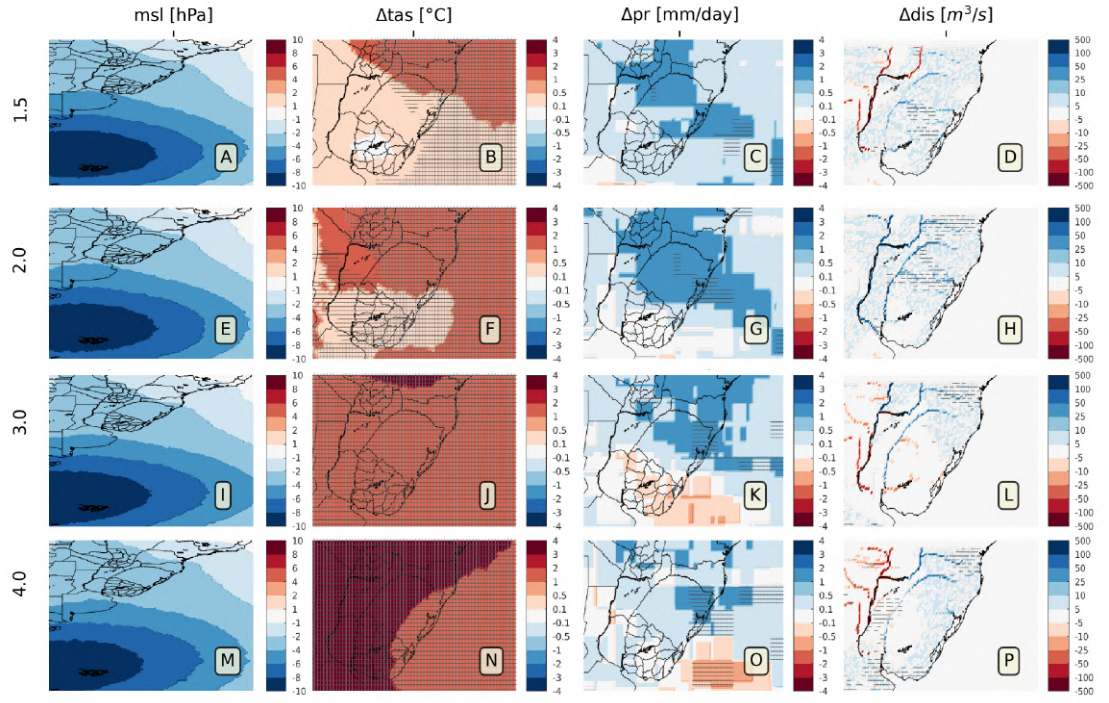

Figure 5.13: Composite of variables associated with analogue events in the CMIP5 ensemble combined with the CHyM model, for different Global Warming Levels serving as F periods, relative to the reference period (CF, 1976-2005). Columns represent: (A,E,I,M) msl during the F period [hPa]; (B,F,J,N) change in temperature anomaly [°C]; (C,G,K,O) change in precipitation [mm/day]; and (D,H,L,P) change in river discharge [$m^3.s^{-1}$]. Changes are calculated relative to the reference period (1976-2005) and, in the change panels, horizontal hatching indicates a consistent signal between at least 80% of models and vertical hatching indicates significance at the 95% confidence level.

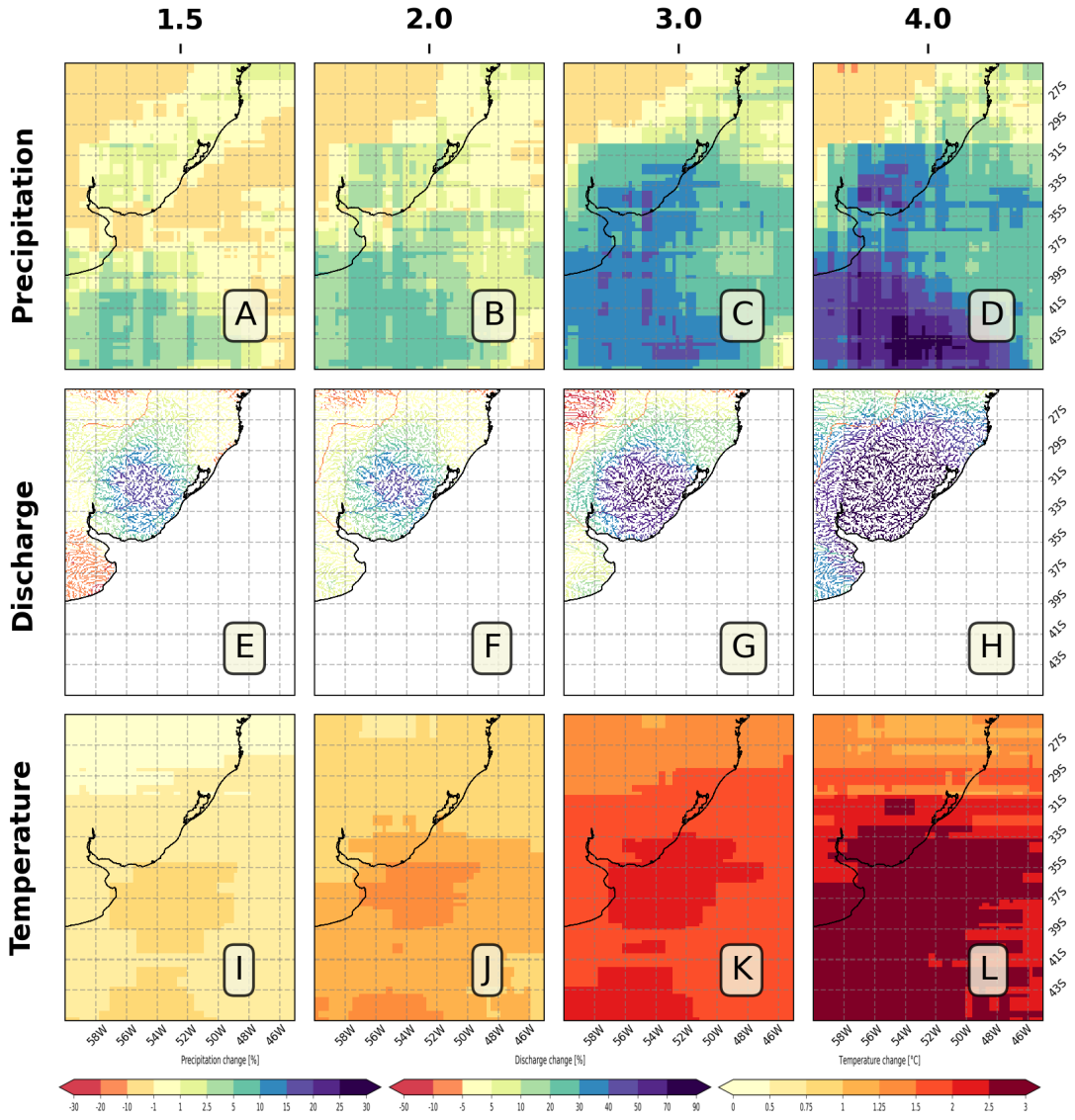

Figure 5.14: Average change for MAMJ period for different GWLs, relative to the reference period (1976-2005) for the CMIP5 ensemble combined with CHyM model outputs. Rows represent: (A-D) change in precipitation [mm/day]; (E-H) change in river discharge [$m^3.s^{-1}$]; and (I-L) change in temperature [°C].

does not include discharge, as previously discussed. The slight weakening in msl anomaly seen in other ensemble is also reproduced here. The CMIP6 ensemble displays the highest and more significant increases in temperature, with most of the region already showing significant warming at GWL 1.5°C. Unlike CMIP5, precipitation does not peak at GWL 2°C, instead it increases steadily with higher degrees of warming, becoming more consistent and significant. The magnitude of change reaches around 1-2mm/day at higher GWLs, slightly weaker than CORDEX increases. No spatial shift of precipitation patterns is visible here. Instead, the same areas present increases that intensify with warming. Spatial variability is also less pronounced than for CORDEX's RCMs, as expected with GCMs, leading to a more uniform signal without any negative precipitation changes over the state. These patterns are consistent with those found for the mean change of the full period (Figure 5.16).

Across the three ensembles, the composite analogue changes indicate increasing intensity of precipitation and discharge under a warming climate. Although it remains difficult to quantify the increases and their detailed spatial distributions, the results are consistent in pointing to a stronger magnitude of precipitation and discharge in similar events in the Rio Grande do Sul region with a warming climate. At higher GWLs, not only does some models project more intense increases, but there is a more consistent signal among different models, reinforcing the confidence in this intensification.

Overall, the analogue attribution study across the different ensembles reveals a consistent signal of intensifying hydrological extremes in Southern Brazil under progressive global warming. Despite variations in spatial patterns and magnitude between the CORDEX, CMIP5, and CMIP6 ensembles, results indicate that events similar to the 2024 flood are expected to become more intense in a warmer climate. Differences between ensembles reflect their spatial resolution and their description of regional processes, but the convergence of their overall trends strengthens confidence in the attribution of such extreme events to anthropogenic climate change. The following section discusses these results in the context of previous findings and their implications for flood adaptation strategies in the region.

5.4 Discussion and applications of hydrological modelling

The extreme event discussed in this chapter was defined by the nine-day average between 26/04/2024 and 04/05/2024, using ERA5 reanalysis data or local observations. The mean sea level pressure anomaly displayed a strong negative anomaly over the ocean east of the coast of Argentina. Although the region is influenced by

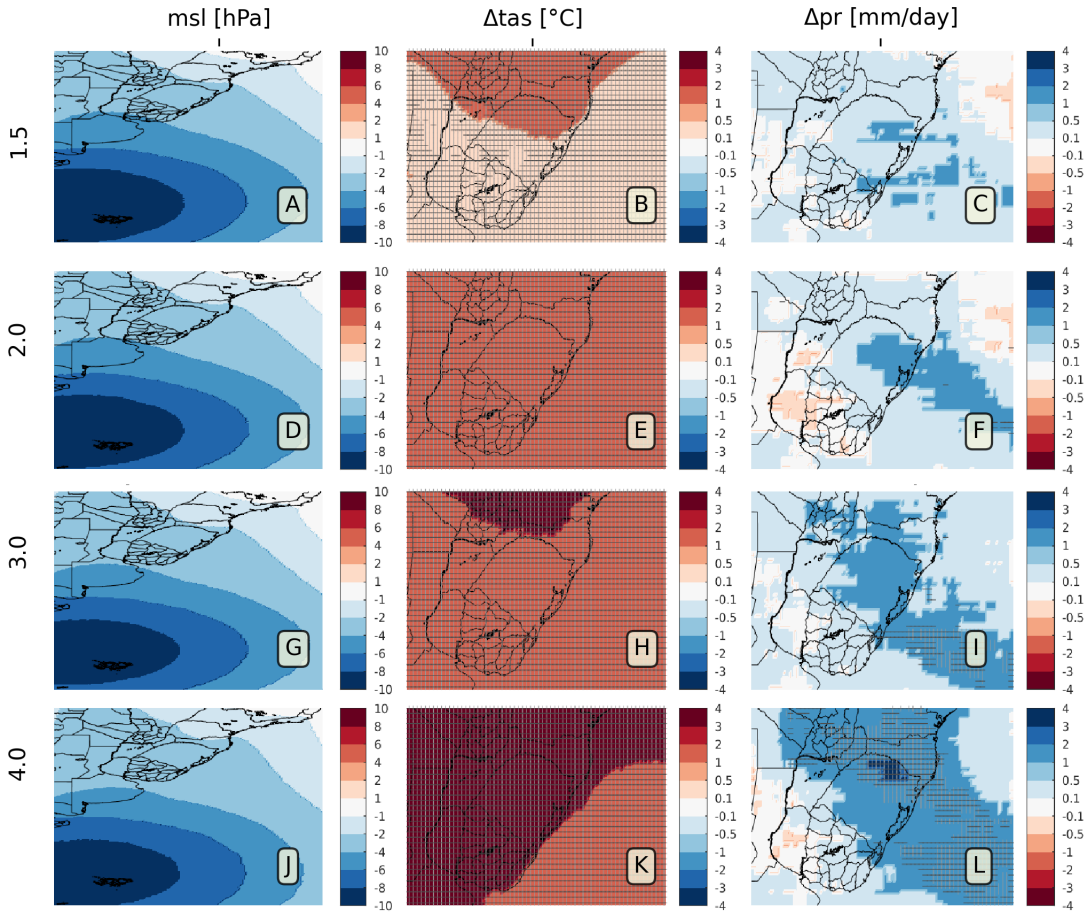

Figure 5.15: Composite of variables associated with analogue events in the CMIP6 ensemble combined with the CHyM model, for different Global Warming Levels serving as F periods, relative to the reference period (CF, 1976-2005). Columns represent: (A,D,G,J) msl during the F period [hPa]; (B,E,H,K) change in temperature anomaly [°C]; and (C,F,I,L) change in precipitation [mm/day]. Changes are calculated relative to the reference period (1976-2005) and, in the change panels, horizontal hatching indicates a consistent signal between at least 80% of models and vertical hatching indicates significance at the 95% confidence level.

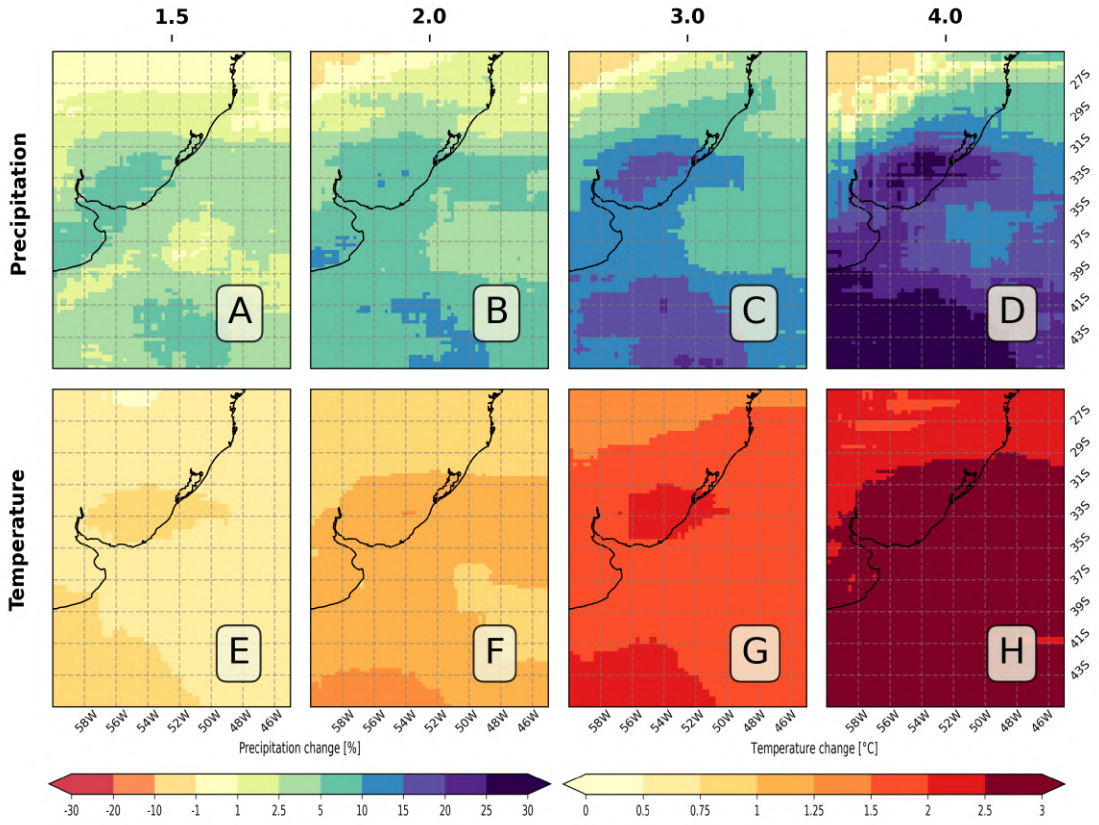

Figure 5.16: Average change for MAMJ period for different GWLs, relative to the reference period (1976-2005) for the CMIP6 ensemble. Rows represent: (A-D) change in precipitation [mm/day]; and (E-H) change in temperature [°C].

ENSO, the weak El Niño conditions during the event are not sufficient to explain its intensity, and, though the region may experience considerable rainfall during April and May, it does not explain such high magnitudes of precipitation. Several stations recorded nine-day average values exceeding 50mm/day, leading to prolonged flood conditions in some regions of the state, including its capital Porto Alegre.

The WWA protocol, applied to local precipitation and discharge data, showed a statistically significant increase in frequency (or decrease in return times) of events of the same or greater magnitude between the counterfactual and the factual period, corresponding to a rise in the global mean surface temperature of 1.2 °C. The analogue attribution combining ERA5 and local stations indicated that natural variability alone cannot explain the observed increase in precipitation and discharge, particularly over the northern part of the state. While the effect of ENSO and PDO on the analogue events cannot be discarded, the weak to neutral El Niño conditions at the time of the event were likely to drive such extreme precipitation. Although ClimaMeter and WWA work with very distinct attribution frameworks, with the former being a conditional protocol and latter not, both analyses consistently indicated amplification of extreme events similar to the floods of April/May 2024 in Southern Brazil under anthropogenic climate change.

The analogue attribution was extended to climate and hydrological model ensembles at different Global Warming levels (1.5°C, 2°C, 3°C and 4°C) relative to a historical period. At all GWLs, both precipitation and discharge increased during analogue events. The CORDEX ensemble exhibited the most intense, though with high spatial variability, changes, whereas CMIP6 has very uniform and consistent increases. CMIP5 models showed a peak in precipitation for GWL 2°C, corresponding to a spatial shift in region of strongest precipitation related to the same msl anomaly. No spatial shift was observed for CORDEX or CMIP6.

This study was made possible by the availability of long-term river discharge observations in Rio Grande do Sul, ensuring the reliability of our approach. The exceptional intensity of the 2024 flood severely damaged several observation stations, leading to data gaps during the event's peak, but the widespread presence of stations in the region guaranteed enough data was available. The long-term dataset included only stations with more than 90% daily data between 1960 and 2023, for a total of 40 stations. Over this period, significant human intervention altered the hydrological regime, as large dams were constructed in the region, specially after 2000, and the urbanization rate went up from 45% to 79% between 1960 and 990 ([117]. These changes likely affected extreme flow behaviour but are not represented in the hydrological model or attribution frameworks employed, which do not account for evolving human forcing.

Despite these limitations, this study successfully used different attribution

frameworks to study the extreme floods that hit Rio Grande do Sul in late April and early May of 2024. The results of a statistical protocol indicated events of similar or greater magnitude have become more frequent with anthropogenic warming. In addition, the analogue based method indicated that events with similar synoptic signatures tend to have higher precipitation and discharge magnitudes as temperatures rise.

The devastating impacts of the 2024 floods underline the urgency of incorporating such findings into adaptation planning. Strengthening flood defences, maintaining hydraulic infrastructure, and improving early warning and evacuation systems have been identified by local experts as critical priorities ([115]). Historically, events of comparable magnitude had not occurred since 1941, yet the analyses presented here suggest that such events may become substantially more frequent under continued warming.

The devastating economical and social impacts of the 2024 floods over Rio Grande do Sul highlight the need for taking into account these findings into adaptation and mitigation measures. Maintaining and updating flood defences and improving early warning systems have been identified as key by local experts ([115]). Similar levels of flooding had not been seen since 1941, however the results displayed in this chapter suggest it may become substantially more frequent under climate change. Beyond taking action to decrease the local contributions to climate change, the region must adapt to this uncomfortable prognostic.

This chapter also highlights the potential of using hydro-climate modelling for event attribution and risk assessment. While the CHyM model was used here in offline mode, without coupling to the driving climate model, future work could benefit from fully coupled hydro-climate simulations. Furthermore, the RCMs and GCMs used here operated at a maximum spatial resolution of 22 km; higher-resolution CP-RCMs, once available for South America, would likely capture small-scale precipitation and topographically driven effects more accurately. The improved performance of CORDEX-driven runs over CMIP5 already demonstrates the advantages of finer resolution.

This chapter also outlines the possibility of applying hydro-climate modelling in extreme event attribution. Offline simulations of the CHyM model were applied to the attribution protocol, with the highest spatial resolution equal to 22km. Provided that a CP-RCM ensemble becomes available over the region, a more detailed signal of precipitation would be likely captured, benefiting the representation of similar extreme events. The validation of CHyM simulations against observations already demonstrates an improved performance of CORDEX versus CMIP5 drive runs with the increased resolution.

Beyond extreme event attribution, hydrological modelling can have several applications inside long-term planning of water resource. Chapter 3 displays how

kilometre-scale hydrological simulations can inform projections of river discharge behaviour under climate change. Long term analysis can support decisions related groundwater management, reservoir operations and control of dams under global warming. Understanding whether river flows are projected to intensify or weaken in the coming decades is essential for environmental impact assessments and sustainable development. The applications of hydro-climate modelling are thus extensive and improvements in the field can support the management of hydrological risks in a warming world. Overall, this case study illustrates the potential of hydro-climate modelling to attribute and understand real-world extreme events, bridging the gap between scientific understanding and practical climate adaptation.

Conclusion

This PhD thesis investigated the projected evolution of the hydrological cycle under climate change. High-resolution modelling, combining hydrological and climate models, was used to study river discharge over the Italian territory. Kilometre scale simulations were validated against local observations and projected changes throughout the 21^{st} century were examined. In parallel to the above analysis, the development of a new structure for a two-way (atmospheric and land-surface) regional model coupled system has been completed to include enhanced land-surface representations by including a physically based hydrological module inside RegCM. The importance of hydroclimate modelling was then illustrated through a real-world application, using hydrological projections for a climate change attribution study.

With increasing temperatures, it is paramount to comprehend how high degrees of warming can impact the hydrological cycle. Although some variables have well-established responses to climate change, considerable uncertainty remains in projecting discharge and runoff. Several regions present large inter-model spreads, and, even when uncertainty is low, projecting extremes and seasonal variability presents further obstacles. Understanding whether a region is likely to become more flood or drought prone, though challenging, is essential for the region's future development and its water resources' management. Research such as this can help to clarify essential societal issues, supporting adaption and planning strategies.

Three research questions were posed at the beginning of this thesis. The first addressed the effects of using kilometre scale convection permitting (CP) climate simulations on the representation of the hydrological cycle and river discharge. Local interactions can strongly influence river discharge, specially over regions of complex topography and/or prone to intense precipitation events. Furthermore, uncertainty is expected to decrease at the CP resolution, given the removal of convective parametrization. However, a regional scale study assessing discharge behaviour using a multiple member CP ensemble had not been previously carried out.

To address this question, an ensemble of kilometre-scale CP regional climate models (CP-RCMs) was used to individually force the hydrological model CHyM,

simulating river discharge across Italy. This ensemble, developed as a part of the CORDEX-FPS convection project, covers the Great Alpine Domain. Hydrological simulations were forced by either runoff or temperature and precipitation fields of CP-RCMs, testing both available CHyM configurations, which were found to be equivalent. An ensemble of reanalysis-driven decade-long simulations (2000-2009) was used for evaluation against observed river discharge, showing good agreement and improved representation compared to lower-resolution ensembles.

Three additional decades (1996-2005, 2040-2049 and 2090-2099) were used to project river discharge under the RCP8.5 scenario. The results indicated an intensification of both drought and flood extremes under climate change, represented by the $Q_{7,10}$ and Q_{100} metrics. These changes were driven respectively by the average precipitation decrease and extreme precipitation increase. Mean discharge was projected to decline across most of Italy, influenced mainly by average autumn and winter precipitation decrease but modulated by the increase in spring and summer extreme precipitation. The seasonality analysis indicated an altitude dependent behaviour, captured only by high-resolution models and tied to changes in the Alpine snow regime. High altitude regions in the Po Valley displayed increased winter and early spring discharge but reduced late spring flow. Detecting such a shift in the seasonality is very relevant for improving the regional water resources and flood management. Additionally, model uncertainty for hydrological projections seems to decrease with higher-resolution modelling. This analysis has been submitted for publication and is currently under review ([118]).

High-resolution CP modelling was shown to have a direct and substantial impact on representing river discharge, particular in regions prone to convective systems and characterized by complex topography, highlighting its value for projecting the evolution of Italian rivers' discharge. The expected alteration in the Alpine snow regime and its subsequent impact on seasonal river flow was only captured in high-resolution ensembles, with local discharge patterns poorly represented in lower resolution simulations.

The second research question examined the impact of enhanced land-surface and hydrological representation within a two-way coupled regional modelling system. Improving discharge projections dependents no only on spatial and temporal resolution, but also on the physical description of hydrological processes represented in climate and hydrological models. Land-surface schemes often simplify these processes and lack physically based river-routing components. These limitations can hinder the description of river discharge, and incorporating enhanced land-surface schemes with robust hydrological modules can improve the reliability of the model simulations.

Therefore, a new coupling framework was developed for the regional climate model RegCM (version 5.0, [3]). The standard RegCM5.0 configuration uses a

rigid single-executable coupling scheme, with CLM4.5 as its default land-surface model. However, CLM5.0 introduced significant improvements in the physical representations of hydrological and various other processes. To integrate this update scheme, a more flexible coupling strategy was implemented using the OASIS3-MCT coupler. This framework requires minimal code alterations and facilitates the integration of independently developed models, while efficiently exchanging information between them. The availability of eCLM, a fork of CLM5.0 adapted to the OASIS3-MCT framework, enabled this integration. CLM5.0's physically based river routing module (MOSART) provides a key advantage, allowing direct estimations of river discharges inside the coupled simulations, without the need of an external hydrological modelling.

Although only preliminary results are currently available for the coupled RegCM-eCLM system, initial offline simulations of this model chain confirmed that the river discharge representation is comparable to the previously validated RegCM forced CHyM simulations. Early coupled results show similar tendencies, although a not yet explained decrease of discharge requires further investigation. The primary difference between RegCM-eCLM offline and RegCM-CHyM simulations was the tendency of the former to slightly underestimate extremes (less intense floods and droughts), whereas the latter simulates higher peak discharges and lower drought flows. These distinctions reflect the impact of land-surface representations and demonstrate the robustness of the new coupled approach.

The second research question therefore remains partially open, but the initial findings are highly promising. The performance of the new system matches the high standard set by previous CP based approaches, and future longer simulations are expected to allow for a more comprehensive evaluation against observations.

The third research question focused on a real-world application of hydrological modelling in climate attribution frameworks. A case-study was conducted for a major flood event in southern Brazil, using river discharge observations and CHyM simulations. This analysis reinforced both the importance of reliable hydrological data for real-world applications and the value of incorporating hydrological modelling in attribution frameworks. Although the CP resolution was not used in this case, the influence of finer spatial grids was evident in the results. An analogue-based protocol revealed an increase in discharge and precipitation in synoptic events similar to the 2024 flood that could not be explained with natural variability alone when comparing past and present climates. Extending the analysis to climate projections revealed further intensification of similar flood events, at higher warming levels. A complementary statistical attribution study based on observations confirmed a significant influence of anthropogenic climate change, suggesting an eight-fold decrease in return periods of extreme precipitation events of similar or higher magnitude. This attribution study will soon be submitted for

publication ([119]).

The results of the attribution study clearly demonstrate the potential of incorporating hydrological modelling in similar studies. The inclusion of hydrological simulations is not only feasible but also led to considerable improvements in understanding the extreme event, highlighting the contribution that such modelling approaches can make to future attribution studies. It also emphasized how improved river discharge projections can be of great use beyond the scientific community through real-world applications, underlining the importance of the modelling efforts and research work conducted to address the first two scientific questions.

The work presented here has also some limitations that are worth highlighting. Hydrological simulations performed by CHyM do not explicitly represent anthropogenic forcing such as dams and water extraction, which can evolve over time. For instance, reservoir operations may reduce flood peaks and modulate drought water flows, processes captured by observations and not by model outputs. Nevertheless, the CHyM simulations showed good validation in all the regions where station observations were available. Moreover, the CORDEX-FPS convection ensemble covers only four decades due to the high computational costs of both executing and storing CP simulations. Longer time series would be advantageous for assessing the influence of natural variability, although such data is not easily obtainable. Finally, the short duration of the coupled simulation available has limited the evaluation and indicated potential issues still to be addressed in the coupled system. While the first two limitations are structural issues and beyond the scope of this work, this last is expected to be overcome in the coming months, as a extended simulations are completed.

In summary, this thesis explored the potential of high-resolution hydroclimate modelling to advance the understanding of river discharge under climate change. Long term discharge trends, extreme events and their seasonality rely on the combined use of hydrological and climate models to be realistically captured. The results clearly show resolution-dependent signals, emphasizing the importance of kilometre-scale modelling and flexible coupling frameworks. Such approaches not only improve scientific projections but also provide critical insights for adaptation and water management in a warming world. Climate change will continue to pose challenges and create obstacles for human society in the coming decades, regardless of the decrease of anthropogenic emissions. Understanding how water resources are expected to evolve is a key step for adaptation and ensuring access to one of the most vital elements for our lives.

Appendix A

Pre-processing Protocol for MOSART

The Model for Scale Adaptive River Transport (MOSART) is a physically based river routing model used to simulate the lateral movement of water through a river network. In this thesis, MOSART was employed to support the hydrological analyses presented in Chapter 4, where its configuration required high-resolution inputs. However, the official MOSART input datasets provided within the Community Climate System Model (CCSM) repository are limited in spatial resolution (up to 0.125°) and do not offer the flexibility required . Therefore, a customized pre-processing protocol was developed to generate the necessary input fields at the desired resolution. The following appendix details this protocol, its required external datasets, and the steps used to produce each variable. All procedures have been made available in a public repository (https://github.com/lvargasheinz/mosart_protocol), including a integrated script for performing all steps necessary. The procedure was developed focused on the Italian domain used in this thesis, but this protocol is applicable to any region.

A.1 External Files

The protocol requires several external inputs. First, the CHyM static file is need, providing notably the drainage area. This variable is essential for the construction of the river network which will be used inside MOSART. CHyM's preprocessing steps are described and all tools are provided at https://github.com/graziano-giuliani/CHyM-roff/. Additional river attributes are needed and can be extracted from the HydroSHEDS Atlas ([120, 121]), which are publicly available online. The information should be converted from the Atlas' shapefiles into NetCDF files, and the conversion is done by the integrated script. Finally, addi-

tional variables are taken directly from the original MOSART files in the CCSM repository, such as specific coefficients not easily derived from external datasets.

A.2 Generation of variables

In this section, each MOSART variable required for the input file is described, along with the procedure used to obtain it.

area [m^2]

Grid cell area obtained directly with the cdo function `gridarea` on the selected grid.

areaTotal [m^2]

Total upstream drainage area. First, compute `areaTotal2` (see below) and then mask out the ocean, filling it with NaN, and obtain `areaTotal` (total upstream drainage area, local unit included; using concept of multi flow direction).

areaTotal2 [m^2]

Total upstream drainage area. Corresponds to the variable obtained within the CHyM framework called `dra`, which should be extracted from the static field and multiplied by $1 * 10^6$ to adjust units.

ID [-]

Cell identification number. Generated with the script `ID.py` script and subsequently masking out the ocean cells.

dnID [-]

The downstream ID can be obtained with the `dnID.py` and subsequently masking out the ocean.

fdir [-]

Flow direction based on a D8 scheme. CHyM preprocessing structure produces values from 1 to 8, whereas MOSART requires 1 to 128. This conversion can be obtained with the `fdir.py` script.

frac [-]

Fraction of the unit draining to the outlet. Variable corresponds to 1 over land and NaN over the ocean. It can be created directly from a land mask.

gxr [m^{-1}]

Drainage density, computed by dividing the length (`rlen`) by the cell area (`area`).

hslp [-]

Topographic slope. Calculated using the cell area and the elevation from CHyM with the script `hslp.py`.

latixy and longxy

Latitude and longitude of each the grid cell centroid. Computed using the scripts `latixy.py` and `longxy.py`.

nr [-] and nt [-]

Manning's roughness coefficient for main channel (`nr`) and tributary flow (`nt`). Based on MOSART's original data, they were assumed to be equal. Values of 0.05 were given for all regions with less than $17000 km^2$ of drainage area, and 0.0477163 for regions above (i.e. large rivers). This empirical estimation is based on the lower resolution information for Italian rivers and should be reassessed for other domains.

nh [-]

Manning's roughness coefficient for overland flow. As it depends primarly on the land-surface characteristics, it was taken from the lower resolution MOSART data and regridded. This approach is expected to be refined in future versions of the protocol.

rdep [m]

Bankfull depth of the main channel. Obtained by dividing HydroSHEDS river volume by its river area, converted from *shapefile* to NetCDF. Values below 2m were set to 2.

rlen [m]

Main channel length. Obtained from the HydroSHEDS Atlas, translated to a NetCDF format and multiplied by 1000 to adjust units.

rslp [-] and tslp [-]

Main channel slope (`rslp`) and mean tributary channel slope averaged through the unit (`tslp`) . Computed with the slope gradient of HydroSHEDS multiplied by 10^{-4} to adjust units. These two variables are considered to be equivalent.

rwid [m]

Bankfull width of main channel. Calculated by dividing the river area by its length, both obtained from the HydroSHEDS Atlas. Units were adjusted and values below 30m were set to 30.

rwid0 [m]

Floodplain width linked to main channel. Values for `rwid` were multiplied by 5, consistent with standard lower resolution MOSART files.

twid [m]

Bankfull width of local tributaries. Obtained from coarse resolution information available in MOSART input files and regridded to the target domain.

Bibliography

[1] Veronika Eyring, Sandrine Bony, Gerald A. Meehl, Catherine A. Senior, Bjorn Stevens, Ronald J. Stouffer, and Karl E. Taylor. "Overview of the Coupled Model Intercomparison Project Phase 6 (CMIP6) experimental design and organization". In: *Geoscientific Model Development* 9.5 (May 2016), pp. 1937–1958. ISSN: 1991-9603. DOI: 10.5194/gmd-9-1937-2016.

[2] William J. Gutowski Jr., Filippo Giorgi, Bertrand Timbal, Anne Frigon, Daniela Jacob, Hyun-Suk Kang, Krishnan Raghavan, Boram Lee, Christopher Lennard, Grigory Nikulin, Eleanor O'Rourke, Michel Rixen, Silvina Solman, Tannecia Stephenson, and Fredolin Tangang. "WCRP COordinated Regional Downscaling EXperiment (CORDEX): a diagnostic MIP for CMIP6". In: *Geoscientific Model Development* 9.11 (Nov. 2016), pp. 4087–4095. ISSN: 1991-9603. DOI: 10.5194/gmd-9-4087-2016.

[3] Erika Coppola, Filippo Giorgi, Graziano Giuliani, Emanuela Pichelli, James M. Ciarlo, Francesca Raffaele, Rita Nogherotto, Michelle Simões Reboita, Chen Lu, Natalia Zazulie, Luiza Vargas-Heinz, Andressa Andrade Cardoso, and Johannes de Leeuw. "The 5th generation regional climate modeling system, RegCM5: the first convection-permitting European wide simulation and validation over the CORDEX-CORE domains". In: *Climate Dynamics* 63.11 (Oct. 2025). ISSN: 1432-0894. DOI: 10.1007/s00382-025-07913-3.

[4] ERIKA COPPOLA, BARBARA TOMASSETTI, LAURA MARIOTTI, MARCO VERDECCHIA, and GUIDO VISCONTI. "Cellular automata algorithms for drainage network extraction and rainfall data assimilation". In: *Hydrological Sciences Journal* 52.3 (June 2007), pp. 579–592. ISSN: 2150-3435. DOI: 10.1623/hysj.52.3.579.

[5] Nikolina Ban et al. "The first multi-model ensemble of regional climate simulations at kilometer-scale resolution, part I: evaluation of precipitation". In: *Climate Dynamics* 57.1–2 (Apr. 2021), pp. 275–302. ISSN: 1432-0894. DOI: 10.1007/s00382-021-05708-w.

[6] Emanuela Pichelli et al. "The first multi-model ensemble of regional climate simulations at kilometer-scale resolution part 2: historical and future simulations of precipitation". In: *Climate Dynamics* 56.11–12 (Feb. 2021), pp. 3581–3602. ISSN: 1432-0894. DOI: 10.1007/s00382-021-05657-4.

[7] Ed Hawkins and Rowan Sutton. "The Potential to Narrow Uncertainty in Regional Climate Predictions". In: *Bulletin of the American Meteorological Society* 90.8 (Aug. 2009), pp. 1095–1108. ISSN: 1520-0477. DOI: 10.1175/2009bams2607.1.

[8] Giorgia Fosser, Marco Gaetani, Elizabeth J. Kendon, Marianna Adinolfi, Nikolina Ban, Danijel Belušić, Cécile Caillaud, João A. M. Careto, Erika Coppola, Marie-Estelle Demory, Hylke de Vries, Andreas Dobler, Hendrik Feldmann, Klaus Goergen, Geert Lenderink, Emanuela Pichelli, Christoph Schär, Pedro M. M. Soares, Samuel Somot, and Merja H. Tölle. "Convection-permitting climate models offer more certain extreme rainfall projections". In: *npj Climate and Atmospheric Science* 7.1 (Feb. 2024). ISSN: 2397-3722. DOI: 10.1038/s41612-024-00600-w.

[9] David M. Lawrence et al. "The Community Land Model Version 5: Description of New Features, Benchmarking, and Impact of Forcing Uncertainty". In: *Journal of Advances in Modeling Earth Systems* 11.12 (Dec. 2019), pp. 4245–4287. ISSN: 1942-2466. DOI: 10.1029/2018ms001583.

[10] P. Shrestha, M. Sulis, M. Masbou, S. Kollet, and C. Simmer. "A Scale-Consistent Terrestrial Systems Modeling Platform Based on COSMO, CLM, and ParFlow". In: *Monthly Weather Review* 142.9 (Sept. 2014), pp. 3466–3483. ISSN: 1520-0493. DOI: 10.1175/mwr-d-14-00029.1.

[11] Anthony Craig, Sophie Valcke, and Laure Coquart. "Development and performance of a new version of the OASIS coupler, OASIS3-MCT$_3$.0". In: *Geoscientific Model Development* 10.9 (Sept. 2017), pp. 3297–3308. ISSN: 1991-9603. DOI: 10.5194/gmd-10-3297-2017.

[12] Ginés Suarez, Omar Bello, and Jack Campbell. *Avaliação dos efeitos e impactos das inundações no Rio Grande do Sul*. Nov. 2024. DOI: 10.18235/0013254.

[13] Walter Collischonn, João Paulo Lyra Fialho Brêda, Sly Wongchuig, Anderson Ruhoff, Rodrigo Cauduro Dias de Paiva, Fernando Mainardi Fan, Rafael Cabeleira de Coronel Machado Filho, and Nicole Ramalho. "Unprecedented April-May 2024 rainfall in South Brazil sets new record". In: *RBRH* 29 (2024). ISSN: 1414-381X. DOI: 10.1590/2318-0331.292420240088.

[14] Sjoukje Philip, Sarah Kew, Geert Jan van Oldenborgh, Friederike Otto, Robert Vautard, Karin van der Wiel, Andrew King, Fraser Lott, Julie Arrighi, Roop Singh, and Maarten van Aalst. "A protocol for probabilistic extreme event attribution analyses". In: *Advances in Statistical Climatology, Meteorology and Oceanography* 6.2 (Nov. 2020), pp. 177–203. ISSN: 2364-3587. DOI: 10.5194/ascmo-6-177-2020.

[15] Davide Faranda, Gabriele Messori, Erika Coppola, Tommaso Alberti, Mathieu Vrac, Flavio Pons, Pascal Yiou, Marion Saint Lu, Andreia N. S. Hisi, Patrick Brockmann, Stavros Dafis, Gianmarco Mengaldo, and Robert Vautard. "ClimaMeter: contextualizing extreme weather in a changing climate". In: *Weather and Climate Dynamics* 5.3 (July 2024), pp. 959–983. ISSN: 2698-4016. DOI: 10.5194/wcd-5-959-2024.

[16] Hans Hersbach et al. "The ERA5 global reanalysis". In: *Quarterly Journal of the Royal Meteorological Society* 146.730 (June 2020), pp. 1999–2049. ISSN: 1477-870X. DOI: 10.1002/qj.3803.

[17] Mathias Hauser, Francois Engelbrecht, and Erich M. Fischer. *Transient global warming levels for CMIP5 and CMIP6*. 2022. DOI: 10.5281/ZENODO.7390473.

[18] John Cook, Dana Nuccitelli, Sarah A Green, Mark Richardson, Bärbel Winkler, Rob Painting, Robert Way, Peter Jacobs, and Andrew Skuce. "Quantifying the consensus on anthropogenic global warming in the scientific literature". In: *Environmental Research Letters* 8.2 (May 2013), p. 024024. ISSN: 1748-9326. DOI: 10.1088/1748-9326/8/2/024024.

[19] John Cook, Naomi Oreskes, Peter T Doran, William R L Anderegg, Bart Verheggen, Ed W Maibach, J Stuart Carlton, Stephan Lewandowsky, Andrew G Skuce, Sarah A Green, Dana Nuccitelli, Peter Jacobs, Mark Richardson, Bärbel Winkler, Rob Painting, and Ken Rice. "Consensus on consensus: a synthesis of consensus estimates on human-caused global warming". In: *Environmental Research Letters* 11.4 (Apr. 2016), p. 048002. ISSN: 1748-9326. DOI: 10.1088/1748-9326/11/4/048002.

[20] Intergovernmental Panel on Climate Change (IPCC). *Climate Change 2021 – The Physical Science Basis: Working Group I Contribution to the Sixth Assessment Report of the Intergovernmental Panel on Climate Change*. Cambridge University Press, June 2023. ISBN: 9781009157896. DOI: 10.1017/9781009157896.

[21] Julie Collignan, Jan Polcher, Sophie Bastin, and Pere Quintana-Segui. "Identifying and Quantifying the Impact of Climatic and Non-Climatic Drivers on River Discharge in Europe". In: *Water Resources Research* 61.4 (Apr. 2025). ISSN: 1944-7973. DOI: 10.1029/2024wr038220.

[22] Sergio M. Vicente-Serrano, Santiago Beguería, and Juan I. López-Moreno. "A Multiscalar Drought Index Sensitive to Global Warming: The Standardized Precipitation Evapotranspiration Index". In: *Journal of Climate* 23.7 (Apr. 2010), pp. 1696–1718. ISSN: 0894-8755. DOI: 10.1175/2009jcli2909.1.

[23] Luis Carlos Serrano Diaz, Brian Smerdon, Daniel S. Alessi, and Monireh Faramarzi. "Assessment of the impacts of climate change on groundwater evapotranspiration in mid-to-high latitude regions". In: *Journal of Hydrology* 660 (Oct. 2025), p. 133294. ISSN: 0022-1694. DOI: 10.1016/j.jhydrol.2025.133294.

[24] Esther Bender, Michael Lehning, and Joel Fiddes. "Changes in Climatology, Snow Cover, and Ground Temperatures at High Alpine Locations". In: *Frontiers in Earth Science* 8 (May 2020). ISSN: 2296-6463. DOI: 10.3389/feart.2020.00100.

[25] Stephen J. Stuart, Samuel M. Dean, Andrew N. Mackintosh, Abha Sood, Peter B. Gibson, Stuart Moore, and Elizabeth J. Kendon. "Precipitation Over Complex Mountain Terrain in a Convection-Permitting Regional Climate Model". In: *Journal of Geophysical Research: Atmospheres* 130.12 (June 2025). ISSN: 2169-8996. DOI: 10.1029/2024jd042773.

[26] Paola Mazzoglio, Marco Lompi, Francesco Marra, Eleonora Dallan, Roberto Deidda, Pierluigi Claps, Salvatore Manfreda, Leonardo Valerio Noto, Alberto Viglione, Mario Raffa, Paola Mercogliano, Marco Marani, Enrica Caporali, and Marco Borga. "Orographic and land-sea contrast effects in convection-permitting simulations of extreme sub-daily precipitation". In: *Weather and Climate Extremes* 49 (Sept. 2025), p. 100798. ISSN: 2212-0947. DOI: 10.1016/j.wace.2025.100798.

[27] Eleonora Dallan, Francesco Marra, Giorgia Fosser, Marco Marani, Giuseppe Formetta, Christoph Schär, and Marco Borga. "How well does a convection-permitting regional climate model represent the reverse orographic effect of extreme hourly precipitation?" In: *Hydrology and Earth System Sciences* 27.5 (Mar. 2023), pp. 1133–1149. ISSN: 1607-7938. DOI: 10.5194/hess-27-1133-2023.

[28] Judith Eeckman, Hélène Roux, Audrey Douinot, Bertrand Bonan, and Clément Albergel. "A multi-sourced assessment of the spatiotemporal dynamics of soil moisture in the MARINE flash flood model". In: *Hydrology and Earth System Sciences* 25.3 (Mar. 2021), pp. 1425–1446. ISSN: 1607-7938. DOI: 10.5194/hess-25-1425-2021.

[29] Francisco Peña, Fernando Nardi, Assefa Melesse, Jayantha Obeysekera, Fabio Castelli, René M. Price, Todd Crowl, and Noemi Gonzalez-Ramirez. "Compound flood modeling framework for surface–subsurface water interactions". In: *Natural Hazards and Earth System Sciences* 22.3 (Mar. 2022), pp. 775–793. ISSN: 1684-9981. DOI: 10.5194/nhess-22-775-2022.

[30] Bibi S. Naz, Wendy Sharples, Yueling Ma, Klaus Goergen, and Stefan Kollet. "Continental-scale evaluation of a fully distributed coupled land surface and groundwater model, ParFlow-CLM (v3.6.0), over Europe". In: *Geoscientific Model Development* 16.6 (Mar. 2023), pp. 1617–1639. ISSN: 1991-9603. DOI: 10.5194/gmd-16-1617-2023.

[31] Selma B. Guerreiro, Hayley J. Fowler, Renaud Barbero, Seth Westra, Geert Lenderink, Stephen Blenkinsop, Elizabeth Lewis, and Xiao-Feng Li. "Detection of continental-scale intensification of hourly rainfall extremes". In: *Nature Climate Change* 8.9 (July 2018), pp. 803–807. ISSN: 1758-6798. DOI: 10.1038/s41558-018-0245-3.

[32] Haider Ali, Hayley J. Fowler, and Vimal Mishra. "Global Observational Evidence of Strong Linkage Between Dew Point Temperature and Precipitation Extremes". In: *Geophysical Research Letters* 45.22 (Nov. 2018). ISSN: 1944-8007. DOI: 10.1029/2018gl080557.

[33] G. Lenderink, R. Barbero, J. M. Loriaux, and H. J. Fowler. "Super-Clausius–Clapeyron Scaling of Extreme Hourly Convective Precipitation and Its Relation to Large-Scale Atmospheric Conditions". In: *Journal of Climate* 30.15 (Aug. 2017), pp. 6037–6052. ISSN: 1520-0442. DOI: 10.1175/jcli-d-16-0808.1.

[34] Herbert Formayer and Alexandra Fritz. "Temperature dependency of hourly precipitation intensities - surface versus cloud layer temperature: PRECIPITATION INTENSITIES: SURFACE VERSUS CLOUD LAYER TEMPERATURE". In: *International Journal of Climatology* 37.1 (Feb. 2016), pp. 1–10. ISSN: 0899-8418. DOI: 10.1002/joc.4678.

[35] Intergovernmental Panel On Climate Change (IPCC). *Climate Change 2013 – The Physical Science Basis: Working Group I Contribution to the Fifth Assessment Report of the Intergovernmental Panel on Climate Change*. 1st ed. Cambridge University Press, July 2013. ISBN: 9781107057991.

[36] Elisie Kåresdotter, Georgia Destouni, Navid Ghajarnia, Richard B. Lammers, and Zahra Kalantari. "Distinguishing Direct Human-Driven Effects on the Global Terrestrial Water Cycle". In: *Earth's Future* 10.8 (Aug. 2022). ISSN: 2328-4277. DOI: 10.1029/2022ef002848.

[37] Tao Tang, Jun Ge, Junji Cao, and Haiyun Shi. "Land water availability altered by historical land use and land cover change". In: *npj Climate and Atmospheric Science* 8.1 (June 2025). ISSN: 2397-3722. DOI: 10.1038/s41612-025-01111-y.

[38] Sofie A. te Wierik, Erik L. H. Cammeraat, Joyeeta Gupta, and Yael A. Artzy-Randrup. "Reviewing the Impact of Land Use and Land-Use Change on Moisture Recycling and Precipitation Patterns". In: *Water Resources Research* 57.7 (July 2021). ISSN: 1944-7973. DOI: 10.1029/2020wr029234.

[39] Shuzhe Huang, Yuan Gan, Nengcheng Chen, Chao Wang, Xiang Zhang, Chuxuan Li, and Daniel E. Horton. "Urbanization enhances channel and surface runoff: A quantitative analysis using both physical and empirical models over the Yangtze River basin". In: *Journal of Hydrology* 635 (May 2024), p. 131194. ISSN: 0022-1694. DOI: 10.1016/j.jhydrol.2024.131194.

[40] David Ketchum, Zachary H. Hoylman, Justin Huntington, Douglas Brinkerhoff, and Kelsey G. Jencso. "Irrigation intensification impacts sustainability of streamflow in the Western United States". In: *Communications Earth amp; Environment* 4.1 (Dec. 2023). ISSN: 2662-4435. DOI: 10.1038/s43247-023-01152-2.

[41] Heng Yan, Zhenghui Xie, Binghao Jia, Ruichao Li, Longhuan Wang, Yuhang Tian, and Yanbin You. "Impact of groundwater overextraction and agricultural irrigation on hydrological processes in an inland arid basin". In: *Journal of Hydrology* 653 (June 2025), p. 132770. ISSN: 0022-1694. DOI: 10.1016/j.jhydrol.2025.132770.

[42] Jorge L. Peña-Arancibia, L. Adrian Bruijnzeel, Mark Mulligan, and Albert I.J.M. van Dijk. "Forests as 'sponges' and 'pumps': Assessing the impact of deforestation on dry-season flows across the tropics". In: *Journal of Hydrology* 574 (July 2019), pp. 946–963. ISSN: 0022-1694. DOI: 10.1016/j.jhydrol.2019.04.064.

[43] G. Forzieri, L. Feyen, R. Rojas, M. Flörke, F. Wimmer, and A. Bianchi. "Ensemble projections of future streamflow droughts in Europe". In: *Hydrology and Earth System Sciences* 18.1 (Jan. 2014), pp. 85–108. ISSN: 1607-7938. DOI: 10.5194/hess-18-85-2014.

[44] Matthias Huss and Regine Hock. "Global-scale hydrological response to future glacier mass loss". In: *Nature Climate Change* 8.2 (Jan. 2018), pp. 135–140. ISSN: 1758-6798. DOI: 10.1038/s41558-017-0049-x.

[45] Josep Cos, Francisco Doblas-Reyes, Martin Jury, Raül Marcos, Pierre-Antoine Bretonnière, and Margarida Samsó. "The Mediterranean climate change hotspot in the CMIP5 and CMIP6 projections". In: *Earth System Dynamics* 13.1 (Feb. 2022), pp. 321–340. ISSN: 2190-4987. DOI: 10.5194/esd-13-321-2022.

[46] Donald A. Wilhite and Michael H. Glantz. "Understanding: the Drought Phenomenon: The Role of Definitions". In: *Water International* 10.3 (Jan. 1985), pp. 111–120. ISSN: 1941-1707. DOI: 10.1080/02508068508686328.

[47] Ashok K. Mishra and Vijay P. Singh. "A review of drought concepts". In: *Journal of Hydrology* 391.1–2 (Sept. 2010), pp. 202–216. ISSN: 0022-1694. DOI: 10.1016/j.jhydrol.2010.07.012.

[48] Wolfgang Kron. "Flood Risk = Hazard • Values • Vulnerability". In: *Water International* 30.1 (Mar. 2005), pp. 58–68. ISSN: 1941-1707. DOI: 10.1080/02508060508691837.

[49] Syukuro Manabe and Richard T. Wetherald. "Thermal Equilibrium of the Atmosphere with a Given Distribution of Relative Humidity". In: *Journal of the Atmospheric Sciences* 24.3 (May 1967), pp. 241–259. ISSN: 1520-0469. DOI: 10.1175/1520-0469(1967)024<0241:teotaw>2.0.co;2.

[50] John Patrick Dunne, Helene T. Hewitt, Julie Arblaster, Frédéric Bonou, Olivier Boucher, Tereza Cavazos, Paul J. Durack, Birgit Hassler, Martin Juckes, Tomoki Miyakawa, Matthew Mizielinski, Vaishali Naik, Zebedee Nicholls, Eleanor O'Rourke, Robert Pincus, Benjamin M. Sanderson, Isla R. Simpson, and Karl E. Taylor. "An evolving Coupled Model Intercomparison Project phase 7 (CMIP7) and Fast Track in support of future climate assessment". In: (Dec. 2024). DOI: 10.5194/egusphere-2024-3874.

[51] Karl E. Taylor, Ronald J. Stouffer, and Gerald A. Meehl. "An Overview of CMIP5 and the Experiment Design". In: *Bulletin of the American Meteorological Society* 93.4 (Apr. 2012), pp. 485–498. ISSN: 1520-0477. DOI: 10.1175/bams-d-11-00094.1.

[52] Andreas F. Prein, Wolfgang Langhans, Giorgia Fosser, Andrew Ferrone, Nikolina Ban, Klaus Goergen, Michael Keller, Merja Tölle, Oliver Gutjahr, Frauke Feser, Erwan Brisson, Stefan Kollet, Juerg Schmidli, Nicole P. M. van Lipzig, and Ruby Leung. "A review on regional convection-permitting climate modeling: Demonstrations, prospects, and challenges". In: *Reviews of Geophysics* 53.2 (May 2015), pp. 323–361. ISSN: 1944-9208. DOI: 10.1002/2014rg000475.

[53] D. P. Dee et al. "The ERA-Interim reanalysis: configuration and performance of the data assimilation system". In: *Quarterly Journal of the Royal Meteorological Society* 137.656 (Apr. 2011), pp. 553–597. ISSN: 1477-870X. DOI: 10.1002/qj.828.

[54] Ronald Gelaro et al. "The Modern-Era Retrospective Analysis for Research and Applications, Version 2 (MERRA-2)". In: *Journal of Climate* 30.14 (July 2017), pp. 5419–5454. ISSN: 1520-0442. DOI: 10.1175/jcli-d-16-0758.1.

[55] E. Kalnay et al. "The NCEP/NCAR 40-Year Reanalysis Project". In: *Bulletin of the American Meteorological Society* 77.3 (Mar. 1996), pp. 437–471. ISSN: 1520-0477. DOI: 10.1175/1520-0477(1996)077<0437:tnyrp>2.0.co;2.

[56] Chiaki Kobayashi and Toshiki Iwasaki. "Brewer-Dobson circulation diagnosed from JRA-55". In: *Journal of Geophysical Research: Atmospheres* 121.4 (Feb. 2016), pp. 1493–1510. ISSN: 2169-8996. DOI: 10.1002/2015jd023476.

[57] Filippo Giorgi, Erika Coppola, Claas Teichmann, and Daniela Jacob. "Editorial for the CORDEX-CORE Experiment I Special Issue". In: *Climate Dynamics* 57.5–6 (Aug. 2021), pp. 1265–1268. ISSN: 1432-0894. DOI: 10.1007/s00382-021-05902-w.

[58] Filippo Giorgi et al. "The CORDEX-CORE EXP-I Initiative: Description and Highlight Results from the Initial Analysis". In: *Bulletin of the American Meteorological Society* 103.2 (Feb. 2022), E293–E310. ISSN: 1520-0477. DOI: 10.1175/bams-d-21-0119.1.

[59] F Giorgi et al. "RegCM4: model description and preliminary tests over multiple CORDEX domains". In: *Climate Research* 52 (Mar. 2012), pp. 7–29. ISSN: 1616-1572. DOI: 10.3354/cr01018.

[60] D. Jacob and R. Podzun. "Sensitivity studies with the regional climate model REMO". In: *Meteorology and Atmospheric Physics* 63.1–2 (1997), pp. 119–129. ISSN: 1436-5065. DOI: 10.1007/bf01025368.

[61] Daniela Jacob, Alberto Elizalde, Andreas Haensler, Stefan Hagemann, Pankaj Kumar, Ralf Podzun, Diana Rechid, Armelle Reca Remedio, Fahad Saeed, Kevin Sieck, Claas Teichmann, and Christof Wilhelm. "Assessing the Transferability of the Regional Climate Model REMO to Different COordinated Regional Climate Downscaling EXperiment (CORDEX) Regions". In: *Atmosphere* 3.1 (Feb. 2012), pp. 181–199. ISSN: 2073-4433. DOI: 10.3390/atmos3010181.

[62] Erika Coppola, Emanuela Pichelli, Francesca Raffaele, and Stefan Sobolowski. "A more in depth analysis of the European Convection Permitting ensemble test case simulations." In: *EGU General Assembly Conference Abstracts*. EGU General Assembly Conference Abstracts. Apr. 2018, p. 16645.

[63] Philippe Lucas-Picher, Daniel Argüeso, Erwan Brisson, Yves Tramblay, Peter Berg, Aude Lemonsu, Sven Kotlarski, and Cécile Caillaud. "<scp>Convection</scp>-permitting modeling with regional climate models: Latest developments and next steps". In: *WIREs Climate Change* 12.6 (Aug. 2021). ISSN: 1757-7799. DOI: 10.1002/wcc.731.

[64] Claudia Tebaldi and Reto Knutti. "The use of the multi-model ensemble in probabilistic climate projections". In: *Philosophical Transactions of the Royal Society A: Mathematical, Physical and Engineering Sciences* 365.1857 (June 2007), pp. 2053–2075. ISSN: 1471-2962. DOI: 10.1098/rsta.2007.2076.

[65] Minh T. Ha et al. "Precipitation frequency in Med-CORDEX and EURO-CORDEX ensembles from 0.44° to convection-permitting resolution: impact of model resolution and convection representation". In: *Climate Dynamics* 62.6 (Dec. 2022), pp. 4515–4540. ISSN: 1432-0894. DOI: 10.1007/s00382-022-06594-6.

[66] Martyn P. Clark, Marc F. P. Bierkens, Luis Samaniego, Ross A. Woods, Remko Uijlenhoet, Katrina E. Bennett, Valentijn R. N. Pauwels, Xitian Cai, Andrew W. Wood, and Christa D. Peters-Lidard. "The evolution of process-based hydrologic models: historical challenges and the collective quest for physical realism". In: *Hydrology and Earth System Sciences* 21.7 (July 2017), pp. 3427–3440. ISSN: 1607-7938. DOI: 10.5194/hess-21-3427-2017.

[67] Alberto Martínez-de la Torre and Gonzalo Miguez-Macho. "Groundwater influence on soil moisture memory and land–atmosphere fluxes in the Iberian Peninsula". In: *Hydrology and Earth System Sciences* 23.12 (Dec. 2019), pp. 4909–4932. ISSN: 1607-7938. DOI: 10.5194/hess-23-4909-2019.

[68] Bridget R. Scanlon, Zizhan Zhang, Himanshu Save, Alexander Y. Sun, Hannes Müller Schmied, Ludovicus P. H. van Beek, David N. Wiese, Yoshihide Wada, Di Long, Robert C. Reedy, Laurent Longuevergne, Petra Döll, and Marc F. P. Bierkens. "Global models underestimate large decadal declining and rising water storage trends relative to GRACE satellite data". In: *Proceedings of the National Academy of Sciences* 115.6 (Jan. 2018). ISSN: 1091-6490. DOI: 10.1073/pnas.1704665115.

[69] Xiaoying Yang, Qun Liu, Yi He, Xingzhang Luo, and Xiaoxiang Zhang. "Comparison of daily and sub-daily SWAT models for daily streamflow simulation in the Upper Huai River Basin of China". In: *Stochastic Environmental Research and Risk Assessment* 30.3 (June 2015), pp. 959–972. ISSN: 1436-3259. DOI: 10.1007/s00477-015-1099-0.

[70] Michael Barlage, Mukul Tewari, Fei Chen, Gonzalo Miguez-Macho, Zong-Liang Yang, and Guo-Yue Niu. "The effect of groundwater interaction in North American regional climate simulations with WRF/Noah-MP". In: *Climatic Change* 129.3–4 (Feb. 2015), pp. 485–498. ISSN: 1573-1480. DOI: 10.1007/s10584-014-1308-8.

[71] Christoph Schär, Daniel Lüthi, Urs Beyerle, and Erdmann Heise. "The Soil–Precipitation Feedback: A Process Study with a Regional Climate Model". In: *Journal of Climate* 12.3 (Mar. 1999), pp. 722–741. ISSN: 1520-0442. DOI: 10.1175/1520-0442(1999)012<0722:tspfap>2.0.co;2.

[72] *Climate Change 2022 – Impacts, Adaptation and Vulnerability*. Cambridge University Press, June 2023, pp. 551–712. ISBN: 9781009325844. DOI: 10.1017/9781009325844.006.

[73] Zhenyu Zhang, Joel Arnault, Patrick Laux, Ning Ma, Jianhui Wei, Shasha Shang, and Harald Kunstmann. "Convection-permitting fully coupled WRF-Hydro ensemble simulations in high mountain environment: impact of boundary layer- and lateral flow parameterizations on land–atmosphere interactions". In: *Climate Dynamics* 59.5–6 (Nov. 2021), pp. 1355–1376. ISSN: 1432-0894. DOI: 10.1007/s00382-021-06044-9.

[74] M.J. Ascott, V. Christelis, D.J. Lapworth, D.M.J. Macdonald, C. Tindimugaya, A. Iragena, D. Finney, R. Fitzpatrick, J.H. Marsham, and D.P. Rowell. "On the application of rainfall projections from a convection-permitting climate model to lumped catchment models". In: *Journal of Hydrology* 617 (Feb. 2023), p. 129097. ISSN: 0022-1694. DOI: 10.1016/j.jhydrol.2023.129097.

[75] Fabio Di Sante, Erika Coppola, and Filippo Giorgi. "Projections of river floods in Europe using <scp>EURO-CORDEX</scp>, <scp>CMIP5</scp> and <scp>CMIP6</scp> simulations". In: *International Journal of Climatology* 41.5 (Feb. 2021), pp. 3203–3221. ISSN: 1097-0088. DOI: 10.1002/joc.7014.

[76] Matilde García-Valdecasas Ojeda, Fabio Di Sante, Erika Coppola, Adriano Fantini, Rita Nogherotto, Francesca Raffaele, and Filippo Giorgi. "Climate change impact on flood hazard over Italy". In: *Journal of Hydrology* 615 (Dec. 2022), p. 128628. ISSN: 0022-1694. DOI: 10.1016/j.jhydrol.2022.128628.

[77] Richard H. Moss, Jae A. Edmonds, Kathy A. Hibbard, Martin R. Manning, Steven K. Rose, Detlef P. van Vuuren, Timothy R. Carter, Seita Emori, Mikiko Kainuma, Tom Kram, Gerald A. Meehl, John F. B. Mitchell, Nebojsa Nakicenovic, Keywan Riahi, Steven J. Smith, Ronald J. Stouffer, Allison M. Thomson, John P. Weyant, and Thomas J. Wilbanks. "The next generation of scenarios for climate change research and assessment". In: *Nature* 463.7282 (Feb. 2010), pp. 747–756. ISSN: 1476-4687. DOI: 10.1038/nature08823.

[78] Marco Verdecchia, Erika Coppola, Barbara Tomassetti, and Guido Visconti. "Cetemps Hydrological Model (CHyM), a Distributed Grid-Based Model Assimilating Different Rainfall Data Sources". In: *Hydrological Modelling and the Water Cycle*. Springer Berlin Heidelberg, pp. 165–201. ISBN: 9783540778431. DOI: 10.1007/978-3-540-77843-1_8.

[79] Erika Coppola, Marco Verdecchia, Filippo Giorgi, Valentina Colaiuda, Barbara Tomassetti, and Annalina Lombardi. "Changing hydrological conditions in the Po basin under global warming". In: *Science of The Total Environment* 493 (Sept. 2014), pp. 1183–1196. ISSN: 0048-9697. DOI: 10.1016/j.scitotenv.2014.03.003.

[80] Lorenzo Sangelantoni, Barbara Tomassetti, Valentina Colaiuda, Annalina Lombardi, Marco Verdecchia, Rossella Ferretti, and Gianluca Redaelli. "On the Use of Original and Bias-Corrected Climate Simulations in Regional-Scale Hydrological Scenarios in the Mediterranean Basin". In: *Atmosphere* 10.12 (Dec. 2019), p. 799. ISSN: 2073-4433. DOI: 10.3390/atmos10120799.

[81] In: *Proceedings of the Royal Society of London. Series A. Mathematical and Physical Sciences* 229.1178 (May 1955), pp. 281–316. ISSN: 2053-9169. DOI: 10.1098/rspa.1955.0088.

[82] Graziano Giuliani. *CHyM-roff*. https://github.com/graziano-giuliani/CHyM-roff. 2025.

[83] B. Tomassetti, E. Coppola, M. Verdecchia, and G. Visconti. "Coupling a distributed grid based hydrological model and MM5 meteorological model for flooding alert mapping". In: *Advances in Geosciences* 2 (Mar. 2005), pp. 59–63. ISSN: 1680-7359. DOI: 10.5194/adgeo-2-59-2005.

[84] Hoshin V. Gupta, Harald Kling, Koray K. Yilmaz, and Guillermo F. Martinez. "Decomposition of the mean squared error and NSE performance criteria: Implications for improving hydrological modelling". In: *Journal of Hydrology* 377.1–2 (Oct. 2009), pp. 80–91. ISSN: 0022-1694. DOI: 10.1016/j.jhydrol.2009.08.003.

[85] Harald Kling, Martin Fuchs, and Maria Paulin. "Runoff conditions in the upper Danube basin under an ensemble of climate change scenarios". In: *Journal of Hydrology* 424–425 (Mar. 2012), pp. 264–277. ISSN: 0022-1694. DOI: 10.1016/j.jhydrol.2012.01.011.

[86] Wouter J. M. Knoben, Jim E. Freer, and Ross A. Woods. "Technical note: Inherent benchmark or not? Comparing Nash–Sutcliffe and Kling–Gupta efficiency scores". In: *Hydrology and Earth System Sciences* 23.10 (Oct. 2019), pp. 4323–4331. ISSN: 1607-7938. DOI: 10.5194/hess-23-4323-2019.

[87] Ugo Maione, Paolo Mignosa, and Massimo Tomirotti. "Regional estimation of synthetic design hydrographs". In: *International Journal of River Basin Management* 1.2 (June 2003), pp. 151–163. ISSN: 1814-2060. DOI: 10.1080/15715124.2003.9635202.

[88] Rutger Dankers and Luc Feyen. "Flood hazard in Europe in an ensemble of regional climate scenarios". In: *Journal of Geophysical Research: Atmospheres* 114.D16 (Aug. 2009). ISSN: 0148-0227. DOI: 10.1029/2008jd011523.

[89] Luc Feyen and Rutger Dankers. "Impact of global warming on streamflow drought in Europe". In: *Journal of Geophysical Research: Atmospheres* 114.D17 (Sept. 2009). ISSN: 0148-0227. DOI: 10.1029/2008jd011438.

[90] Fred Kucharski, Franco Molteni, and Annalisa Bracco. "Decadal interactions between the western tropical Pacific and the North Atlantic Oscillation". In: *Climate Dynamics* 26.1 (Nov. 2005), pp. 79–91. ISSN: 1432-0894. DOI: 10.1007/s00382-005-0085-5.

[91] Erika Coppola, Francesca Raffaele, and Filippo Giorgi. "Impact of climate change on snow melt driven runoff timing over the Alpine region". In: *Climate Dynamics* 51.3 (Aug. 2016), pp. 1259–1273. ISSN: 1432-0894. DOI: 10.1007/s00382-016-3331-0.

[92] IMPETUS4CHANGE. *Improving Near-Term Climate Predictions for Societal Transformation*. Nov. 2022. DOI: 10.3030/101081555.

[93] M. L. Bettolli, S. A. Solman, R. P. da Rocha, M. Llopart, J. M. Gutierrez, J. Fernández, M. E. Olmo, A. Lavin-Gullon, S. C. Chou, D. Carneiro Rodrigues, E. Coppola, R. Balmaceda Huarte, M. Barreiro, J. Blázquez, M. Doyle, M. Feijoó, R. Huth, L. Machado, and S. Vianna Cuadra. "The CORDEX Flagship Pilot Study in southeastern South America: a comparative study of statistical and dynamical downscaling models in simulating daily extreme precipitation events". In: *Climate Dynamics* 56.5–6 (Jan. 2021), pp. 1589–1608. ISSN: 1432-0894. DOI: 10.1007/s00382-020-05549-z.

[94] Justin L. Huntington and Richard G. Niswonger. "Role of surface-water and groundwater interactions on projected summertime streamflow in snow dominated regions: An integrated modeling approach". In: *Water Resources Research* 48.11 (Nov. 2012). ISSN: 1944-7973. DOI: 10.1029/2012wr012319.

[95] Nancy Collins, Gerhard Theurich, Cecelia DeLuca, Max Suarez, Atanas Trayanov, V. Balaji, Peggy Li, Weiyu Yang, Chris Hill, and Arlindo da Silva. "Design and Implementation of Components in the Earth System Modeling Framework". In: *The International Journal of High Performance Computing Applications* 19.3 (Aug. 2005), pp. 341–350. ISSN: 1741-2846. DOI: 10.1177/1094342005056120.

[96] Keith Oleson et al. *Technical description of version 4.5 of the Community Land Model (CLM)*. en. Tech. rep. 2013. DOI: 10.5065/D6RR1W7M.

[97] Allison L. Steiner, Jeremy S. Pal, Sara A. Rauscher, Jason L. Bell, Noah S. Diffenbaugh, Aaron Boone, Lisa C. Sloan, and Filippo Giorgi. "Land surface coupling in regional climate simulations of the West African monsoon". In: *Climate Dynamics* 33.6 (Mar. 2009), pp. 869–892. ISSN: 1432-0894. DOI: 10.1007/s00382-009-0543-6.

[98] Robert Dickinson, A Henderson-Sellers, and P Kennedy. *Biosphere-atmosphere Transfer Scheme (BATS) Version 1e as Coupled to the NCAR Community Climate Model*. en. Tech. rep. 1993. DOI: 10.5065/D67W6959.

[99] David Lawrence, Fisher Rosie, Charles Koven, Keith Oleson, Sean Swenson, Mariana Vertenstein, Ben Andre, Gordon Bonan, Bardan Ghimire, Daniel Kennedy, Erik Kluzek, Ryan Knox, Peter Lawrence, Fang Li, Hongyi Li, Danica Lombardozzi, Yaqiong Lu, Justin Peket, William Riley, and Chonggang Xu. *CLM5.0 Technical Description*. May 2018.

[100] Stefan Poll, Paul Rigor, Marco van Hulten, Kaveh Patakchi Yousefi, Daniel Caviedes Voullieme, Klaus Goergen, and Stefan J. Kollet. "The new version of the Terrestrial Systems Modeling Platform (TSMP2) based on ICON, eCLM, and ParFlow". In: *AGU Fall Meeting Abstracts*. Vol. 2024. AGU Fall Meeting Abstracts. Dec. 2024, A32F-01, A32F–01.

[101] T. K. Tesfa, H.-Y. Li, L. R. Leung, M. Huang, Y. Ke, Y. Sun, and Y. Liu. "A subbasin-based framework to represent land surface processes in an Earth system model". In: *Geoscientific Model Development* 7.3 (May 2014), pp. 947–963. ISSN: 1991-9603. DOI: 10.5194/gmd-7-947-2014.

[102] Patrick Marsaleix, Francis Auclair, Jochem Willem Floor, Marine Julie Herrmann, Claude Estournel, Ivane Pairaud, and Caroline Ulses. "Energy conservation issues in sigma-coordinate free-surface ocean models". In: *Ocean*

Modelling 20.1 (Jan. 2008), pp. 61–89. ISSN: 1463-5003. DOI: 10.1016/j.ocemod.2007.07.005.

[103] Centre for High-Performance Scientific Computing in Terrestrial Systems (HPSC-TerrSys). *eCLM Fork of Community Land Model v5.0*. https://github.com/HPSCTerrSys/eCLM. 2025.

[104] Adriano Fantini. "Climate change impact on flood hazard over Italy". https://hdl.handle.net/1 PhD thesis. University of Trieste, 2019.

[105] Elisabeth A. Lloyd and Theodore G. Shepherd. "Environmental catastrophes, climate change, and attribution". In: *Annals of the New York Academy of Sciences* 1469.1 (Feb. 2020), pp. 105–124. ISSN: 1749-6632. DOI: 10.1111/nyas.14308.

[106] Theodore G. Shepherd. "A Common Framework for Approaches to Extreme Event Attribution". In: *Current Climate Change Reports* 2.1 (Feb. 2016), pp. 28–38. ISSN: 2198-6061. DOI: 10.1007/s40641-016-0033-y.

[107] Nathalie Schaller et al. "Human influence on climate in the 2014 southern England winter floods and their impacts". In: *Nature Climate Change* 6.6 (Feb. 2016), pp. 627–634. ISSN: 1758-6798. DOI: 10.1038/nclimate2927.

[108] Michelle Simões Reboita, Enrique Vieira Mattos, Bruno César Capucin, Diego Oliveira de Souza, and Glauber Willian de Souza Ferreira. "A Multi-Scale Analysis of the Extreme Precipitation in Southern Brazil in April/May 2024". In: *Atmosphere* 15.9 (Sept. 2024), p. 1123. ISSN: 2073-4433. DOI: 10.3390/atmos15091123.

[109] Walter Collischonn et al. "The exceptional hydrological disaster of April-May 2024 in southern Brazil". In: *RBRH* 30 (2025). ISSN: 1414-381X. DOI: 10.1590/2318-0331.302520240119.

[110] Leonardo Laipelt, Fernando Mainardi Fan, Rodrigo Cauduro Dias de Paiva, Matheus Sampaio, Walter Collischonn, and Anderson Ruhoff. "Mechanisms and scenarios of the unprecedent flooding event in South Brazil 2024". In: (May 2025). under review. DOI: 10.5194/egusphere-2025-1285.

[111] Joel Avruch Goldenfum, Anderson Ruhoff, Fernando Mainardi Fan, Rodrigo Paiva, Walter Collischonn, Fernando Dornelles, Fernando Meirelles, Gean Paulo Michel, and Masato Kobiyama. *Nota sobre a cheia ocorrida nos dias 4 e 5 de setembro na Bacia do rio Taquari-Antas*. Tech. rep. Insitituto de Pesquisa Hidráulicas, 2023.

[112] Leandra Zanger, Axel Bücher, Frank Kreienkamp, Philip Lorenz, and Jordis S. Tradowsky. "Regional pooling in extreme event attribution studies: an approach based on multiple statistical testing". In: *Extremes* 27.1 (Dec. 2023), pp. 1–32. ISSN: 1572-915X. DOI: 10.1007/s10687-023-00480-y.

[113] Davide Faranda, Gabriele Messori, Camargo Suzana J., Vargas-Heinz Luiza, and Erika Coppola. *May 2024 South Brazil floods locally exacerbated by both human-driven climate change and natural variability*. 2024. DOI: 10.5281/ZENODO.14163505.

[114] Chen Lu, Rita Nogherotto, Tommaso Alberti, Gabriele Messori, Erika Coppola, and Davide Faranda. "Models confirm that recent European wildfires are exacerbated by anthropogenic climate change". working paper or preprint. Jan. 2025.

[115] Agência Nacional de Águas e Saneamento Básico. *As Enchentes no Rio Grande do Sul – Lições, Desafios e Caminhos para um Futuro Resiliente*. 1st ed. Agência Nacional de Águas e Saneamento Básico, Apr. 2025. ISBN: 9786588101735.

[116] Yoav Benjamini and Yosef Hochberg. "Controlling the False Discovery Rate: A Practical and Powerful Approach to Multiple Testing". In: *Journal of the Royal Statistical Society Series B: Statistical Methodology* 57.1 (Jan. 1995), pp. 289–300. ISSN: 1467-9868. DOI: 10.1111/j.2517-6161.1995.tb02031.x.

[117] Governança e Gestão Secretaria de Planejamento. *Atlas Socioeconômico do Estado do Rio Grande do Sul*. 8th ed. Departamento de Planejamento Governamental, Nov. 2024. ISBN: 9786501245805.

[118] Luiza Vargas-Heinz, Matilde García-Valdecasas Ojeda, and Erika Coppola. "Impacts of climate change on Italy's river network: An assessment using high-resolution climate projections". In: *Journal of Hydrology* (2025). under review. DOI: 10.2139/ssrn.5601993.

[119] Luiza Vargas-Heinz, Chen Lu, and Erika Coppola. "Attribution of the 2024 Southern Brazil Floods to Climate Change". in preparation.

[120] Bernhard Lehner, Mathis L. Messager, Maartje C. Korver, and Simon Linke. "Global hydro-environmental lake characteristics at high spatial resolution". In: *Scientific Data* 9.1 (June 2022). ISSN: 2052-4463. DOI: 10.1038/s41597-022-01425-z.

[121] Simon Linke, Bernhard Lehner, Camille Ouellet Dallaire, Joseph Ariwi, Günther Grill, Mira Anand, Penny Beames, Vicente Burchard-Levine, Sally Maxwell, Hana Moidu, Florence Tan, and Michele Thieme. "Global hydro-environmental sub-basin and river reach characteristics at high spatial resolution". In: *Scientific Data* 6.1 (Dec. 2019). ISSN: 2052-4463. DOI: 10.1038/s41597-019-0300-6.